The production of ionization and Cerenkov radiation by cosmic ray muons

K.M. Pathak

The Production of Ionization and Cerenkov Radiation by Cosmic Ray Muons.

A Thesis submitted to the
University of Durham for the
Degree of Doctor of Philosophy

by

K.M. Pathak

September, 1967

CONTENTS

ABSTRACT

The details of the construction of a new horizontal spectrograph using neon flash tubes, plastic scintillators and an air-gap magnet are given. A detailed description of a water Cerenkov counter is also presented.

Both the Cerenkov radiation loss in water and the ionization loss in a plastic scintillator have been investigated using cosmic ray muons in the momentum range 0.355 - 100 GeV/c.

The results on the Cerenkov loss show that there is no significant change of Cerenkov intensity at particle momentum above 1 GeV/c. As such, the results are in good agreement with the classical theory of Frank and Tamm, and do not support the suggested suppression effect of Tsytovich (1963). Similarly they contradict the experiment, at high momentum, by Bassi et al. (1952), in which an anomalously large increase in Cerenkov loss was found.

The results on the ionization loss in the momentum range 10 - 100 GeV/c are consistent with the theory of Sternheimer (1952, 1953). No significant decrease was found in the values of most probable ionization loss in the above momentum range, again in contradiction to the theory of Tsytovich.

PREFACE

This thesis describes the construction of a new horizontal spectrograph and a Cerenkov counter with which a study has been made of the Cerenkov radiation loss of cosmic ray muons in water as a function of momentum up to 100 GeV/c.

The responsibility for the design and construction of the spectrograph was shared with author's colleagues, but the operation of the spectrograph, and the design and construction of the Cerenkov counter were the responsibility of the author alone.

In addition to the study of Cerenkov loss, the ionization loss of cosmic ray muons in a plastic scintillator has also been investigated. Here, the responsibility of the author was to analyse the final data.

The work was carried out in the Physics Department of the Durham University, under the supervision of Professor A. W. Wolfendale and Dr. M. G. Thompson.

CHAPTER 1.

1.1. Brief Introduction to the Cosmic Radiation Phenomena.

It has been known for almost sixty years that some type of ionizing radiation is continuously bombarding the earth's atmosphere from outer space. This ionizing radiation is termed the 'Cosmic Radiation'.

The mystery of the origin of this penetrating radiation is not yet fully solved. However, it is now generally accepted that the low energy part of the radiation is of solar origin, while the more energetic primaries are supposed to have galactic origin, and those of the very highest energies may well be of extra galactic origin.

At energies of a few tens of GeV, the primary cosmic ray flux at the top of the atmosphere is composed of 85 - 88% protons, about 10% alpha particles, 1 or 2% heavier nuclei and a small flux of electrons, gamma rays and neutrons. In addition there is expected to be a significant flux of neutrinos, most of which will be of solar origin. The energy range of the charged primaries varies from about 10^9 eV to 10^{20} eV, the lower limit depending on the geomagnetic latitude. The flux of the primary particles decreases rapidly with increasing energy and the 'upper limit' of 10^{20} eV may arise only from the very low rate of particles involved.

On entering the earth's atmosphere, the primary cosmic

rays interact with the nuclei of the air molecules with a mean free path of about 80 gm cm^{-2}. Thus, most of the interactions takes place in the first few hundred gm cm^{-2} of the atmosphere, and very few of the primary particles survive down to sea level. As a result of the primary interactions various secondary particles such as pions, kaons, nucleons and other baryons are produced. The number of the secondary products is attenuated exponentially in the atmosphere with an attenuation length of about 120 gm cm^{-2}. Unless the energy of the interacting primary is sufficiently high (few tens of GeV) none of the secondary particles reach the sea level.

The neutral pions (π^{o}) produced in the primary interactions decay almost immediately (half-life $\simeq 1.8 \times 10^{-16}$ sec.) giving rise to photons. If the latter are energetic they will create electron-pairs. The fast electrons thus produced radiate photons and the whole process is repeated giving rise to electron-photon cascades which propagate through the atmosphere. If the energy of the primary is above 10^{15} eV, the number of electrons arising from a neutral pion will be so great that a dense shower of particles, mainly electrons, will arrive at ground level. These showers are known as 'extensive air showers'.

Of the charged pions ($\pi^{\pm}$) produced, only the very energetic ones (energy $>$ 20 GeV) have a chance of interacting with the nuclei of the atmosphere, before undergoing

π-μ decay. The rest will decay into muons and neutrinos. The muons are very weakly interacting particles and have a much longer mean-life (2.20×10^{-6} sec.) against decay. As such, very many of them reach sea level and the more energetic ones even penetrate far underground. They constitute the hard component of the cosmic rays at sea level. Those muons which decay give rise to electrons and neutrinos. Some of these electrons may produce further electron-photon multiplications. These decay electrons as well as the electrons from the electron-photon cascades mainly initiated by neutral pions, give rise to the soft - component of cosmic rays.

Thus at sea-level, the cosmic ray flux mainly consists of muons, electrons, photons and neutrinos, with a small proportion of pions, nucleons and other baryons.

1.2 Cosmic Ray at Large Zenith Angle:-

It has been mentioned already that the number of cosmic ray particles dwindles as they propagate through the atmosphere. This effect will be more pronounced in the near-horizontal direction, since the thickness of the atmosphere along this direction is about 36 times more than that in the vertical direction. Only high energy muons can survive through such a great depth of the atmosphere.

The variation of the muon intensity with zenith angle is very interesting. At low energies, the relative intensity of muons in the vertical direction is much higher than that in the near horizontal direction. This is because in the latter direction, a muon loses more energy due to longer path length and has a much bigger probability of μ-e decay. Consequently, the number of low energy muons in the near - horizontal direction is reduced very much, but their median energy is much higher and at 90°, it is $\approx$ 80 GeV. At high energies, i.e. at energies greater than 100 GeV, the overall intensity of muons in the near - horizontal direction is significantly higher than that in the vertical direction. This is due to the fact that high energy pions (or kaons) travelling in the near - horizontal direction have a greater probability of decay into high - energy muons than pions of similar energy travelling in the vertical direction where at the corresponding point, the atmosphere is comparatively dense.

From the experimental points of view, the study with muons in the large zenith angle has two chief advantages: First, one can get a more or less uncontaminated muon flux of extremely high energy; secondly, the intensity

of the low energy muons being small, the measurements and the analysis are less complicated compared to those in the vertical direction where the low energy flux is very high.

1.3 Measurements on High Energy Muons.

The present day accelerating machine can produce highly interacting particles such as $\pi^{\pm}$, $K^{\pm}$, protons etc., up to an energy of about 30 GeV or so. But it is very difficult to get a pure beam of muons of energy more than a few GeV from the machine, because the fast pions from which the muons are produced have a comparatively long life-time. As such, cosmic rays are the only source at present of high energy muons. It has been indicated earlier that in the near - horizontal direction the flux of energetic muons is quite high. With the help of a magnetic spectrograph the momenta of these muons can be found precisely. Thus a magnetic spectrograph selecting particles in the near- horizontal direction may be used as a source of high energy muons of known momentum and sign. Such spectrographs are widely used now-a-days for the measurement of the momentum - spectrum and the charge - ratio of muons. Also, they are used for invest-

igating the interactions of muons with the atomic electrons and nuclei of the material through which they traverse. The spectrograph in the present experiment has been used for the latter type of investigation.

1.4 The Present Work:-

The present work includes the design and construction of a new cosmic - ray horizontal spectrograph and a water - Cerenkov counter which have been used to study the variation of energy loss (ionization and Cerenkov losses) with momentum of cosmic ray muons.

The present introduction is followed by Chapters 2 and 3 where the theoretical aspects of the problems of ionization and Cerenkov losses are discussed. A brief review of the previous work on energy loss is incorporated in Chapter 4. Chapter 5 contains the description of the new spectrograph. A detailed description of the Cerenkov counter is given in Chapter 6. The analyses of the experimental results on ionization loss and Cerenkov radiation loss are given in Chapter 7. Finally, the conclusions from the present experiment both on the ionization loss and Cerenkov loss are drawn in Chapter 8.

CHAPTER 2.

Theories of Energy Loss:

2.1 Introduction.

A fast charged particle in its passage through matter may lose its energy in one or more of the following processes:

a) Ionization and excitation

b) Bremsstrahlung

c) Direct pair production

d) Nuclear interaction

e) Cerenkov radiation

Of these, the energy losses by ionization and excitation of the atoms of the penetrated medium are the dominant mechanisms for muons up to energies of about 10^{11} or 10^{12} eV; at higher energies bremsstrahlung, pair - production and nuclear interactions make important contributions.

Cerenkov radiation is emitted whenever the velocity of the particle exceeds the velocity of light in the medium. However, compared to other kinds of losses, its contribution is very small.

As has been mentioned earlier (Chapter 1), the

aim of the present experiment is to estimate the ionization and Cerenkov loss of relativistic cosmic ray muons. In this chapter, we shall confine ourselves mainly to the theories of ionization loss. Theories of Cerenkov loss will be dealt with in the next chapter.

2.2 Theories of the Average Energy Loss by Collisions:

When a fast charged particle, heavier than an electron, passes through matter, it loses energy predominantly by inelastic collisions with atomic electrons, causing ionization or excitation. The theory of energy loss by the above processes was established by Bohr (1913) through a semiclassical procedure. Later Bethe (1930, 1932, 1933) developed a quantum mechanical theory for the collision losses. The Bohr and Bethe theories apply to substances where the atoms are well separated i.e. gases.

In all the theories developed so far, the possible energy transfers to atomic electrons in a single collision have conveniently been divided into two classes: (a) distant collisions and (b) close collisions. A distant collision is one in which an (atomic) electron of energy smaller than a predetermined value η is

ejected, whereas in a close collision, an electron of energy greater than η is ejected. In determining the value of η, however, the following two conditions are imposed:

(a) η must be large compared with the binding energies of electrons in the atom; and

(b) η must be sufficiently small that for energy transfers of order η and less, the effective impact parameter is large compared with atomic dimensions, and consequently the charged particle can be represented as a point charge.

For a fast particle, a value of η between 10^4 and 10^5 eV satisfies the above two conditions simultaneously (Rossi 1952, Uehling 1954).

An atomic electron may receive in a single collision an amount of energy between a minimum value and some maximum value Em. The actual energy transferred E^1 in any collision depends upon the impact parameters of the particular collision.

The minimum value is, in practice, equal to the mean excitation or ionization potential I (z) of the atom, and is a measure of the smallest amount of energy which can be transferred, on the average, to a bound

electron. The quantity I (z) can be deduced from experimental results or can be calculated theoretically, (Bloch (1933), Wick (1941 & 1943), Hallpern and Hall (1948), Baker and Segre (1951) and Mather and Segre (1951). For most calculations, the formula

$$I(z) = I_H z \qquad \text{.. .. .. 2.1}$$

where I_H = 13.5 eV = the energy corresponding to the Rydberg frequency, can be used.

The maximum energy that can be transferred to an electron, mass m, by a particle of mass M in a single collision was shown by Bhabha (1937) to be:

$$E_m = \frac{E_o^2 - M^2 c^4}{M c^2 \left(\frac{M}{2m} + \frac{m}{2M} + \frac{E_o}{Mc^2}\right)} \qquad \text{.. 2.2}$$

where E_o = total energy of the particle,
= E + M c^2 where E is the Kinetic energy.

If $E_o << \frac{M^2 c^2}{m}$ & $M >> m$ .. 2.3

then, $E_m \approx 2 m c^2 \frac{\beta^2}{1-\beta^2}$ 2.4

Where $\beta c = v$, the velocity of the particle.

Bethe (1930, 1932) computed the energy loss per gm cm^{-2} resulting from distant collisions, by taking into account the binding of the electrons to the atoms. Considering the system formed by an atom and the incident particle, he calculated the probabilities for the various possible transitions leading to excitation or ionization of the atom. He obtained the following result:

$$K_{Coll(<\eta)}(E) = \frac{2C\ mc^2}{\beta^2}\left(\ln\frac{2\ mc^2\beta^2\eta}{(1-\beta^2)I^2(Z)} - \beta^2\right) \quad \ldots\ldots 2.5$$

$$\text{where } C = \pi N \frac{Z}{A} r_e^2 = 0.150 \frac{Z}{A} g^{-1}\ cm^2 \quad \ldots\ldots 2.6$$

where Z and A are the charge and mass number of the material, N is the Avogadro's number, and

$$r_e = \frac{e^2}{mc^2} = \text{classical radius of the electron.}$$

Equation(2.5) holds good for particles of unit charge, positive or negative, and with velocities large compared with the velocity of atomic electrons.

For close collisions, the energy loss per gm cm^{-2}, $K_{Coll(>\eta)}(E)$ can be computed from the following expression:

$$K_{Coll(>\eta)}(E) = \int_{\eta}^{Em} E^{1} \phi_{Coll}(E, E^{1})\, dE^{1} \quad \ldots\ \ldots\ \ldots \quad 2.7$$

where $\phi_{coll}(E, E^{1})\, dE^{1}$ is the collision probability.

For particles of mass M and spin $\frac{1}{2}$, Bhabha in 1938 and Massey and Corben (1939) showed this probability to be

$$\phi_{Coll}(E, E^{1})\, d E^{1} = \frac{2C\, mc^{2}\ \ d E^{1}}{\beta^{2}\ (E^{1})^{2}} \left[1 - \beta^{2}\frac{E^{1}}{Em} + \frac{1}{2}\left(\frac{E^{1}}{E + Mc^{2}}\right)^{2}\right] \quad \ldots\ \ \ldots\ \ \ldots \quad 2.8$$

So for singly charged particle, heavier than electron, one gets from equations 2.7 and 2.8

$$K_{Coll\ (>\eta)}(E) = \frac{2\ C\ mc^{2}}{\beta^{2}} \left\{ \ln \frac{Em}{\eta} - \beta^{2} + \frac{1}{4}\left(\frac{Em}{E + Mc}\right)^{2} \right\} \quad \ldots \quad 2.9$$

provided that $E_{o} << \frac{M^{2} e^{2}}{m}$

Thus the total energy loss by collision per gm cm^{-2} is the sum of the equations 2.5 and 2.9 and is given by

$$-\frac{(dE)}{(dx)_{av}} = K_{Coll\ (<\eta)}(E) + K_{Coll\ (>\eta)}(E)$$

$$= \frac{2\ C\ mc^{2}}{\beta^{2}} \left\{ \ln \frac{2m\ \beta^{2} c^{2}\ Em}{(1 - \beta^{2})\ I^{2}(z)} - 2\beta^{2} + \frac{1}{4}\left(\frac{Em}{(E + Mc^{2})}\right)^{2} \right\} \quad \ldots \quad 2.10$$

The equation 2.10 gives the average rate of energy loss. The last term within the bracket, which is due to the spin of the particle, affects the rate of energy loss only at high energies. For muons in water, the correction is about 0.2% at an energy of 20 GeV (Cousins & Nash, 1962). Moreover, it may be mentioned here that most experiments measure not the average but the most probable ionization loss which, being determined almost entirely by the distant collisions, will not be affected by spin (Price 1955). So neglecting the spin term, and using equation 2.3 and 2.4, the equation 2.10 can be written as

$$-\left(\frac{dE}{dx}\right)_{av} = \frac{2\,C\,mc^2}{\beta^2}\left\{\ln\frac{4\,m^2c^4\beta^4}{(1-\beta^2)^2 I^2(Z)} - 2\beta^2\right\} \quad .. \quad 2.11$$

The condition $E_o \ll \frac{M^2c^2}{m}$ limits the validity of equation 2.11 to muon energies of up to a few GeV.

From equation 2.11 it is obvious that the average energy loss is a function of the velocity β of the incident particle. It may be mentioned here that for an incident particle of charge Z, $-\left(\frac{dE}{dx}\right)_{av}$ is proportional to Z^2. Further, the average loss does

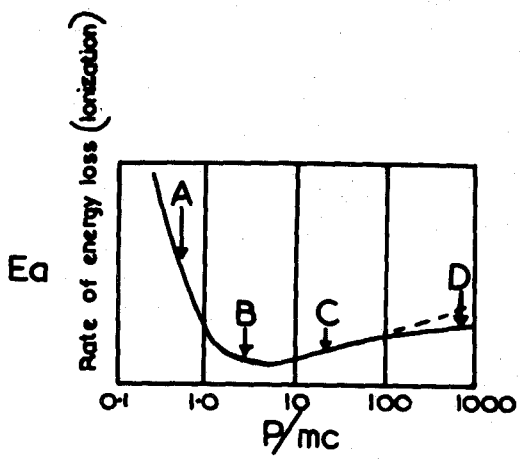

FIG 2·1 The form of the variation of rate of average energy loss with momentum

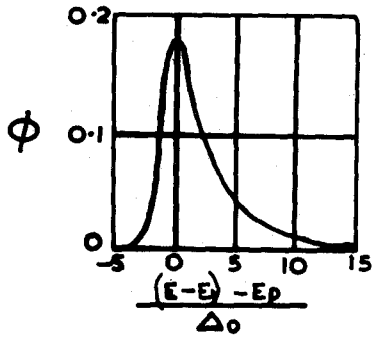

FIG 2·2 Probability ϕ of an energy loss $(E-E_1)$ as a function of the most probable energy loss Ep & Δ_0 The latter being defined by

$$\Delta_0 = 2C\, mc^2\, x/\beta^2$$

(Landau 1944)

not depend separately on the momentum and on the mass of the incident particle, but only on the ratio of these two quantities. This means that for all particles of unit charge, the graph of $-\left(\frac{dE}{dx}\right)_{av}$ against β will be a universal curve.

2.3 The Average Energy Loss Curve:-

Figure 2.1 depicts schematically the nature of the variation of average energyloss with momentum. The whole curve may be divided into 4 different regions A, B, C and D as indicated. In the region A, the region of sub-relativistic energies ($0.96 > \beta > 0.1$), the energy loss falls off as $\frac{1}{\beta^2}$ as the velocity of the particle is increased. This is due to the fact that, for a given impact parameter, the time spent by a passing particle in the vicinity of an electron becomes shorter and shorter as the velocity of the particle increases. Consequently the interaction between the particle and electron becomes less and less effective. But when β approaches nearly equal to its limiting value unity, the factor $\frac{1}{\beta^2}$ becomes practically constant. No further reduction can occur and the region B, i.e. the region of minimum ionization, is reached. After

this flat minimum ($\beta > 0.97$) the energy loss begins to show a slow increase (region C) with increasing momentum, due to the factor $(1 - \beta^2)$ in the logarithm of the equation 2.11. Physically this increase is partly due to the increase in the maximum transferable energy E_m with E_o and partly due to the relativistic deformation of the coulomb field of the incident particle which causes the particle to be effective at larger distances from its geometric path. The logarithmic rise is considerably reduced at very high momenta (region D) by the so called 'density effect' to be described in the following section.

The factor $C \left(= 0.150 \ \frac{Z}{A} \right)$ in the equation 2.11 shows that the rate of energy loss (per gm cm^{-2}) is somewhat less for heavy elements as $\frac{Z}{A}$ falls with increasing Z. This means that light elements are more effective in slowing down ionizing particles.

2.4 The Density Effect:

In the theory discussed so far, it has been assumed that the atoms are isolated and are thus independent of their neighbours atoms. This is

permissible to a large extent when the absorbing medium is gas and it also holds good, in general, for all close collisions. But for distant collisions, the presence of neighbouring atoms cannot be neglected, particularly in the case of dense media. For such collisions, the screening of the electric field of the passing particle by the intervening atoms of the medium needs to be considered. This factor becomes more and more important with the increase of the velocity of the particle and the screening reduces the strength of the interaction and therefore, decreases the energy loss. The magnitude of the reduction depends in a fairly complicated way on the dispersive properties of the medium, and the detected energy loss depends critically on the techniques of observations. It may be mentioned here that the density effects are independent of the nature of the penetrating particle.

Swann in 1938 first pointed out the possible influence of the density on the ionization loss due to distant collisions. Fermi (1939, 1940) investigated the whole problem quantitatively. He considered the electrons of the absorber as classical oscillators, with a single characteristic frequency, ν_j set in

motion by the passage of a charged particle. Further he considered only losses occurring at relatively large distances from the geometric track of the particle. The latter assumption helped him in treating the absorbing medium as continuous and the energy loss as a classical process. Thus Fermi showed that a factor, Δ, should be subtracted from the energy loss expression for the isolated atoms. For singly charged particles, Δ, according to Fermi, is given by the following equations:

$$\Delta(\beta) = \frac{2C\ mc^2}{\beta^2} \ln K \quad \text{for} \quad \beta < \frac{1}{\sqrt{K}} \qquad \ldots\ldots \quad 2.12$$

$$\Delta(\beta) = \frac{2C\ mc^2}{\beta^2} \left(\frac{K-1}{1-\beta^2} + \frac{1 - K\beta^2}{K-1} \right) \qquad \ldots \quad 2.13$$

for $\beta > \frac{1}{\sqrt{K}}$

where $$K = 1 + \frac{4\pi ne^2}{m w_o^2} \qquad \ldots\ldots\ldots\ldots\ldots \quad 2.14$$

is the dielectric constant of the medium for low frequencies, and m, e, n are the mass, charge and number of electrons per unit volume. $\frac{W_o}{2}$ is the frequency of the electronic oscillator when E = 0.

The quantity $\Delta(\beta)$ given by equation 2.12 is usually small. So in the low energy region, the corrected energy loss is not appreciably different

from that given by Bethe - Bloch theory equation 2.11. But at higher energies when the particle velocity exceeds the velocity of light in the medium, the correction given by equation (2.13) has to be subtracted from the average energy expression (2.11) or from the expression for the most probable energy loss Ep (Equation 2.22). The latter at high energies, for a traversal of x gm cm^{-2} of the absorber, becomes

$$Ep = \frac{2C\ mc^2\ x}{\beta^2} \left(ln \frac{4C\ m^2\ c^4\ x}{(K-1)\ I^2(z)} - \frac{1-\beta^2}{K-1} + j \right) \ldots 2.15$$

Since the factors $(1-\beta^2)$ in the logarithmic term cancel out in the expression (2.15) for corrected Ep, the probable energy loss tends towards a constant value (see fig. 2.3), the so called 'Fermi Plateau', independent of the particle velocity.

However, from fig 2.1, it is obvious that in spite of the reduction of energy loss due to the density effect, the curve shows an increase in average energy loss at high values of $\frac{P}{Mc}$. This is due to the fact that the average energy loss is, to a considerable extent, dependent on close collisions, which are hardly affected by polarization. With the increase of momentum of the particle, the maximum transferable energy, E_m, increases entirely from the close collisions. So the

increase of the rate of energy loss is due mainly to the close collisions. But on the other hand, since the most probable energy loss is mainly determined by the distant collisions, the relativistic rise beyond a certain value, determined by the properties of the medium, is eliminated altogether (figs. 2.3, and 2.4).

According to Fermi, there remains a finite energy loss even when the impact parameter b is allowed to tend to infinity. This was interpreted by Fermi as that part of the energy which is emitted as Cerenkov radiation, which then forms part of the total loss calculated with the aid of the theory and not additional to it (See Chapter 3). On the basis of the Fermi's theory, as has been pointed out first by Bohr (1948) and later by Messel and Ritson (1950), Schoenberg (1951) and Fowler and Jones (1953), the whole of the most probable energy loss beyond the minimum and up to the beginning of the plateau should be ascribed to this Cerenkov radiation. Fermi showed that the energy loss for the impact parameter $b \longrightarrow \infty$ was

$$W_\infty = \frac{2C\, mc^2\, x}{\beta^2} \left\{ -\beta^2 - \ln(1 - \beta^2) \right\} \text{ for } \beta < \frac{1}{\sqrt{K}} \qquad \ldots\ldots\ 2.16a$$

and $$W_{\infty} = \frac{2\,C\,mc^2\,x}{\beta^2}\left(-\frac{1-\beta^2}{K-1} + \ln\frac{K}{K-1}\right) \text{ for } \beta > \frac{1}{\sqrt{K}} \quad .. \ 2.16b$$

W_{∞}, according to Fermi, represents that part of the energy lost by the particle that is emitted in the form of Cerenkov radiation.

Thus, the most probable ionization loss (including excitation) with density correction can be obtained by subtracting equation (2.16b) from equation (2.15), and is given by

$$E_{p\ \text{ionization}} = \frac{2\,Cmc^2\,x}{\beta^2}\left\{\ln\frac{4C\,m^2c^4x}{K\,I^2(z)} + j\right\} \quad .. \ 2.17$$

Since the above equation (2.17) does not contain β in the logarithmic term, it implies that according to Fermi's theory, there should be no relativistic increase in energy loss except for that due to Cerenkov radiation (Fig. 2.3 curve C and fig 2.4 curve D).

The Fermi theory was later extended by Halpern and Hall (1940, 1948) to cover the case of several dispersion frequencies. They concluded that the correction factors given by the equations (2.12) and (2.13) assuming a single frequency of the electron, were an over estimate of the reduction in the collision loss. Extensions of the Fermi theory have also been

made by Wick (1940, 1941, 1943), Schoenberg (1950, 1952) and Sternheimer (1952, 1953).

Thus from the Fermi's original theory and all the later extensions to it (as mentioned above) one comes to the conclusion that there should be no relativistic increase in the ionization loss. The whole increase of the loss at relativistic energies is due to the emission of Cerenkov radiation which will escape. That is to say, an experiment that observes only the ionization loss should not detect any relativistic increase in the most probable energy loss. The experimental results of Occhialini (1949) as well as those of Bower and Roser (1951) seemed to support the above conclusion.

But Ghosh et al. (1952, 1954) and Pickup and Voyvodic (1950, 1951) observed a relativistic increase in the detected ionization loss. In view of this discrepancy, the contribution of Cerenkov radiation to the energy loss has been thoroughly re-investigated.

Huybrechts and Schoenberg (1952) pointed out that the treatment of Fermi did not take into account the fact that the frequency bands in which a large part of Cerenkov radiation was emitted would be modified by interactions between the adjacent atoms.

They overcame the difficulty by distinguishing the close collisions from distant collisions by selecting a critical impact parameter $R = \left(\frac{mc^2}{4\pi ne^2} \right) = 5.3 \times 10^5 n^{-\frac{1}{2}}$ cm (which is of the order of 10^{-8} cm) where n is the electron density of the medium. They showed that the close collisions (impact parameter $<$ R) would lead mainly to the ionization and excitation, and the Cerenkov radiation was the principal result of the distant collisions (impact parameter $>$ R) and would be smaller than the Fermi's theory. Thus from the theory of Huybrechts and Schoenberg, it appears that any experimental observation of the ionization loss would include not only the 'primary' ionization and excitation loss but also the 'secondary' ionization and excitation produced by the absorption of Cerenkov radiation near the track. Since the Cerenkov radiation would increase with the increasing velocity of the traversing particle, one should expect, according to the above theory of Huybrechts and Schoenberg, a relativistic rise in the most probable ionization loss. Thus, the above theory could explain satisfactorily the experimental results of Ghosh et al. (1952, 1954). However, in the case of photographic emulsion they predicted a smaller relativistic rise than was found experimentally.

Fowler and Jones in 1953 extended the above theory by modifying slightly the magnitude of the impact parameter, R, for close collisions. They pointed out that for distances greater than the atomic dimensions ($\approx 10^{-8}$ cm), the medium should be treated as a homogeneous dielectric having a complex dielectric constant. The latter assumption would give rise to a heavily damped Cerenkov radiation which would be entirely absorbed within a distance of $\approx 10^{-4}$ cm from the track of the particle. Consequently the observed ionization loss would show a relativistic increase.

Sternheimer (1953, 1954, 1956) and Budini (1953) have analysed the problem by making a similar distinction between 'Primary' ionization and excitation, and the 'Secondary' effects caused by the reabsorption of Cerenkov radiation. This is discussed in detail in the next chapter which deals with the Cerenkov radiation loss.

2.5 Statistical Fluctuations in Energy Loss by Collisions and the most probable Energy Loss.

In practice, the ionization loss measured in a detector is due to the contribution from two sources:

(a) Primary ionization i.e. the ionization produced by the traversing charged particle in direct interactions

with the atomic electrons of the absorber, and

(b) Secondary ionization i.e. the ionization produced by the electrons ejected from the primary ionization.

The energy loss due to primary ionization is a result of large numbers of independent ionizing collisions. The ionizing events thus follow a Poisson distribution. Further, a wide range of energies can be lost by the fast particle in a single inelastic collision as can be seen from equation (2.8). Consequently there will be a great deal of fluctuations in the observed rate of energy loss which will be found to have the characteristic skew probability distribution as shown in the fig. 2.2. This distribution has been predicted by Landau (1944) assuming (a) that the energy loss of a particle in passing through an absorber of thickness x is small compared with its initial energy, and (b) that $\Delta_o \left\{= \frac{2\,C\,mc^2\,x}{\beta^2}\right\}$ is large compared with the average ionization potential $I = I_H Z$ of the electrons in the absorber. The result of the fluctuations of the energy loss is often called the "Landau effect".

A qualitative explanation for the shape of the

curve in fig. 2.2 can be given as follows:
In the majority of the ionizing collisions suffered by a particle while passing through an absorber, the energy transferred to the struck electron is very small, as can be seen from the $\frac{dE^1}{(E^1)^2}$ term in equation (2.8). Such low energy collisions give rise to an approximately Gaussian distribution of the energy loss. On the other hand, there will be a few collisions in which a large amount of energy will be transferred to the electron. These collisions give rise to a high energy tail on the distribution.

It is due to this Landau distribution, especially the high energy tail of the distribution that the experimental determination of the average energy loss becomes extremely complicated. Further, the average is very sensitive to the relatively infrequent high energy collisions which cannot be studied satisfactorily due to experimental limitations, such as the saturation of the detector or its amplifier. On the other hand, the Gaussian region of the peak, which is due to the more frequent small energy transfers, remains more or less unaffected by the fluctuations. So it is usually

preferable to study the mode i.e. the most probable value of the ionization loss rather than the mean.

Again, on comparing the two curves in fig 2.1, and fig 2.3 C, one would notice that the logarithmic rise in the curve E_{av} vs momentum is much higher than that in Ep vs momentum. It is so because the increasing values of the maximum transferable energy E_m do not influence the magnitude of the mode values. It is seen that compared to E_a vs momentum, the study of E_p as a function of momentum of the particle reveals the onset of the density effect more sharply, and hence, in the latter case, it is easier to detect.

The problem of fluctuations has also been investigated by other workers, eg. Bohr (1915), Williams (1929), Symon(1948) and Sternheimer (1952, 1953, 1956). Rossi (1952) has summarised the complete solution of the problem obtained by Symon (1948), and now-a-days, usually this solution is used for calculating the distribution of the energy loss.

Symon (1948) gave a complete solution of the problem considering separately the case of a thin absorber ($E_a(x) \geq 0.9\ E_o$) and the case of thick absorber ($E_a(x) < 0.9\ E_o$). Symon showed that the most probable energy loss E_p of a singly charged heavy particle traversing an absorber of thickness x gm cm^{-2}

is given by

$$E_p = \frac{2\,C\,mc^2\,x}{\beta^2}\left\{ \ln \frac{4\,C\,m^2\,c^4\,x}{(1-\beta^2)\,I^2(Z)} - \beta^2 + j \right\} \quad .. \quad 2.22$$

Where j is a function of the parameter $G = \frac{2\,C\,mc^2\,x}{\beta^2 E_m}$.

Curves for j vs G, and also the probability distribution as a function of the energy loss according to Symon's theory have been given by Rossi (1952).

For $G < 0.05$, Symon's formula eqn. (2.22) is the same as that of Landau, j having the constant value of 0.38. But for $G > 0.05$, Symon's method must be used.

2.6 Expected most probable energy loss E_p for relativistic muons in (a) plastic scintillator NE 102A and (b) water:

On taking the density effect into consideration the equation (2.22) may be written as

$$E_p = \frac{2C\,mc^2\,x}{\beta^2}\left\{ \ln \frac{4\,C\,m^2\,c^4\,x}{(1-\beta^2)\,I^2(Z)} - \beta^2 + j - \delta(\beta) \right\} \quad 2.23$$

In order to compute a theoretical curve for the most probable energy loss E_p as a function of the momentum, the density corrections given in equations

(2.13) and 2.14) by Fermi, or analytical expressions given by Sternheimer (1956) may be used. The latter are:

$$\delta(\beta) = 4.606\, x + C_1 + a(x_1 - x)^m \quad \text{when } (X_0 < X < X_1)$$

and $$\delta(\beta) = 4.606\, x + C_1 \quad \text{when } X > X_1$$

where $x = \log \frac{P}{Mc}$, P being the momentum and M the mass of the charged particle, c velocity of light. a, m, C_1 are constants which depend on the absorber. Xo is the value of X which corresponds to the momentum below which $\delta(\beta) = 0$; X_1 corresponds to the momentum above which the relation between $\delta(\beta)$ and X can be considered linear.

Rearranging equation (2.23) after Sternheimer (1952, 1953, 1956) and taking $j = 0.37$, one gets

$$E_p = \frac{Ax}{\beta^2} \left\{ 1.06 + B + 2 \ln \frac{P}{Mc} + \ln \frac{Ax}{\beta^2} - \beta^2 - \delta(\beta) \right\} \quad \ldots\ldots 2.24$$

where $A = 2\, C\, mc^2$

and $B = \ln \left\{ \frac{mc^2\ (10^6)\ eV}{I^2\ (Z)} \right\}$

M = mass of the muon = 105.66 MeV.

The value of X_1 for phosphor as well as for water as quoted by Sternheimer (1956) and Crispin (1965) is 2.0 so when $X < X_1$, $\log \frac{P}{Mc} < 2$

i.e. $P < 10.57$ GeV/c.

Thus, for muons of momentum less than 10.57 GeV/C, the equation (2.24) becomes

$$E_p = \frac{Ax}{\beta^2}\left(1.06 + B + \ln\frac{Ax}{\beta^2} - \beta^2 - C_1 - a(X_1 - \log\frac{P}{Mc})\right)^m \quad .. \quad .. \quad .. \quad 2.25$$

and for $P > 10.57$ GeV/C,

$$E_p = \frac{Ax}{\beta^2}\left(1.06 + B + \ln\frac{Ax}{\beta^2} - \beta^2 - C_1\right) \quad .. \quad 2.26$$

From the equations (2.25) and (2.26) it is obvious that the most probable energy loss E_p depends on the constants of the absorber and the velocity β, of the indident particle. For momentum greater than 10.57 GeV/C, then $\beta \approx 1$, and consequently the E_p, for all practical purposes, is constant for particle of momentum greater than 10.57 GeV/C.

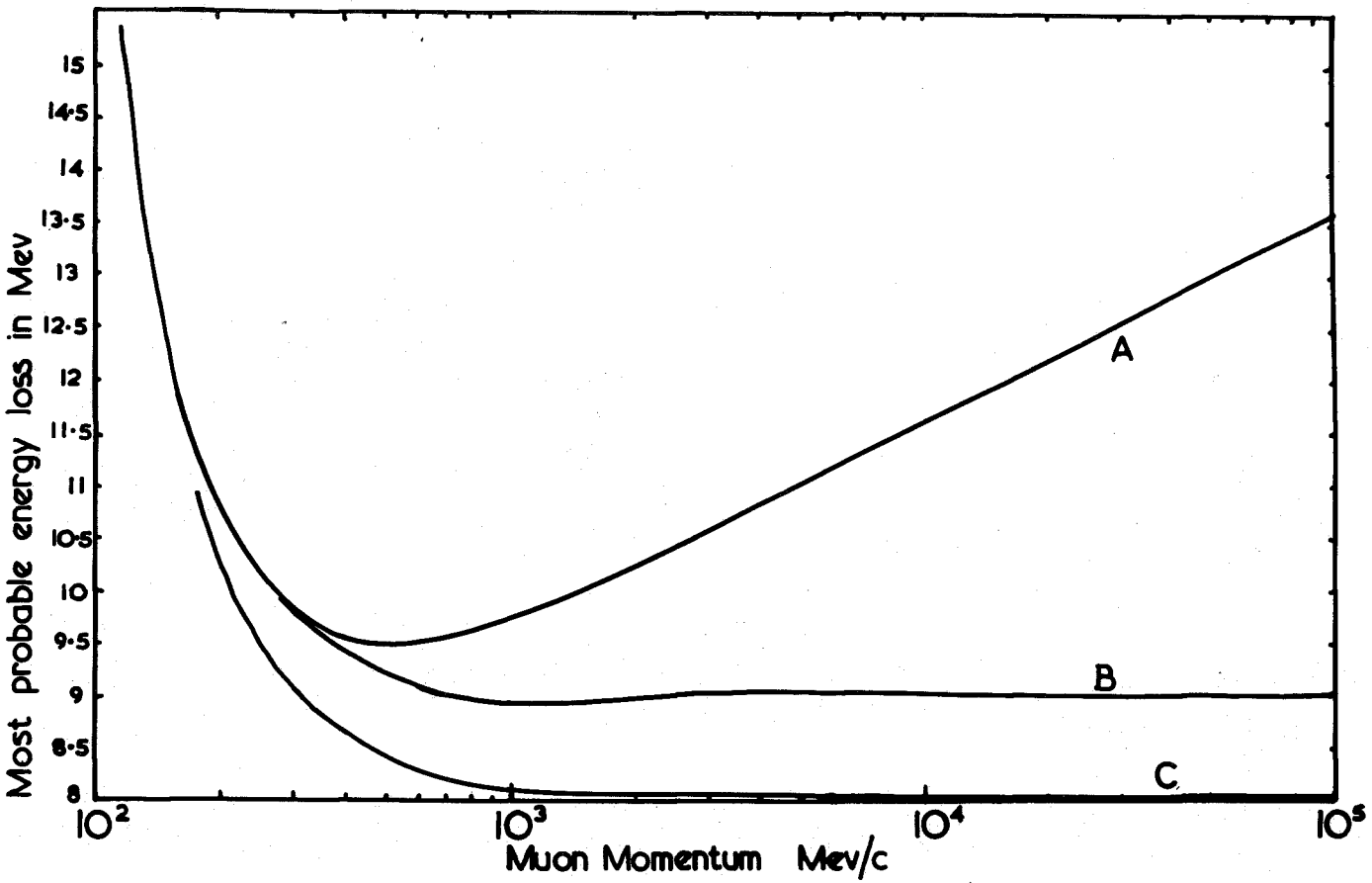

FIG 2·3 VARIATIONS OF THE MOST PROBABLE ENERGY LOSS WITH MOMENTUM IN THE PLASTIC SCINTILLATOR (5·16 gm cm^{-2})

A. Uncorrected for density effect (Symon)
B. The same with Sternheimer density correction
C. Ionization loss according to Fermi after correction for density effect and Cerenkov radiation loss.

2.6a The most probable energy loss in phosphor NE 102A

The constants for the phosphor NE 102A have the following values (Sternheimer 1956, Crispin 1965, NE catalogue September 1965):

$A = 0.0833$ MeV gm^{-1} cm^{2} $\quad a = 0.514$

$B = 18.69 \quad C_1 = 3.13$

$I(Z) = 62.6$ eV $\quad m = 2.595$

$X_o = 0.044$

$X_1 = 2.$

Using the above constants, expected values of E_p in a 5 cm thick NE 102A plastic scintillator have been calculated and results are shown in fig.2.3B.

From the theoretical curve it is found that the relativistic rise beyond the minimum is about 1.3%.

Crispin (1965) used another variety of plastic scintillator NE 102 which has properties and composition similar to those of NE 102A but slightly inferior light transmission. Using the Sternheimer density correction, he calculated a rise of 1.48% in energy loss beyond the minimum. His experimental results were found to be in good agreement with the theory up to 10 to 15 GeV/C. But at higher momenta, the results showed a rise in the

most probable energy loss which was greater than the predicted value. At 100 GeV/C, he observed an increase of about 2.2% above the predicted rise.

On the other hand, Barnaby (1961), using the same variety of plastic scintillator NE 102 showed that the relativistic rise was less than 1% for muons of energy between 0.5 and 10 GeV, i.e. less than the predicted value of Crispin. The reason for this discrepancy is not known.

2.6b The most probable energy loss in water.

Theoretical estimates for the most probable ionization loss in water, using the density corrections of Sternheimer in equation (2.25) and (2.26) have been made and the results are shown in the fig. 2.4. Also shown, for comparison, are the results of Fermi's density correction. The following are the constants used in estimating Sternheimer's density correction:

$A = 0.0853$ MeV gm^{-1} cm^2	$a = 0.519$
$B = 18.35$	$m = 2.69$
$I(Z) = 67.5$ eV	$X1 = 2$
	$X0 = 0.23$

The relativistic rise beyond the minimum is found to be $\approx$ 2.5% (fig. 2.4 Curve C).

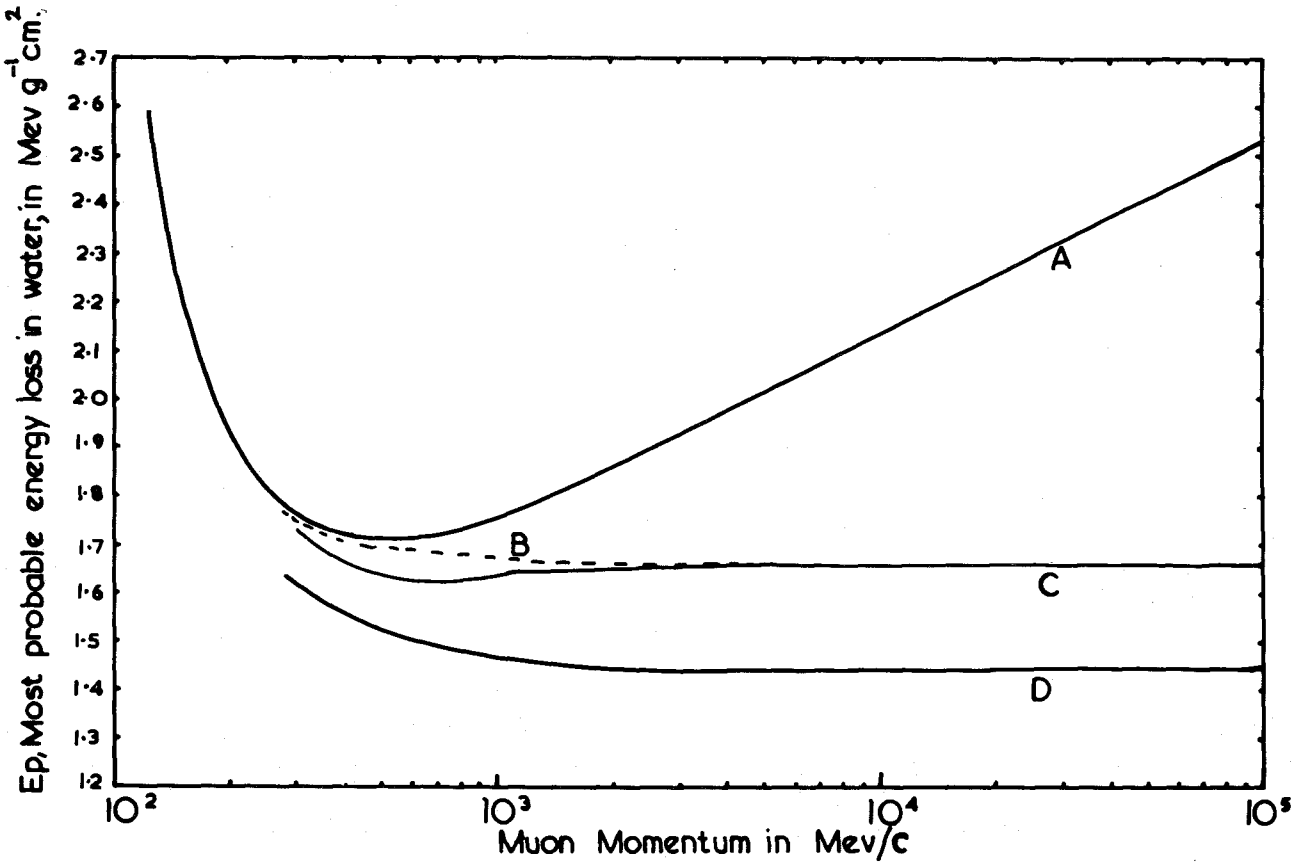

FIG 2·4 THEORETICAL VARIATIONS OF THE MOST PROBABLE ENERGY LOSS OF MUONS WITH MOMENTUM IN WATER

A. Uncorrected for density effect (Symon)
B. With Fermi's density correction.
C. With Sternheimer density correction
D. With Fermi's density & Cerenkov radiation loss correction (only ionization)

In estimating Fermi's density correction, the dielectric constant K has been calculated from equation (2.14) as follows:

$$K = 1 + \frac{4\pi ne^2}{m W_o^2}$$

$$= 1 + \frac{ne^2}{\pi m \nu_o^2}$$

Putting $I(Z) = h\nu_o = 67.5$ ev, $= 1.632 \times 10^{16}$/sec,

and $n = \frac{NZ}{A} = 3.041 \times 10^{23}$ per c.c.

Thus, $K = 1.092$.

It will be seen from the curve B fig 2.4 that the most probable ionization loss, after being corrected for density effect according to Fermi, does not show any rise at all. It falls off rather smoothly and attains a steady plateau value at about 10 Gev/c.

2.6 C Magnitude of the Density Effect in Water and Phosphor:

A comparison of the magnitude of the density correction $\delta(\beta)$ in plastic scintillator and in water has been made and the results are shown graphically in fig. 2.5. It is seen that the $\delta(\beta)$ in water is less than that in a plastic scintillator.

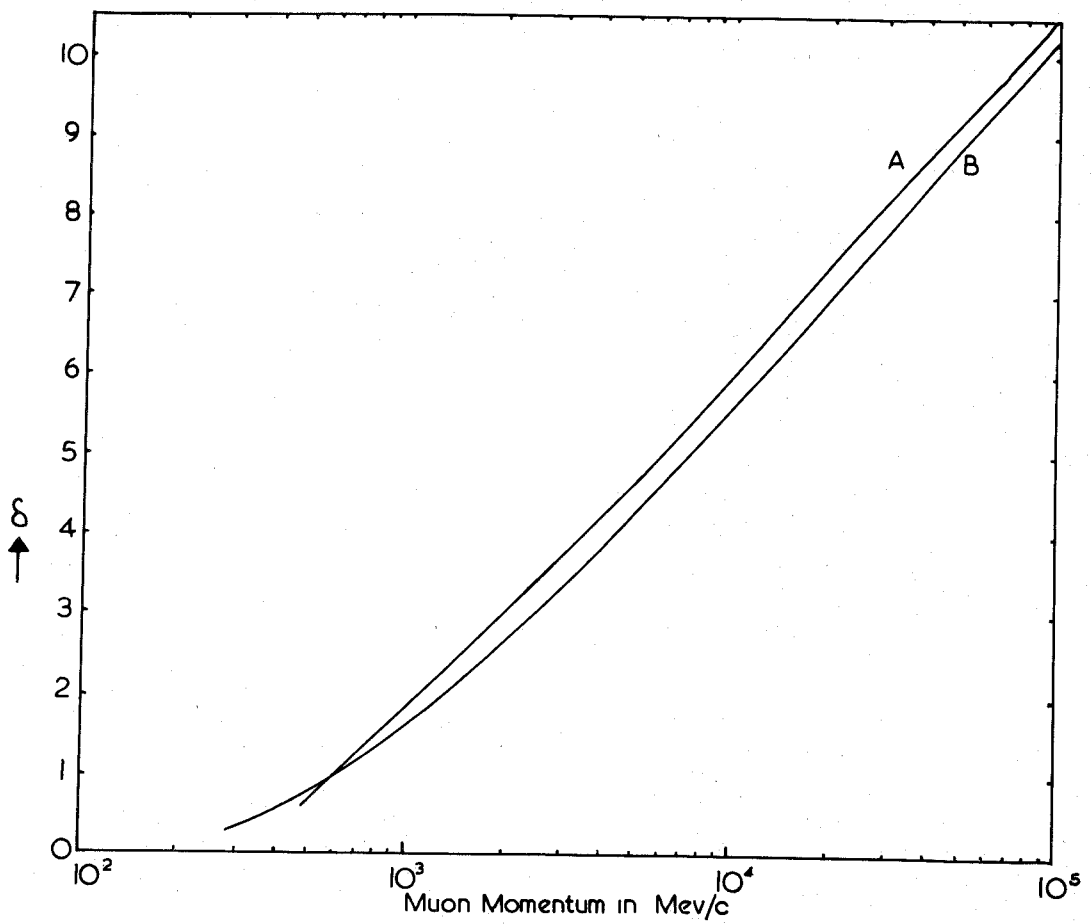

FIG 2·5 VARIATION OF THE DENSITY EFFECT WITH MOMENTUM IN PLASTIC(A) & IN WATER (B) (Sternheimer density correction)

The difference in $\delta(\beta)$ in two substances may arise due to two factors: (1) density, ρ , and (11) effective atomic number, Z . Since the density of water (ρ = 1 gm/cc) is nearly the same as that of plastic scintillator (ρ = 1.032 gm/cc), the calculated difference in $\delta(\beta)$ is mainly due to the difference in their Z values. The polarization effect in a medium of higher Z is comparatively less, and so the corresponding energy loss is higher. This means that the correction factor $\delta(\beta)$ in a medium of higher Z is smaller than that in a medium of low Z .

The effective Z of water is 7.23, whereas that of plastic is 3.5. So the density correction factor $\delta(\beta)$ in water is small compared with that in a plastic scintillator.

2.6 d Difference between the Fermi and Sternheimer Density Corrections.

Let us write the Fermi's density correction (equation 2.13) $\Delta(\beta)$ for $\beta > \frac{1}{\sqrt{K}}$ as

$$\Delta(\beta) = A \frac{\delta}{\beta^2}$$

so, $$\delta = \ln \frac{K-1}{1-\beta^2} + \frac{1-K\beta^2}{K-1},$$

where $$K = 1 + \frac{ne^2}{\pi m \nu_0^2}$$

Substituting this relationship in the correction factor, and using the fact that the plasma frequency

$$\nu_p = \left(\frac{ne^2}{\pi m}\right)^{\frac{1}{2}} \quad \text{gives}$$

$$(K-1) = \left(\frac{h\nu_p}{h\nu_0}\right)^2 \quad \text{one gets,}$$

$$\delta = \ln(K-1) + \ln\left(\frac{1}{1-\beta^2}\right) - 1 \quad \text{for } \beta \approx 1.$$

$$= \ln\left(\frac{h\nu_p}{h\nu_0}\right)^2 + \ln\left(\frac{P}{\beta \cdot MC}\right)^2 - 1$$

$$= \ln\left(\frac{h\nu_p}{h\nu_0}\right)^2 + \ln\frac{1}{\beta^2} + 2\ln\frac{P}{MC} - 1$$

$$= -2\ln\left(\frac{h\nu_0}{h\nu_p}\right) - 1 + 2\ln\frac{P}{MC}$$

$$= 4.606\,x + C_1, \quad \text{where } C_1 = -\left(2\ln\frac{I(z)}{h\nu_p} + 1\right)$$

This is identical with the expression given by Sternheimer for $X > X_1$. Since $X_1 = 2$ for both the

phosphor and water, for a muon of momentum greater than 10.57 Gev/C there should be no difference between Fermi's and Sternheimer's calculations. The curves B and C in the fig 2.4 justify this.

2.7 Radiative Corrections:

New interests in the study of the energy loss by relativistic particles have been aroused by the recent works of Tsytovich (1962, 1963) who made radiative corrections to the energy losses by ionization as well as by Cerenkov radiation. Tystovich finds that at very high energy, the energy loss is reduced, by 7 to 10% on Fermi Plateau, by higher order corrections in the fine structure constant α . He has shown that the collisions which are most affected are those in which small energy transfers are involved i.e. the so-called resonant collisions. Physically, these corrections to the basic theory result from the multiple virtual emissions of the photons by the incident particle. Tsytovich emphasizes that the interaction of the virtual photons with the material magnifies the effect greatly for extremely high particle energy and high density of the material (Fano 1963). Very recently, however, Fowler and Hall (1965) have made a critical study of the various classical and

semi classical theories of energy loss of relativistic charged particles mainly to clarify the ambiguity arising out of Tsytovich's works. They predicted, on the basis of their perturbation theory calculations, a logarithmic increase in ionization similar to that predicted by Sternheimer (1953). Further they showed that the higher order corrections i.e. the radiative corrections arise from the successive acts of Cerenkov quantum emission. This can only affect the observed ionization loss if one accepts the view that the latter arises from Cerenkov conversion, which is open to question. Fowler and Hall, further, pointed out that the sign of the correction would be opposite for positive and negatively charged particles. Thus measurement on Cosmic rays muons without charge separation would fail to detect this type of correction. They concluded that the approximations made in deriving the theoretical expressions introduced errors of the same order (5%) of magnitude as the higher order corrections. That is to say, a small reduction (radiative correction) in the energy loss can be regarded as well - established, provided the predictions of the theory without corrections be known accurately.

Zhdanov et al.(1963) and Alekseeva et al.(1963), studied the ionization loss of electrons in nuclear emulsion. They supported Tsytovich prediction of the reduction in the ionization loss for $\gamma \gg 100\text{-}200$. But recently Bushkirk (1964) and Kushwala (1965) who also worked with electrons of γ = 100 to 5000 in nuclear emulsions, did not find any significant evidence for the existence of the effect. Ashton et al.(1965) and Crispin & Hayman (1964) studied the energy loss of Cosmic ray muons of relativistic energies in scintillators. They also could not find any decrease in energy loss due to radiative corrections. Further, Crispin observed no significant difference (at least less than 1%) between the ionization loss of negative and positive muons.

Thus the problem of the radiative corrections is yet to be resolved and calls for further intensive study.

CHAPTER 3.

CERENKOV RADIATION LOSS.

3.1 Introduction.

In the year 1934, Cerenkov, while studying the luminescence of solutions of Uranyl salts bombarded with gamma rays, discovered that a very weak radiation was visible even from pure solutions (i.e. solutions having none of the usual properties of fluorescing materials). Moreover, the radiation appeared to be localised in a cone about the direction of the gamma radiation. It may be mentioned here that Mallet (1926, 1928, 1929) was the first to study the phenomenon. But unfortunately he did not attempt to offer an explanation for the origin of the radiation. Cerenkov's results were first interpreted by Frank and Tamm (1937) on the basis of classical electromagnetic theory. Hence forward the phenomenon came to be known as 'Cerenkov Radiation'.

3.2 Physical Nature of Cerenkov Radiation.

When a fast charged particle traverses a dielectric medium at constant velocity, the associated electromagnetic pulse temporarily polarizes the dielectric medium in the vicinity of the track. Each atom of the medium thus polarized radiates an electromagnetic wave. The resulting

electromagnetic wave, in general, is cancelled by destructive interference in all directions if $\beta n < 1$ (where β is the velocity of the particle in the units of the velocity of light c and n is the refractive index of the dielectric medium). However, if $\beta n > 1$, i.e. if the velocity of the particle is greater than the phase velocity of light ($\frac{c}{n}$) in the medium, there will be one direction Φ in which constructive interference takes place.

The effect may be better explained with reference to the Huygens construction shown in fig. 3.1. If the particle moves from A to B in the same time interval Δt during which light travels from A to C, or A to E, the wavelets originating from the different points on the track AB will be coherent, and they will reinforce each other to form a plane wavefront BC or BE. From the condition of coherence, one gets

$$\text{Sin } \phi = \text{Cos } \theta = \frac{C\ \Delta t}{n} \cdot \frac{1}{\beta c \cdot \Delta t} = \frac{1}{\beta n} \quad .. \quad 3.1$$

Thus the resulting Cerenkov radiation is emitted on a conical surface CBE of half angle ϕ .

Beside the condition set in equation 3.1, there are two more conditions to be satisfied for getting coherence;

(1) the path length l of the particle in the medium shall be large compared with the wavelength λ of the radiation in question, otherwise due to diffraction effects light will be distributed over an angle $\delta\theta \simeq \lambda / l \sin \theta$,

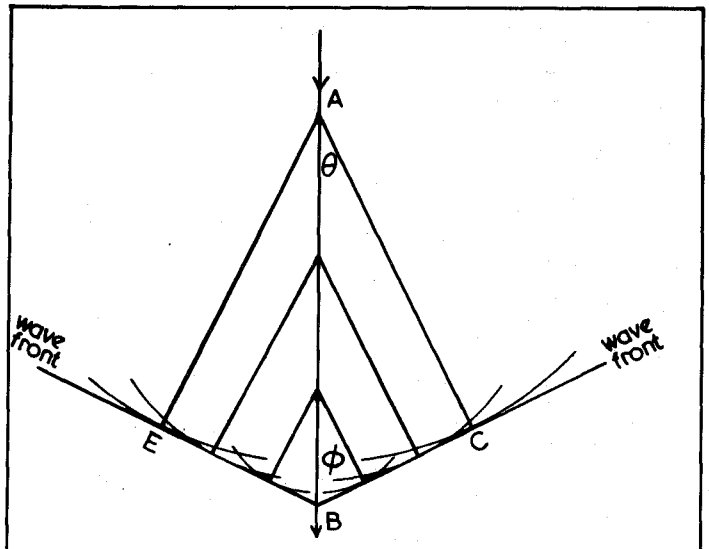

FIG 3·1 HUYGENS CONSTRUCTIONS FOR PARTICLES EMITTING CERENKOV RADIATION.

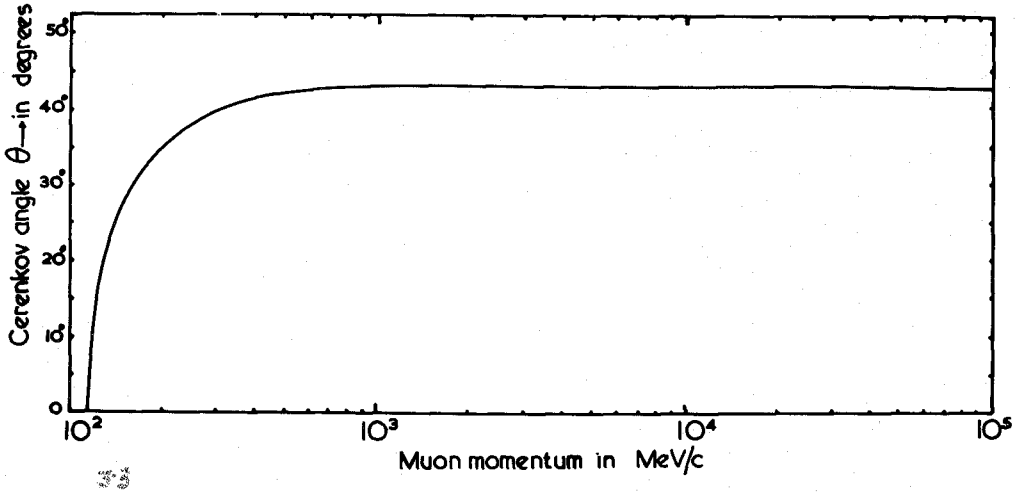

FIG 3·4 ANGLE OF EMISSION OF CERENKOV RADIATION IN WATER, (n·1·368)

instead of appearing at only one angle (Jelley 1953);

(2) the velocity of the particle must be constant during its passage through the medium.

From the relation 3.1 it is easy to see that no radiation is emitted if $\beta n < 1$, as mentioned earlier. The condition $\beta n \geq 1$ for this emission of Cerenkov radiation sets a threshold energy limit (corresponding to a minimum value of β) which varies with the mass of the particle. The following table shows the threshold energies for electrons, muons and the protons in air and in water.

Table 3.A.

Particle	Threshold energy in Air n = 1.00029	Threshold energy in Water n = 1.33
Electron	21 MeV	260 KeV
Muon	4.4 Gev	54 MeV
Proton	39 GeV	475 MeV.

At the threshold energy, the radiation is parallel to the direction of the particle.

3.3 Theories of Cerenkov Radiation Loss:

Fermi (1940) first pointed out that the Cerenkov radiation originates in small energy transfers from fast charged particles to distant atoms, which is subsequently emitted as a coherent radiation. Thus, Cerenkov radiation is a

particular form of energy loss in very soft collisions, and not an added amount of energy loss.

The problem of the emission of Cerenkov radiation has been studied theoretically by several workers by the methods of classical electrodynamics as well as quantum mechanics. It is interesting to note that the basic theory of Frank and Tamm (1937) based on the classical electromagnetic theory still remains valid and can explain the phenomenon rather satisfactorily, as has been shown by later, more refined, calculations. An excellent account of the various theories has been given by Jelley (1958). We shall first discuss the Frank and Tamm theory.

3.3 A. The Classical Theory of Frank and Tamm.

Frank and Tamm (1937) showed from classical theory that "an electron moving in a medium radiates light, even if it is moving uniformly, provided that its velocity is greater than the velocity of light in the medium".

They considered only the macroscopic structure of the medium by treating the latter as a continuous non-dispersive isotropic dielectric. Using Maxwell's electromagnetic equations, they showed the total energy radiated by an electron of charge e, moving through a medium at a constant velocity V to be equal to

$$\frac{dW}{dx} = \frac{e^2}{c^2} \int_{\beta n} \left(1 - \frac{1}{\beta^2 n^2}\right) w \, dw \quad \text{ergs/cm} \quad .. \; 3.2$$

where n is the refractive index and w is the frequency of the molecular oscillators of the medium.

The integration is to be carried out over all frequencies for which $\beta n > 1$.

By generalising the above equation for a particle of charge Ze, the energy loss per unit path is

$$\frac{dW}{dx} = \frac{Z^2 e^2}{c^2} \int_{\beta n > 1} \left(1 - \frac{1}{\beta^2 n^2}\right) w \, dw \quad \text{ergs/cm} \quad .. \quad 3.3$$

Thus it is seen that, the Cerenkov loss, like ionization, varies as the square of the particle charge Z.

3.3 A (i) <u>Magnitude of the Cerenkov Loss:-</u>

A comparison of the Cerenkov effect with other sources of energy losses by a charged particle traversing matter can be easily made with the help of the equation 3.2, as shown below.

The approximate value of the refractive index n may be written as (Sommerfield, 1954)

$$\left.\begin{aligned} n^2(w) &= 1 + \frac{A}{W_o^2 - W^2} \\ n^2(0) &= K = 1 + \frac{A}{W_o^2} \end{aligned}\right\} \quad .. \; .. \; . \; 3.4$$

where K is the dielectric constant, A is another constant, and w_o is some average molecular frequency of the medium.

Substituting equation 3.4 in equation 3.2 one obtains the approximate expression for the Cerenkov radiation loss per unit path for a fast electron ($\beta \simeq 1$).

$$\frac{dW}{dx} = \frac{e^2 Wo^2}{2c^2} \left(K - 1 \right) \ln \frac{K}{K-1} \quad .. \quad .. \quad 3.5$$

In a typical medium, Wo = 6 x 10^{15}/sec, so that $\frac{dW}{dx}$ is of the order of several KeV per cm or $\simeq$ 0.1% of the energy loss by ionization for a relativistic particle.

3.3 A (ii) Spectral Distribution of the Cerenkov Radiation.

The spectral distribution of the Cerenkov radiation can be deduced from the equation 3.3 as follows:

If ν is the frequency of an individual photon, then

$$W = Nh\nu \quad ,$$

where N = total number of photons of frequency

and h = Planck's constant

and, $w = 2\pi\nu$.

We get from the equation 3.3, assuming the refractive index n as constant over the visible region of the spectrum,

$$\frac{dW}{dx} = \frac{Z^2 e^2}{c^2}\left(1 - \frac{1}{\beta^2 n^2}\right) w\, dw \quad \text{ergs/cm} \quad \ldots \quad 3.3$$

$$= \frac{4\pi^2 Z^2 e^2}{c^2}\left(1 - \frac{1}{\beta^2 n^2}\right) \nu\, d\nu \quad \text{ergs/cm} \quad 3.6$$

$$= \frac{4\pi^2 Z^2 e^2}{}\left(1 - \frac{1}{\beta^2 n^2}\right) \frac{d\lambda}{\lambda^3} \quad \text{ergs/cm} \quad 3.7$$

and,

$$\frac{dN}{dx} = \frac{2\pi Z^2 \alpha}{}\left(1 - \frac{1}{\beta^2 n^2}\right) \frac{d\lambda}{\lambda^2}$$

photons/ cm. 3.8

where α = fine structure constant

$$= \frac{e^2}{\hbar c} = \frac{1}{137}$$

For a muon, the number of photons per unit cm path within a spectral region defined by the wavelengths λ_1, and λ_2, is equal to

$$\frac{dN}{dx} = \frac{2\pi\alpha}{}\left(1 - \frac{1}{\beta^2 n^2}\right)\left(\frac{1}{\lambda^2} - \frac{1}{\lambda_1}\right) \text{ photons/cm} \quad 3.9$$

From the equation 3.7 above, it is obvious that the Cerenkov radiation is concentrated at the violet end of the spectrum.

3.3 B Extension to the Basic Theory.

In 1939, Tamm alone made a rigorous analysis of the

whole problem. He investigated the effects of slowing down of the particle by ionization and other processes. However, the final expression obtained for the radiation loss is identical with the equation 3.2.

The problem of the emission of Cerenkov radiation has also been studied theoretically by Fermi (1940), Schiff (1940) and others.

In Fermi's calculations on the polarisation effect, as has been mentioned earlier, the Cerenkov radiation appears as a contribution to the total energy loss of a particle traversing a condensed material and forms part of the energy loss calculated by the Bohr theory of ionization. (see equation 2.16).

A.Bohr (1948), Messel and Ritson (1950) and Schoenberg (1951) have shown that for a medium with no absorption and described by a single type of dispersion oscillator, the relativistic rise of the ionization loss should escape as Cerenkov radiation. This result is, however, in disagreement with the observed rise in ionization loss in crystals (Whitemore and Street, 1949) and in emulsion experiments (Bowen and Roser, 1952).

Developing Fermi's theory on the basis of his multi-frequency dispersion oscillators, Sternheimer (1952) has shown that energy escape as Cerenkov radiation is small (less than 0.01 Mev gm^{-1} cm^2) both for macroscopic crystals

and for emulsion. Further in the visible region, where the absorption is negligible, Sternheimer's expression for Cerenkov radiation loss is in agreement with the result of Frank and Tamm, for a single dispersion oscillator. Moreover, Sternheimer has shown that the Cerenkov radiation loss reaches a saturation value in the region $\frac{P}{MC} > \nu_i \, f_i^{-\frac{1}{2}}$ where f_i is the oscillator strength for the i^{th} transition whose frequency is ν_i. In emulsion, the asymptotic value is around $\frac{P}{MC} \simeq 20$. Sternheimer has also pointed out that "Cerenkov loss decreases somewhat with increasing Z, atomic number of the material".

The Cerenkov radiation loss in relation to the ionization loss has also been extensively investigated by Budini (1953) and Fowler and Jones (1953) as has been mentioned in Chapter 2. Budini has suggested that the whole of the increase of energy loss beyond the minimum should appear as Cerenkov radiation only in the case of a perfectly transparent, hence physically impossible, medium. His theory, although on the lines of the Fermi's theory, is mainly based on the correlation between the breadth of the spectroscopic lines of the absorber and the structure of the Cerenkov bands. Budini has obtained the following expression for the Cerenkov radiation loss in an idealized dispersive medium with no absorption:

$$\frac{dW}{dx} = \frac{e^2}{c^2} \int \left\{ 1 - \frac{Re(\ K(w)\ )}{\beta^2\ |K(w)|^2} \right\} w\ dw \qquad 3.10$$

where Re(K(w)) is the real part of the frequency dependent dielectric constant K (w) of the medium.

K (w) is given by

$$K(w) = 1 + \alpha \sum \frac{f_i}{w_i^2 - w^2 - i\, g_i\, w}$$

where $\alpha = \frac{4\pi Ne^2}{m}$ (N is the number of electrons per c.c , and e and m are the charge and mass of the electron respectively), while w_i and f_i are the frequency and oscillator strengths of the i^{th} resonance, and g_i the corresponding damping coefficient responsible for the absorption. The equation 3.10 reduces to the Frank and Tamm expression 3.2, when $g_i = o$. The integration in 3.10 is carried out over all frequencies for which the condition $Re(\ K(w)\ ) > \frac{1}{\beta^2}$ is satisfied.

But in practice, no real medium is free from absorption so that $g_i \neq 0$. The dielectric constant at the peak of a given resonance is

$$Re\ (\ K(w_i)\ ) \simeq 1 + \tfrac{1}{2} \left(\frac{4\pi\ Ne^2 f_i}{m\ g_i\ w_i} \right)$$

and the threshold for radiation in this band is then

$$(\beta E)^2 = \left(\frac{\beta^2}{1-\beta^2} \right) > 2 \left(\frac{m\ g_i\ w_i}{4\pi Ne^2\ f_i} \right)$$

The total output of radiation, covering resonance regions with damping, and observable at a radial distance r from the track of the particle, is then:

$$\frac{dW}{dx} = \frac{e^2}{c^2} \int \exp\left\{ -\frac{w}{V}\beta^2 \; r \; \mathrm{Im}\, K(W) \right\}$$

$$\left\{ 1 - \frac{\mathrm{Re}\,[K(w)]}{\beta^2 \, |K(w)|^2} \right\} w \, dw \qquad \ldots \qquad \ldots \qquad 3.11$$

where V is the particle velocity.

The first factor in the integrand contains the absorption, showing that radiation of a given frequency will only be seen, at a distance r , if the condition

$$\left\{ \frac{w}{V} \beta^2 r. \qquad \mathrm{Im}\, K(w) \right\} \ll 1 \quad \text{is satisfied.}$$

Budini concludes that for dense media with narrow spectroscopic lines, there should be a simultaneous relativistic increase of Cerenkov radiation along with a relativistic increase of ionization loss. Such an effect has been reported by Bassi et al. (1952).

3.3 C <u>Quantum Treatment of the Cerenkov Effect:-</u>

In the classical theory of Frank and Tamm, the velocity of the particle has been assumed as constant during the emission of the Cerenkov light. Thus, no account has been taken of the reaction of the emitted quanta on the traversing particle. Ginsburg (1940) first considered, on the

basis of the quantum theory, the possible recoil, experienced by the particle, due to the emitted photon. Quantum treatments haye also been made by Sokolov (1940), Beck (1948), Schiff (1949) and Tidman (1956). Since the energies of the radiated quanta are small compared with the Kinetic energy of the particle, the modifications introduced by such (quantum) treatment are naturally expected to be small. The expression for the radiation condition and the energy loss obtained on the basis of the quantum theory differ slightly from those obtained in the classical theory, as can be seen from the following expression for the radiation output from a particle of charge e, and without a magnetic moment, deduced by Ginsburg (1940a).

$$\frac{dW}{dx} = \frac{e^2}{c^2} \int \left[1 - \frac{1}{\beta^2 n^2 (w)} \left\{ 1 + \frac{n^4}{4} \left(\frac{\hbar w}{mc^2} \right)^2 + n^2 \left(\frac{\hbar w}{mc^2} \right) \right\} \right] w \, dw \qquad .. \quad .. \quad 3.12$$

the symbols carry their usual significance. This equation 3.12 differs from the classical one (equation 3.2) only by the presence of two small terms of higher order.

Ginsburg also considered the possible effect on Cerenkov radiation emission from a particle having both electric and magnetic moment. He showed that at very high energies there would be no magnetic radiation.

3.3 C (i) Effects of Spin on the Cerenkov Loss.

Sokolov and Loskutov (1957) (see Jelley 1958) have shown that the radiation yield, the threshold condition and the polarisation of the emitted Cerenkov radiation are slightly modified for a particle with a spin.

For a particle of half-integral spin, there is an additional contribution for the quantum spin effect. And the expression for the total radiation yield takes the form:

$$W = \frac{e^2}{c^2} \int_0^{W_{max}} \left(1 - \frac{1}{\beta^2 n^2} \right) w \, dw + \frac{e^2}{c^2} \int_0^{W_{max}} \frac{n^2 w^2 \hbar^2}{4 c^2 p^2} \left(1 - \frac{1}{n^2} \right) w \, dw \qquad .. \quad .. \quad 3.13$$

The symbols have their usual meaning.
The first term in this equation 3.13 is due to the particle of zero spin and the corresponding radiation is linearly polarized in the plane containing the photon and the particle, whereas the second term is due to the spin effect, and the radiation is orthogonal i.e. the E - vector tangential to the Cerenkov cone.

Thus from the above equation 3.13, it is seen that if $\hbar \longrightarrow 0$ (classical approximation), the radiation, as for a particle with zero spin, becomes completely linearly

polarized.

Spin effect has also been studied by Ginsburg (1942 and 1943).

3.3 D. Radiative Corrections to the Cerenkov Loss.

Recently Tsytovich (1963) has made radiative corrections to the basic theories of Frank and Tamm (1937) and of Fermi (1940), by taking into account the second order perturbations. On the basis of his theory, he had predicted a reduction in the intensity of Cerenkov loss for particles of ultra relativistic energies. An estimate for the magnitude of the corrections has been given below:

The relative corrections, neglecting the spatial dispersion, can be written in the form:

$$\frac{W - W_o}{W_o} = - \frac{e^2}{\pi \hbar c} \Delta^t \qquad .. \qquad .. \quad 3.14$$

where Wo is the Cerenkov loss in the first approximation of the theory, Δ^t is the transverse part of the radiative corrections.

For ultra relativistic velocities, Tsytovich gives, in the case of a single dispersion oscillator,

$$\Delta^t = 2 \ln^2 \frac{E}{MC^2} + 2\left(\ln \frac{2E}{MC^2} - 1 \right) \left(\ln \frac{M^2 C^4}{E^2 \psi_o^2} - 1 \right) + 0.1696$$

$$\text{for } \frac{E}{MC^2} << \frac{1}{|\psi_o|} \qquad .. \quad 3.15$$

and $$\Delta^{t} = \frac{7}{2} - \frac{\pi^2}{6} + \frac{1}{2} \ln^2 \frac{1}{2.72\Psi_0^2}$$

$$\text{for } \frac{E}{MC^2} >> \frac{1}{|\Psi_0|} \quad .. \quad .. \quad .. \quad .. \quad 3.16$$

Where E is the total energy of the muon of mass M, and Ψ_0 is a function of the total concentration N of the electrons of the medium and of all natural frequencies W_s, and is given by (Zhdanov et al. 1963).

$$\Psi_0 = \frac{e^2}{\hbar C} \frac{Wo}{\langle Ws \rangle} \ln \frac{C}{\langle V \rangle} \quad .. \quad .. \quad 3.17$$

In this equation, $\langle Ws \rangle$ is the effective natural frequency of the atomic electrons, $\langle V \rangle$ is their mean velocity, and Wo is 2π times the plasma frequency.

Since in the study of Cerenkov loss, we are chiefly concerned with small energy transfers, we calculate the radiative corrections in a limiting case for which the energy transfer is less than the ionization potential (= 67.5 eV) in water.

First we estimate Ψ_0 as follows:

The $\frac{C}{\langle V \rangle}$ is calculated assuming that the electrons of the atoms move in simple orbits according to Bohr's theory in which the velocity V of an electron moving in a n^{th} orbit around a nucleus of charge Ze is $V = \frac{Ze^2}{n\hbar}$

$$\frac{V}{C} = \frac{Ze^2}{n\hbar C} = \frac{Z}{137\, n} \quad \text{where } \frac{e^2}{\hbar c} = \alpha = \frac{1}{137}$$

$$n = 1, 2, 3 \text{ etc.}$$

Thus,

(1) $\frac{V}{C}$ for an electron (2) in a Hydrogen atom $= \frac{1}{137}$

(11) $\frac{V}{C}$ for an inner electron (2) in an Oxygen atom $= \frac{8}{137}$

(111) $\frac{V}{C}$ for an outer electron (6) in an Oxygen atom $= \frac{4}{137}$

Therefore the mean $\langle \frac{V}{C} \rangle = \frac{1}{137 \times 10} (2 + 8 \times 2 + 4 \times 6) = \frac{4.2}{137}$

$\langle W_s \rangle = 2 \pi \nu_s = \frac{2 \pi I}{h}$ where I = ionization potential = 67.5 eV.

The plasma frequency $\nu_p = \sqrt{\frac{Nc^2}{\pi m}} = 4.95 \times 10^{15}/\text{sec}$

$$\therefore \frac{W_o}{\langle W_s \rangle} = \frac{2 \pi \nu_p}{2 \pi \nu_s} = \frac{h \nu_p}{I} = \frac{20.47}{67.5}$$

$$\therefore \quad \psi_o = 7.718 \times 10^{-3}$$

Therefore the limiting value of $E/MC^2 = \frac{1}{\psi_o} = 0.1296 \times 10^3$

Thus for muons of energy E $\ll$ 13.67 GeV, equations 3.15 and for E $\gg$ 13.67 GeV, equations 3.16 should be used in computing the relative corrections. But, according to Tsytovich, the radiative corrections are only appreciable for particles of energy $\rangle$ 10 GeV. The magnitude of the

correction in water for muons of energy $>$ 10 Gev is found to be 3.8%. Since the limiting energies are not known precisely, it is not possible to give the expected shape of the curve or the point where the reduction begins. However, in fig 3.2 C, the variations of the absolute number of Cerenkov photons, after applying radiative correction above 10 Gev, are shown. If Tsytovich's effect is real, it is expected to be detected over the energy range 10 - 100 GeV.

3.4 Theoretical calculations on

(A) the rate of Cerenkov Loss in water,

and (b) the variations of the angle of emission, θ, with muon momentum.

3.4 A <u>The Rate of Cerenkov Loss in Water</u>.

A theoretical estimate on the number of Cerenkov photons emitted by a fast muon over a spectral band $\lambda_2 \rightarrow \lambda_1$, on its passage through water can be made using equation 3.9:

$$\frac{dN}{dx} = \frac{2\pi\alpha}{} \left(1 - \frac{1}{\beta^2 n^2}\right) \left(\frac{1}{\lambda_2} - \frac{1}{\lambda_1}\right) \text{ photons/cm.}$$

$$= F(\beta, n) \left(\frac{2\pi\alpha}{} \left(\frac{1}{\lambda_2} - \frac{1}{\lambda_1}\right)\right) \text{ photons/cm.}$$

where $F(\beta, n) = \left(1 - \frac{1}{\beta^2 n^2}\right)$

Considering the transmission characteristic of the water used and the absorption spectra of the wavelength shifter Popop, it will be shown in chapter 6 that the useful wavelength range in this experiment is from 2500 to 4000 A.U. and the corresponding average refractive index over this spectral range is n = 1.368. The threshold momentum for the Cerenkov emission = 103 MeV/C when n = 1.388.

Using the above value of the refractive index n, the function $F(\beta, n)$ which gives the relative number of photons in water has been plotted against the momentum of the muon Fig. 3.2.

The absolute number of photons can be obtained by multiplying $F(\beta, n)$ by the term $\left(\frac{2\pi\alpha}{} \left(\frac{1}{\lambda_2} - \frac{1}{\lambda_1} \right) \right)$ and has been shown in the fig 3.2 B. It is seen from the fig 3.2 B that starting from the threshold momentum, the number of photons emitted per cm increases very rapidly, and then becomes constant (= 320 photons/cm) at about 10 Gev/C.

It may be pointed out here that in calculating the absolute number of photons, the velocity β for a particular incident energy has been assumed constant. In other words, the change in energy of the incident muon is assumed to be small. But for a thick detector and especially near the threshold energy region the change in the energy of the incident muon due to ionization loss should

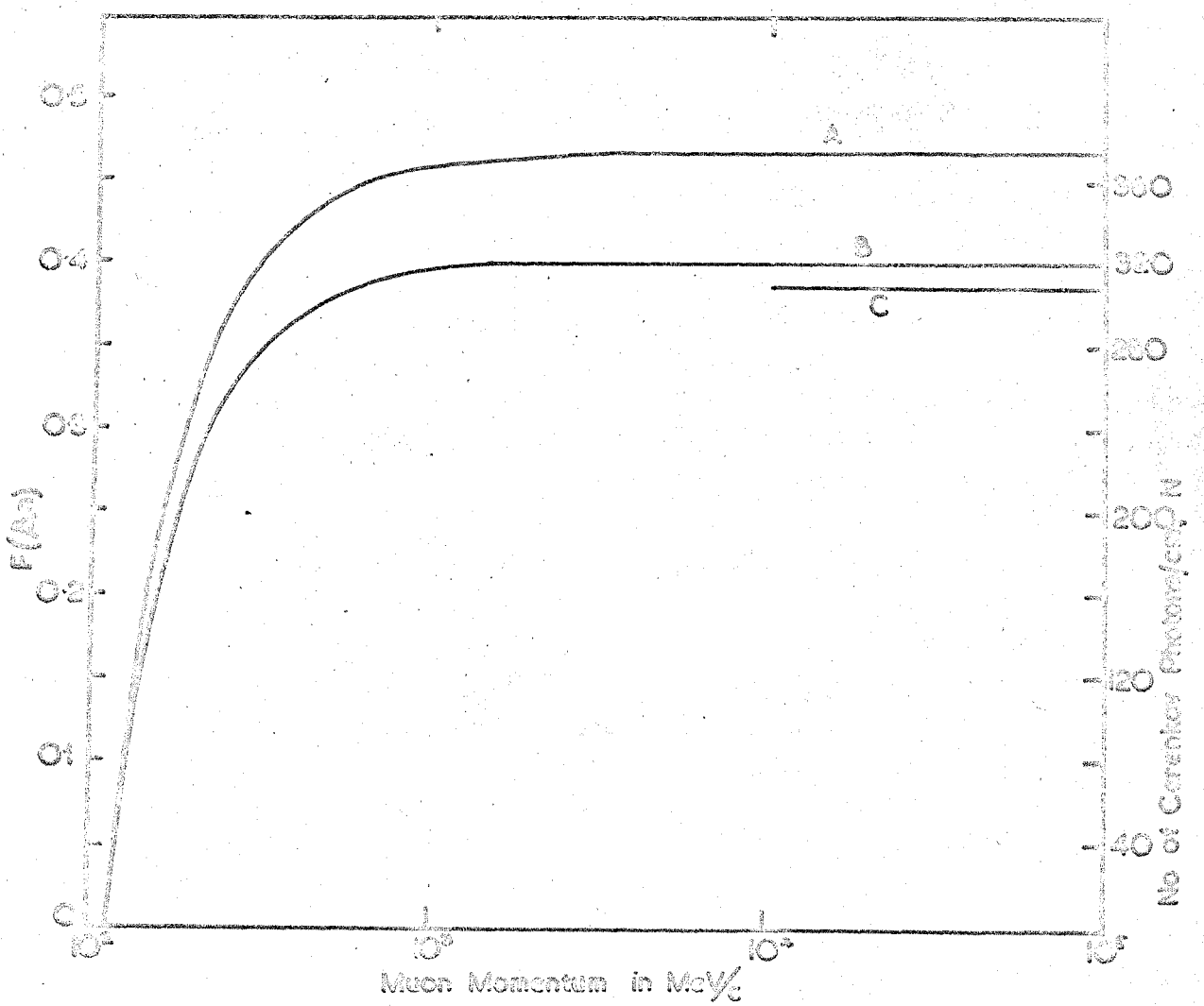

FIG 22. A. Relative rate of quanta emission according to Frank & Tamm's theory
B. Variations of the absolute number of Cerenkov photons with muon momentum in water over the spectral band 2500 to 4[illegible] AU & n = 1.333.
C. Taylovich correction to 'B'

be taken into account. Since in the present experiment, the energy range is $\gg$threshold, and the radiator is also comparatively thin, the change in β due to ionization loss in the radiator will be neglected.

3.4 B Variations of the Angle of Emission with Muon Momentum:-

It is seen from the equation 3.1 that the angle of emission of Cerenkov radiation which is given by

$$\theta = \cos^{-1} \frac{1}{\beta n}$$

depends on β , the velocity i.e. the momentum of the muon.

In the fig 3.3, the variation of θ with the muon momentum has been shown. Starting from the zero value at the threshold , it goes on increasing and attains a maximum value = 43° at about 10 GeV/C.

3.5 Contribution of the Knock-On Electrons:-

When a fast muon passes through water, it will produce δ - rays (i.e. electrons produced with energies between a few KeV and a few hundreds of KeV) as well as energetic knock-on electrons. δ-rays and knock-on electrons will emit Cerenkov photons, if they have energies greater than the threshold energy (260 KeV). Considering the threshold

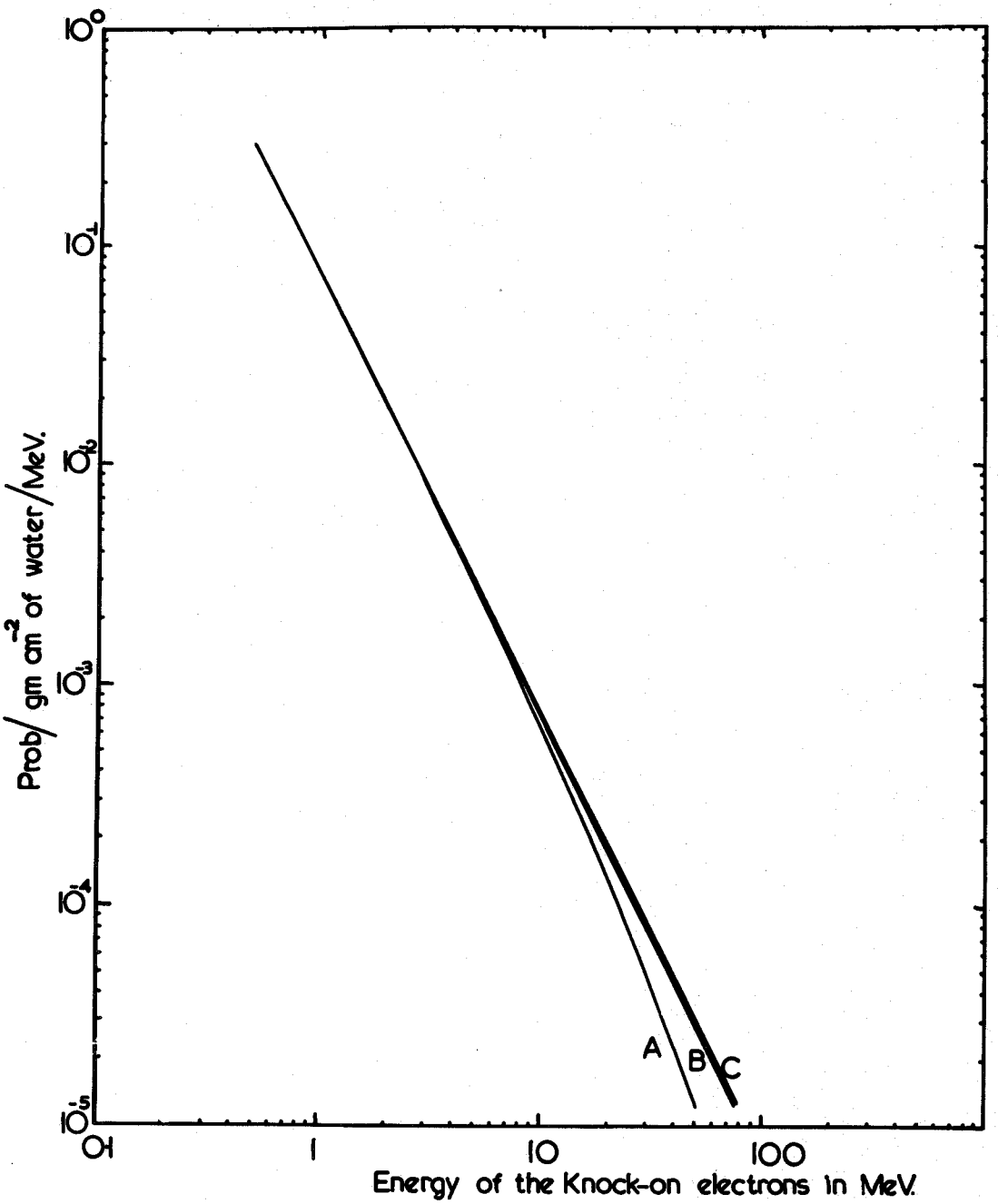

FIG 3·4 PROBABILITY OF KNOCK ON ELECTRONS IN WATER DUE TO
A: 1 GeV/c muon
B: 10 GeV/c muon
C: 100 GeV/c muon

energy as well as the energy loss in water, it may reasonably be assumed that the δ-rays will contribute very little to the total production of Cerenkov radiation. The main contribution will be from the knock-on electrons. The calculation is given below.

It may be shown in fig 3.4 that the probability of the production of low energy knock-on electrons by relativistic muons in water is nearly the same for muons of all energies greater than 1 GeV. Further, it is seen from fig 3.4 that the probability of emission of high energy knock-on electrons is very small.

In fig 3.5, the variation of the angle of emission of the knock-on electrons as a function of the energy of the knock-on has been shown. From this, it is seen that all the knock-on electrons (with energy greater than 8 MeV) are ejected within a cone of semi-vertical angle 20° with the direction of motion of the muon. Consequently the contributions from such energetic muons will be quite appreciable.

The differential cross-section per electron for the production of a knock-on electron with energy limits E^1 and $(E^1 + dE^1)$ by a primary muon of spin $\frac{1}{2}$ and kinetic energy E is given by Bhabha (1938)as

$$\sigma(E, E^1)\, dE^1 = \frac{2\pi r_e^2 mc^2}{\beta^2} \left\{ \left(1 - \beta^2 \frac{E^1}{E_{max}} \right) + \frac{1}{2} \left(\frac{E^1}{E_{max} + MC^2} \right)^2 \right\} \left(\frac{dE^1}{E^1} \right)^2 \quad . \quad 3.18$$

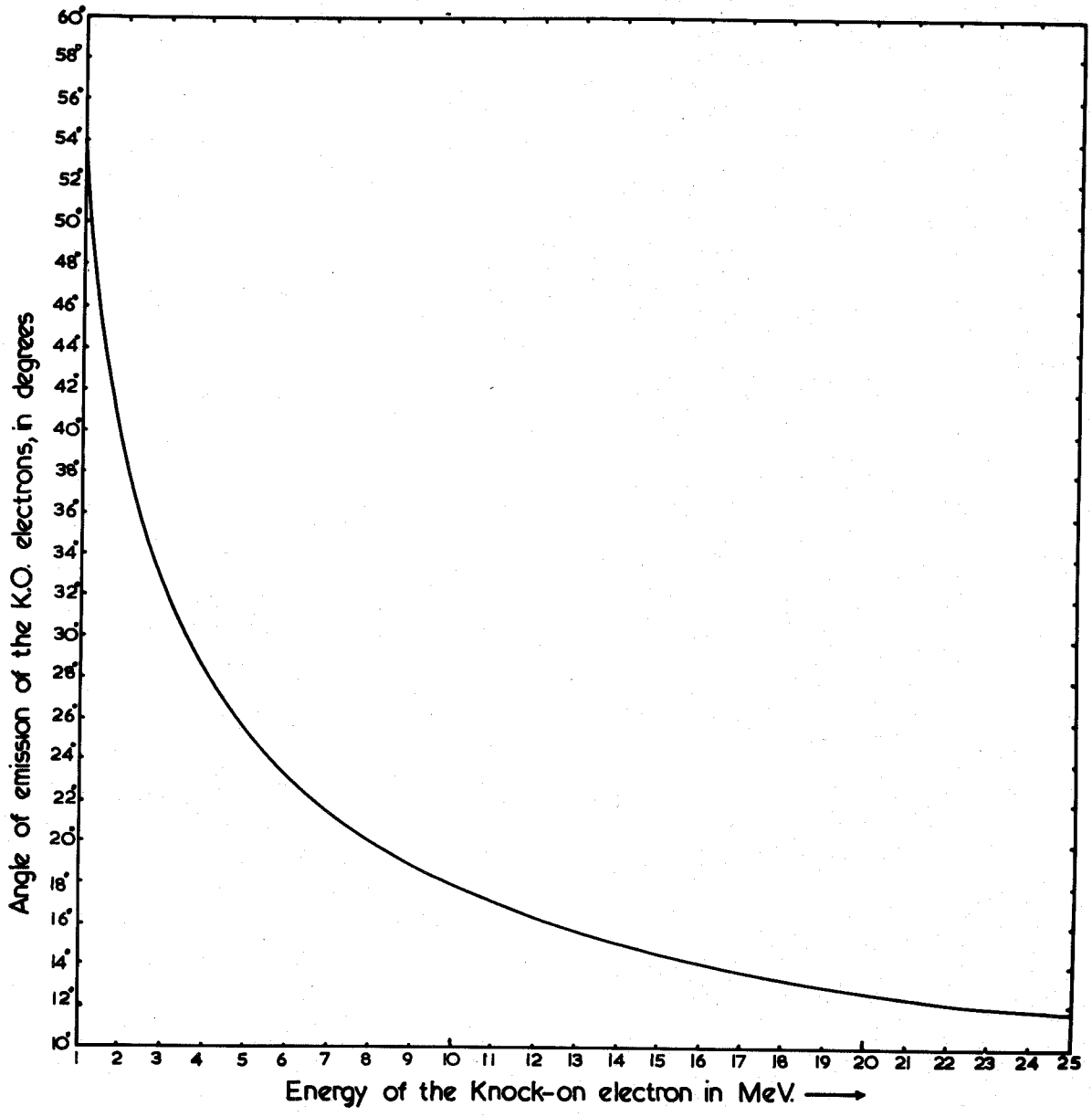

FIG 3·5 ANGLE OF EMISSION OF THE K.O. ELECTRONS AS A FUNCTION OF THE ENERGY OF THE K.O. ELECTRONS.

where the symbols have their usual significance.

So the number of knock-on electrons produced with energy E^1 within dE^1 in 1 cm of water is

$$N_\delta = \left(\frac{NZ}{A}\right) \sigma(E, E^1)\, dE^1 \quad \ldots\ldots\ldots\ldots\ldots\ldots\ldots\ldots 3.19$$

$$= 0.0775 \left\{1 - \frac{E^1}{E_m}\right) \frac{dE^1}{\left(E^1\right)^2} \quad \text{for} \quad \beta \simeq 1$$

$$\text{where} \quad E_m \equiv \frac{E^2}{E + 11.1} \text{ Gev.}$$

In the following table (table 3.B.), the number of knock-on electrons produced by a 10 GeV/C muon in water is given.

TABLE 3B

(1) K.O. electron energy interval	(2) Mean in MeV	(3) Mean Range Re in cm.	(4) N_δ/cm	(5) N_δ Re.10^{-2}	(6) N photons per cm	(7) No= Total No. of Cerenkov photons	(8) Corr. factor f	(9) No. f
2 - 4	3	1.5	0.0837	5.81	314	18.24	0.50	9.12
4 - 8	6	3.1	0.0193	5.98	318	19.02	0.60	11.41
8 - 16	12	6.4	0.0097	6.20	320	19.84	0.79	15.67
16 - 32	24	12.9	0.00484	6.24	320	19.99	0.90	17.94
32 - 64	48	25.9	0.00242	6.27	320	20.06	0.95	19.06
64 - 100	82	44.5	0.00068	3.02	320	9.66	0.95	9.18
100 - 200	150	81.3	10^{-5}	-	-	-	-	-
200	-	-	-	-	-	-	-	-

In the column (3) of the above table, the electron ranges have been calculated by using the following range energy relation,

$$Re = 0.543\ E_{max} - 0.160 \quad \text{(Wilkinson, 1950)}$$

where E_{max} is the electron energy in MeV, and Re is measured in gm/cm^2. The above relation is almost independent of the material of the absorber when the latter is light. In the column (6), the number of Cerenkov photons emitted by a knock-on electron has been computed using equation 3.9 over the spectral band 2500 to 4000 A.U, in water. Column (7) shows the number of Cerenkov photons, No., per cm from the different energy interval. But this has to be corrected for the possible Coulomb scattering. The contributions from the low energy knock-on electrons ($E^1 < 5$ MeV) will be reduced very much due to the multiple Coulomb scattering of the electrons in water. Assuming an isotropic distribution of these low energy knock-on electrons, only about 50% of them may be expected to move in the forward direction contributing Cerenkov photons at the detector level. On the other hand, the knock-on electrons of energy ≥ 5 MeV will initially be emitted within a forward cone of semi-vertical angle $< 25^{\circ}$ (fig 3.5) with the primary direction, and will also be scattered less. So it is reasonable to assume that the contribution from such energetic knock-on electrons will

not be affected very much. A correction factor f has been used to take into account the effect of scattering on the contribution from knock-on electrons. The following two empirical equations have been used in calculating f (column 8)

$$f = 0.5 \quad \text{for } E^1 < 5 \text{ MeV}$$

$$f = \frac{(E^1 - 5) + 5 \times 0.5}{E^1} \quad \text{when } E^1 \geq 5 \text{ MeV}$$

The total number of Cerenkov photons per cm contributed by knock-on electrons is thus $\sum$ Nof = 82.11. This can be compared with the number of Cerenkov photons/cm in water due to a relativistic muon, 320/cm. Therefore, the contribution from the knock-on electrons is 25.7%.

Thus there will be an increase in the total quanta produced of about 25.7%. This may affect the pulse height distribution in two ways: (a) by shifting the most probable energy loss to a higher value, and (b) by adding a tail to the high energy side of the distribution. The former will be caused by the photons from the knock-on electrons of energy $\leq$ 16 MeV, as $N\delta$ /cm $\simeq$ 0.01 for E $\lesssim$ 16 MeV. (See Column 4, table 3B). So in a path of 100 cm in water, such knock-on electrons will contribute everytime whenever a fast muon traverses the counter. The number of photons/cm, arising due to the knock-on electrons of energy $\lesssim$ 16 MeV, is $\sum$ Nof = 36. Therefore, this may increase the true most probable pulse-height by 36/320 $\simeq$ 11%.

Again, the depth of water in the counter is about 2.8 radiation lengths. So, whenever the energy of a knock-on electron is >> 83.8 MeV, the critical energy in water, it will produce showers. But the frequency of occurrence of such an energetic knock-on electron is small, as can be seen from fig 3.4. Consequently, the contribution from such occasional high energy knock-on electrons will give rise to the tail of the distribution.

3.6 Concluding Comments.

It is worthwhile to sum up the whole problem of energy loss at this point. So far, the theoretical predictions on the logarithmic rise in the energy loss is concerned, we are confronted with three different views:

(1) According to the Fermi theory, the whole of the increase of energy loss beyond the minimum should appear as Cerenkov loss which is saturated at high energies. This is quite in agreement with the classical theory of Frank and Tamm;

(11) Budini differs in that he predicts that the logarithmic rise in the energy loss curve is partly due to the increase in ionization and excitation loss, and partly due to the Cerenkov loss. Further he opines that there should

be a simultaneous relativistic increase of Cerenkov loss along with the relativistic increase of ionization loss;

(iii) On the other hand, Tsytovich, although he seems to support the basic theories of Fermi and of Frank and Tamm, predicts a reduction in the ionization as well as in the Cerenkov loss for particles at ultra relativistic velocities.

These differences in the theoretical predictions obviously demand more precise experimental results. But so far as the study of Cerenkov loss is concerned, the number of experiments performed so far is very few (see chapter 4). Further, only a couple of experiments (Bassi et al. 1952, and Millar and Hincks, 1957) have been carried on in the GeV range, the highest energy covered being less than 4.5 GeV. Moreover, the methods of momentum measurements in these experiments were not very precise.

Thus, a rigorous experiment to study the variation of Cerenkov intensity with momentum in the region 1 to 100 GeV, especially to test the recent prediction of Tsytovich, is felt very necessary. The present work is an attempt to carry out such an experiment by using a water Cerenkov counter and a new horizontal spectrograph for precise measurements of the momentum of the cosmic ray muons. In the actual experiment as will be described in the latter chapters, the electrical pulses due to Cerenkov photons will be studied

as a function of the particle momentum. In the fig. 3.2, the expected relative variation of the most probable pulse heights as a function of the muon momentum is shown. If the Cerenkov radiation loss follows the classical theory, the curve as shown in fig 3.2 will rise monotonically to a plateau value. But if Tsytovich theory holds good, the curve will fall off, instead of attaining a plateau value monotonically, by about 4% for particles of momenta P $>$ 10 GeV/c, and then will reach its asymptotic value.

CHAPTER 4.

Review of Previous Experiments on Energy Loss by (A) Ionization, and (B) Cerenkov Radiation:

4.A. Measurements on Ionization Loss.

The ionization loss of fast charged particles through matter has been studied in an extensive way, both theoretically and experimentally. Prior to the recent theory of Tsytovich (1962) about the reduction in energy loss due to radiative corrections, the experimental results were found to support the theoretical predictions quite satisfactorily. The main interest in all the experiments on ionization loss has centred more or less on the study of the logarithmic increase and the density effect. Since the latter is small in gases, the logarithmic rise in the energy loss is most easily observed. As such, we shall first discuss the measurements of ionization in gaseous detectors, such as (a) proportional counters and high pressure ionization chambers, and (b) cloud chambers. Next the experiments in dense media, namely, (c) nuclear emulsions, and (d) crystal counters and scintillators, will be discussed. Since the experiments performed are very large in number, we shall confine ourselves with only the most relevant and conclusive early work together with recent results.

4.A.(a) Experiments with Proportional Counters and High Pressure Ionization Chambers:

Quite a few experiments have been performed using these types of detectors. Experiments with relativistic muons all follow the same general pattern: one or more proportional counters are placed in the beam of a Geiger counter telescope, and the ionization produced is measured, the momentum of each particle passing through the system being determined either by its residual range or by deflection in a magnetic field. A typical arrangement used for this type of measurement is shown in fig 4.1. The value of the experimental results mainly depends on the precision of the momentum measurement. Using proportional counters, the ionization losses at high particle energies have been measured by Price et al. (1953), Parry et al. (1953), Yeliseyer et al. (1953), Eyeions et al. (1955), Kharitonov (1952), and Kharitonov and Barski (1953). West in 1953 showed that the observed width of the ionization distribution would be dependent on the product of the gas pressure and track lengths. It has been found experimentally that the observed width approaches to the Landau's theoretical value at high pressures. Some workers, eg. Palmatier et al. (1954) designed their counters to use higher pressures and longer track lengths. Lanou and Kraybill (1959) measured the

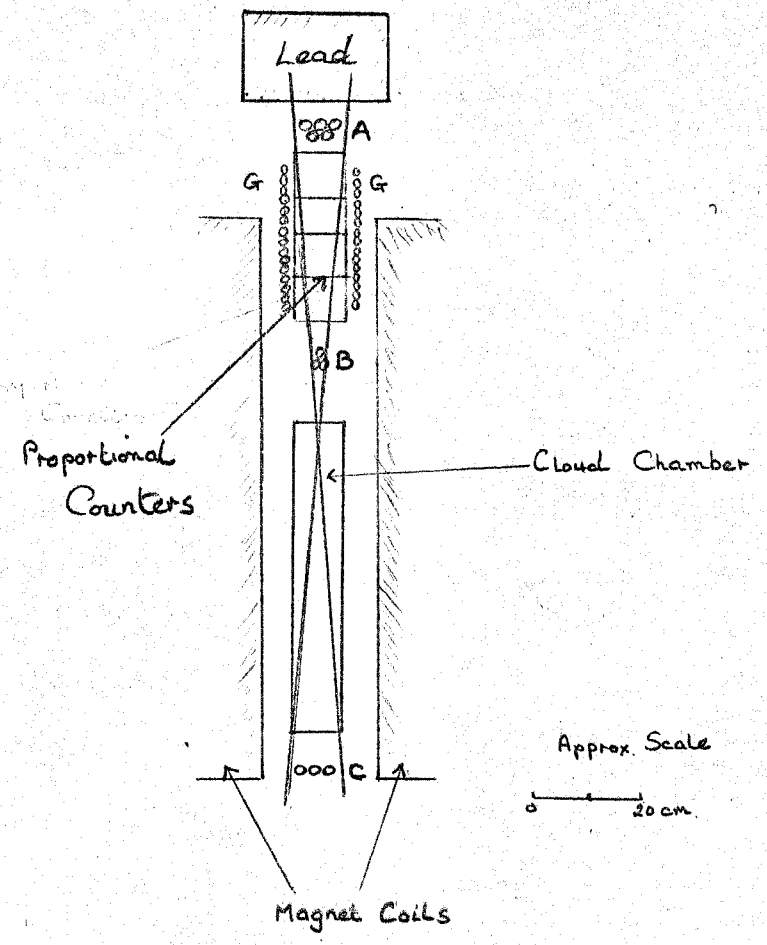

Fig. 4.1 Typical experimental arrangement used by Price et al. (1953) for the determination of the probable ionization of Cosmic Ray muons.

ionization loss of cosmic ray muons in helium gas with proportional counters. The momentum, in their experiment, was measured with a magnetic spectrograph which resolved particles in the momentum region from 3.3 GeV/c to 140 GeV/c. Their results were in good agreement with Sternheimer's theoretical values. Using proportional counters with neon-methane mixtures, Jones et al.(1963) studied the rate of energy loss of cosmic ray muons as a function of momentum over the range 0.3 - 30 GeV/c. They used Durham cosmic ray spectrograph (Brook et al. 1962) for the measurement of muon momentum. Their results, when normalized to the Landau theory at one momentum, were in good agreement with the theoretical values over the whole range.

All the results published so far show the expected relativistic increase of most probable energy loss with momentum. However, only three groups of workers, namely, Parry et al. (1953), Eyeions et al. (1955), and Lanou and Kraybill (1959) have reached the high energy plateau region.

4.A.(b) Experiments with Cloud Chambers:-

The ionization losses have been studied using cloud chambers by Sengupta (1940), Hazen (1944, 1945) and Hayward (1947). They verified the existence of the logarithmic rise for electrons, but their results on muons were inconclusive. Accurate experimental results on the relativistic

rise in ionization loss have been obtained by Ghosh, Jones and Wilson (1952, 1954), who used muons in a cloud chamber, and a high resolution magnetic spectrometer. Their measurements extended over a momentum range from 500 MeV/c to about 30 GeV/c and showed a relativistic rise which agreed with theory and also showed the existence of the density effect, but did not reach the plateau. Their results are shown in fig. 4.2, together with the theoretical curves of Budini and Sternheimer. Kepler et al. (1958) measured the ionization losses of relativistic muons and electrons to cover the energy range $\beta\gamma = 3$ (minimum ionization) to $\beta\gamma = 1000$, in helium, argon and xenon, with a cloud chamber. Their experimental results agreed well with the theory in the case of helium. In argon, and particularly in xenon, the observed relativistic rise was less than that predicted theoretically. In short, the relativistic rise in the gaseous detectors was found to be about 40 to 50%.

4.A. (c) Experiments with Nuclear Emulsions.

Experiments using nuclear emulsions have been many. Occhialini in 1949, and Corsen and Keck in 1950, working with electron tracks in emulsions established the existence of a plateau at high energies although they did not detect any variation of grain density for electrons from 7.5 to 500 MeV, and from 10 to 180 MeV, respectively. Since their investigations were confined to electrons, their measurements

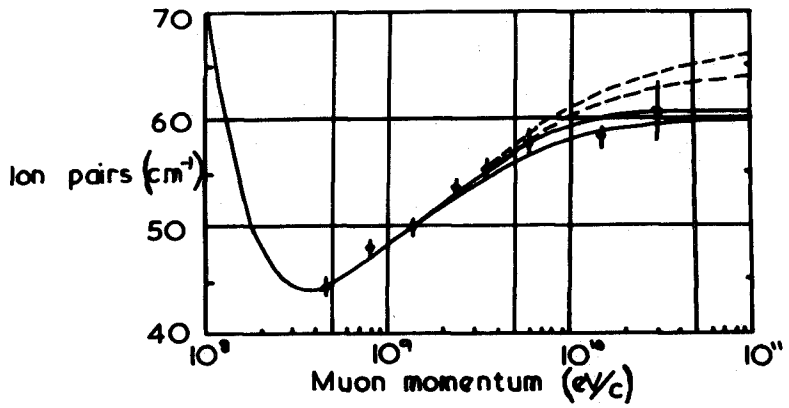

FIG. 4·2. The average specific ionization of muons in oxygen at S.T.P. arising from encounters of energy transfer less than 1 keV. (see text for details)

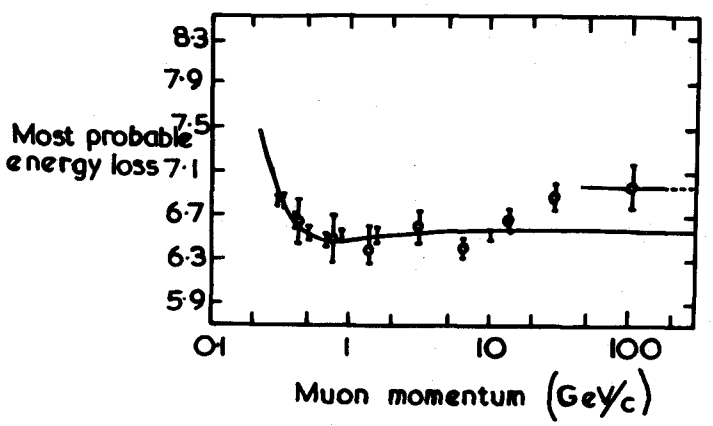

FIG. 4·5. The most probable energy loss due to ionization as a function of the muon momentum: (Crispin & Hayman)

— Theoretical curve (Sternheimer)
Barnaby (1961)
Crispin & Hayman (1964)

were not extended down to the minimum of ionization, and hence could not yield a value for the magnitude of the relativistic rise. However, Pickup and Voyvodic (1950) found a difference of about 10% between the plateau value of ionization for extreme relativistic particles and the minimum value. This rise in the energy loss has been substantiated by latter workers, namely, Daniels et al. (1952(, Stiller and Shapiro (1953), Michaelis and Violet (1953), Fleming et al. (1953), Jaunean and Tremberly (1953), Alexander and Johnston (1957), Jongejans (1960), Herz and Stiller (1964). The relativistic rise obtained by Herz and Stiller, and Michaelis & Violet was a little smaller than values commonly found i.e. in the range 10 - 14%. Prior to 1962, all the experimental evidence pointed to the existence of plateau up to the highest mementa measured.

In 1962, Tsytovich predicts, as has been mentioned in chapter 2, that in emulsion the ionization loss may not rise monotonically to a plateau value. It may instead decrease after γ = 100 to 200, and reach, at γ = 600 to 1000, an asymptotic value which is about 6 to 8% less than the earlier recognised plateau. The experimental investigations of Alekseyeva et al. (1962) and of Zhdanov et al. (1963, 1964) support Tsytovich's calculations. Unlike other workers using the emulsions, the above Russian results also exhibit a maximum in the region γ = 100. The results of Zhdanov

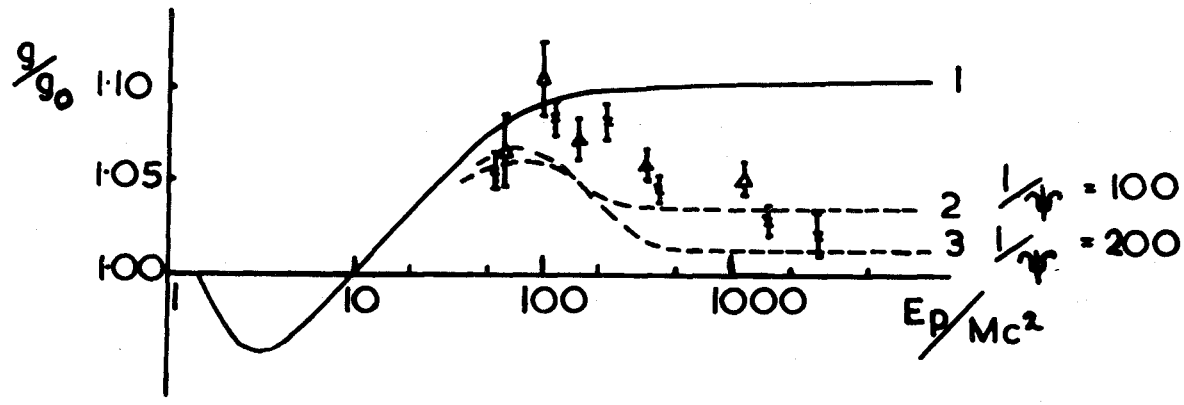

FIG. 4·3. Experimental results of Zhdanov et al., compared with the theory of Tsytovich.

△ Ilford G-5 emulsion.

× NIKFI–R emulsion.

Curves (1) Theoretical curve neglecting the radiative correction.

(2,3) Asymptotic theoretical curves taking radiative corrections into account.

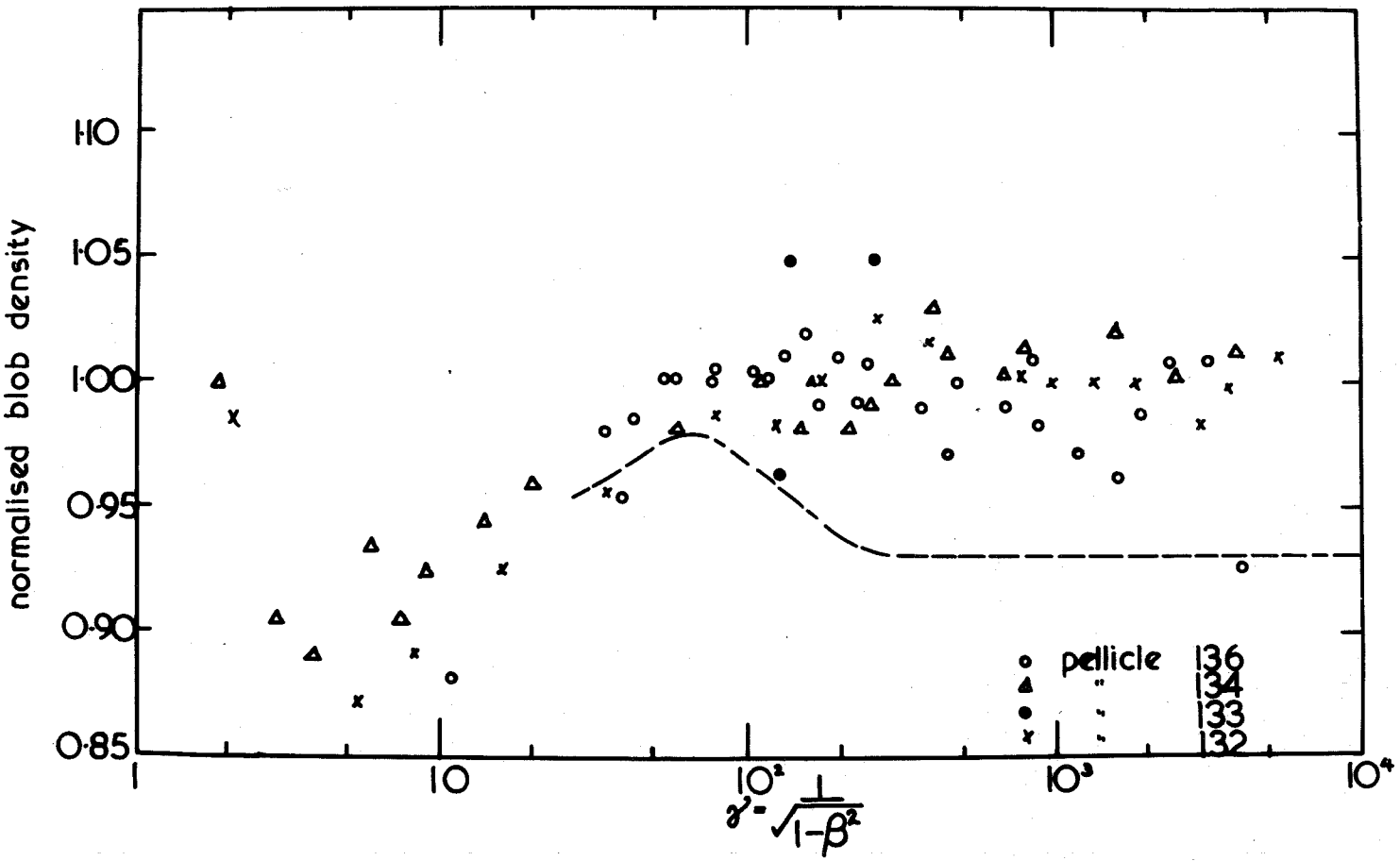

FIG. 4·4. Experimental results of Brushkirk et al. (1964). The dotted curve shows the theoretical prediction of Tsytovich.

et al. (1963) is shown in fig.4.3. However, more recent emulsion results of Bushkirk et al. (1964), of Herz and Stiller (1964), and of Kushwala (1965) working over the same energy range as the Russians, do not show any evidence for the existence of the Tsytovich effect. The experimental results of Bushkirk et al. (1964) along with the theoretical predictions of Tsytovich are shown in fig. 4.4. One other point as observed in emulsion may be mentioned here. It has been found that there is no significant difference (less than 1.5%) between the ionizing ability of the particles with different sign.

4.A. (d) Experiments with Crystal Counters and Scintillators:

Crystal counter in the measurement of ionization loss of a charged particle was first introduced by Whittemore and Street (1949) who used a silver chloride crystal in the energy loss measurement. They compared the light out-put from the ionization of muons of energy greater than 1.6 GeV with that from muons at the minimum ionization (0.3 GeV) and found a definite relativistic increase. Their results were quantitatively consistent with the predictions of the Halpern and Hall theory regarding the density corrections. But the method being effectively an integral one, is not a source of detailed information. Bowen and Roser (1952), using anthracene and cosmic ray muons, showed that for energies between 0.3 and 3 GeV, the rise in the most prob-

able energy loss was less than 2%. Bowen (1954), working with a sodium iodide crystal and cosmic ray muons, found that the relativistic increase was 10.9% for energies up to 5 GeV, but using a liquid scintillator over the same energy range as in his earlier experiment, he found that the relativistic increase did not exceed 2%. This agrees with previous results on similar organic materials (Baskin and Winckler (1953), Meshkovskii and Shebanov (1952)) and with theory (Sternheimer, 1952, 1956). Barnaby (1961), using a large area plastic scintillator (NE 102) and cosmic ray muons, found the relativistic rise in the most probable energy loss to be less than 1%, between 0.5 and 10 GeV. More recently Crispin and Hayman (1964), using the same type of phosphor NE 102, studied the ionization loss of cosmic ray muons. Since this group of workers used a magnetic spectrograph (Durham vertical cosmic ray spectograph), the momentum measurement in their experiment was obviously more precise than that of Barnaby. Their results shown in fig. 4.5 along with those of Barnaby, were compatible with Sternheimer's density correction to the ionization loss theory of Bethe-Bloch up to 10-15 GeV/c. But at higher momenta, the observed most probable energy loss was about 3% above the predicted rise. They did not find any reduction, due to Tystovich effect, in the energy loss at high energies. Further, separated analysis of their data for positive and negative

muon showed no difference of ionization loss greater than 1%. Very recently Ashton and Simpson (1965) have studied the ionization loss of the relativistic cosmic ray muons in liquid scintillator. Their results confirm the existence of the density effect to the highest momentum measured ($\simeq$ 200 GeV/c), but they also did not find, in their final result, any evidence for a decrease of energy loss at higher energies. The momentum, in this experiment, was measured with the Durham horizontal cosmic ray spectrograph.

Thus, so far as the energy loss in organic scintillator is concerned, although there is good general agreement between the theory and experiment there is still some uncertainty as to the magnitude of the rise, if any, in the energy loss beyond the minimum of the energy loss curve. Further, the Tsytovich effect has not yet been tested thoroughly. So one aspect of the present work is to study the ionization loss of cosmic ray muons in an organic scintillator (NE 102A) at relativistic energies.

4B Measurements on Cerenkov Radiation Loss.

The energy loss by Cerenkov radiation is usually studied by estimating the intensity of Cerenkov light emitted in a radiator (a transparent dielectric medium) by the passage of a charged particle through it. The Cerenkov light intensity is very low, so a highly sensitive detector is needed to make any meaningful study of it. In the early

stage of research, the Cerenkov light was recorded by means of the photographic method. But now-a-days, photomultiplier tubes which are extremely light sensitive, are invariably used. However, the normal procedure in this type of investigation is to compare either the observed absolute intensity of radiation, or the most probable pulse-height distribution as recorded with photmultiplier tubes, with the theoretically predicted values.

Depending on the source of the charged particles producing Cerenkov radiation, the experiments performed so far can be classified into the following 3 categories:

(a) Experiments using radio-active sources,

(b) Experiment using machine accelerated particles,

and (c) Experiment using cosmic ray particles.

(a) Experiments with radio-active sources:-

Most early experiments on Cerenkov radiation were done, using radio-active sources emitting β-and γ-rays. Normally, an estimate of the absolute yield of Cerenkov light per particle was made in order to compare it with the theoretical yield given by the classical theory of Frank and Tamm. Estimates of this kind were performed first by Cerenkov himself who studied the luminescence of strong β-source in benzene. A more systematic study of the variations of the intensity of Cerenkov radiation emitted by β- particles in water as a function of the energies of

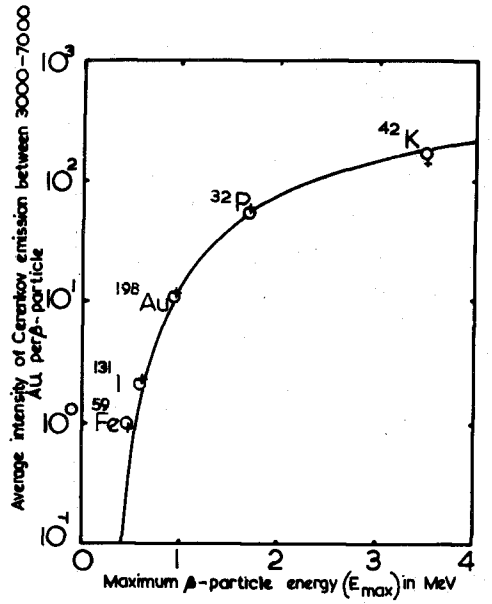

Fig 4·6 Results of Belcher's experiment. The continuous curve is constructed from the theory of Frank and Tamm. The isotopes used in this work are indicated beside the experimental points.

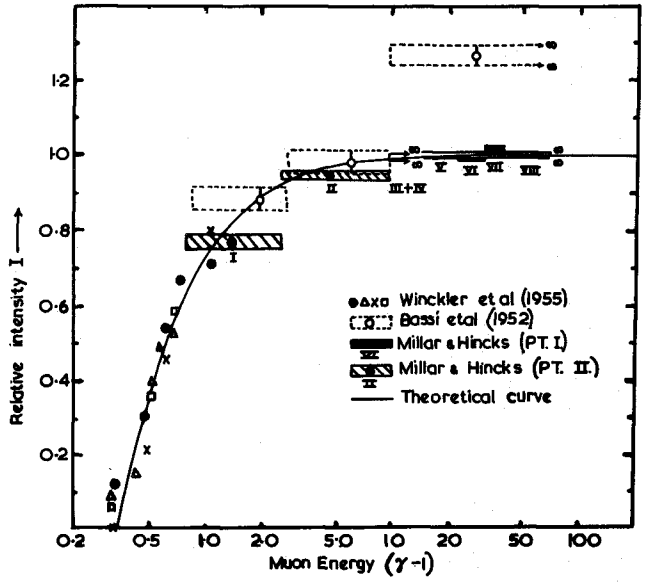

Fig 4·7 Comparision with theory of various experimental observations of relative Cerenkov light intensity as a function of muon energy. The results from different experiments have been independently normalized (Millar & Hincks, 1957)

the particles was made by Belcher (1953). He used various aqueous solutions of radio-active isotopes. His results shown in fig. 4.6 are in good agreement with the Frank and Tamm theory.

(b) Experiments with machine-accelerated particles:-

Collins and Reiling (1938) were the first to study the properties of Cerenkov radiation of machine-accelerated particles. Using a photographic recording system, they measured the absolute intensity of Cerenkov radiation emitted by a 10 μA beam of 2 MeV electrons from an electrostatic generator, in thin foils of mica, glass and cellophane. Their experimental results agreed to within a factor of 2 with that predicted by the Frank and Tamm theory.

Winkler et al. (1955) studied the intensity variations of Cerenkov light in lucite by using cyclotron accelerated π^+ and π^- mesons, up to a maximum energy of 168 MeV (π^-). Their experimental results (see fig. 4.7) indicated that the average pulse size from a photomultiplier coupled to a lucite Cerenkov radiator varies with energy in a manner very close to that predicted theoretically. They also made a search for any possible difference in Cerenkov response to positive and negative pions of same energy. They found that the effect, if any, was less than 3% and smaller than the magnetic effects on photomultipliers due to reversing the clyclotron.

(C.1) Experiments with Cosmic Rays:-

Ascoli-Balzanelli and Ascoli (1957) measured the absolute intensity of Cerenkov radiation due to cosmic ray muons in gas and vapours. In 1959, Caglioti et al., using a large area non-focusing Cerenkov counter also measured the absolute yield of Cerenkov light produced by cosmic ray muons in several transparent materials eg. water, lucite, heptane, and toluene. They found that the observed results were in good agreement with those predicted theoretically.

The first real attempt to study the variations of the Cerenkov intensity as a function of the energy of the cosmic ray muons was by Bassi et al. (1952). They used plexiglass as the radiator and the Cerenkov light was collected by photo-multiplier tubes. The momentum was measured with lead absorbers, using a Geiger telescope. They observed a relativistic rise above that predicted by the Frank and Tamm theory, as shown in fig. 4.7. Their results were, however, not inconsitent with the theoretical prediction of Budini (1953). But the statistics of the experiment were poor.

The possibility of the deviation of Cerenkov yield from the Frank and Tamm theory was latter investigated, rather more thoroughly, by Millar and Hincks (1957). They studied the most probable pulse height distribution due to Cerenkov light produced in plexiglass by cosmic ray muons. The muon energies were selected by lead absorbers in a scinti-

llator telescope. They did not, however, find any high energy anomaly in the intensity of Cerenkov radiation up to muon energies somewhat above 4.2 GeV (β = 0.99970C). In the low energy region (near threshold), the observed radiation was slightly less than the theoretically predicted values. But this departure was attributed by them to an optical effect in the apparatus rather than to a true deviation from the theory. They made a comparative study of their results with those of other workers as has been shown in fig. 4.7. They concluded that the theoretical Cerenkov intensity was valid to within a few per cent from the threshold up to a velocity β = 0.99970, well into the saturation region.

Thus, from the above discussion it is obvious that the number of experiments performed so far to investigate the variation of Cerenkov intensity as a function of the velocity of the particle is very few indeed. It is more so in the high energy region. The maximum energy covered so far is only about 4.2 GeV. No experiment has yet been performed to make a rigorous test of the contradictory theories of Budini and Tsytovich. An investigation of the variation of the Cerenkov light yield at higher energies will be very useful for this purpose. In the present experiment as has been mentioned in chapter 3, an attempt has been made to study the variation of Cerenkov intensity with the momentum of the cosmic ray muon in the GeV region. The

experimental details are given in the following two chapters.

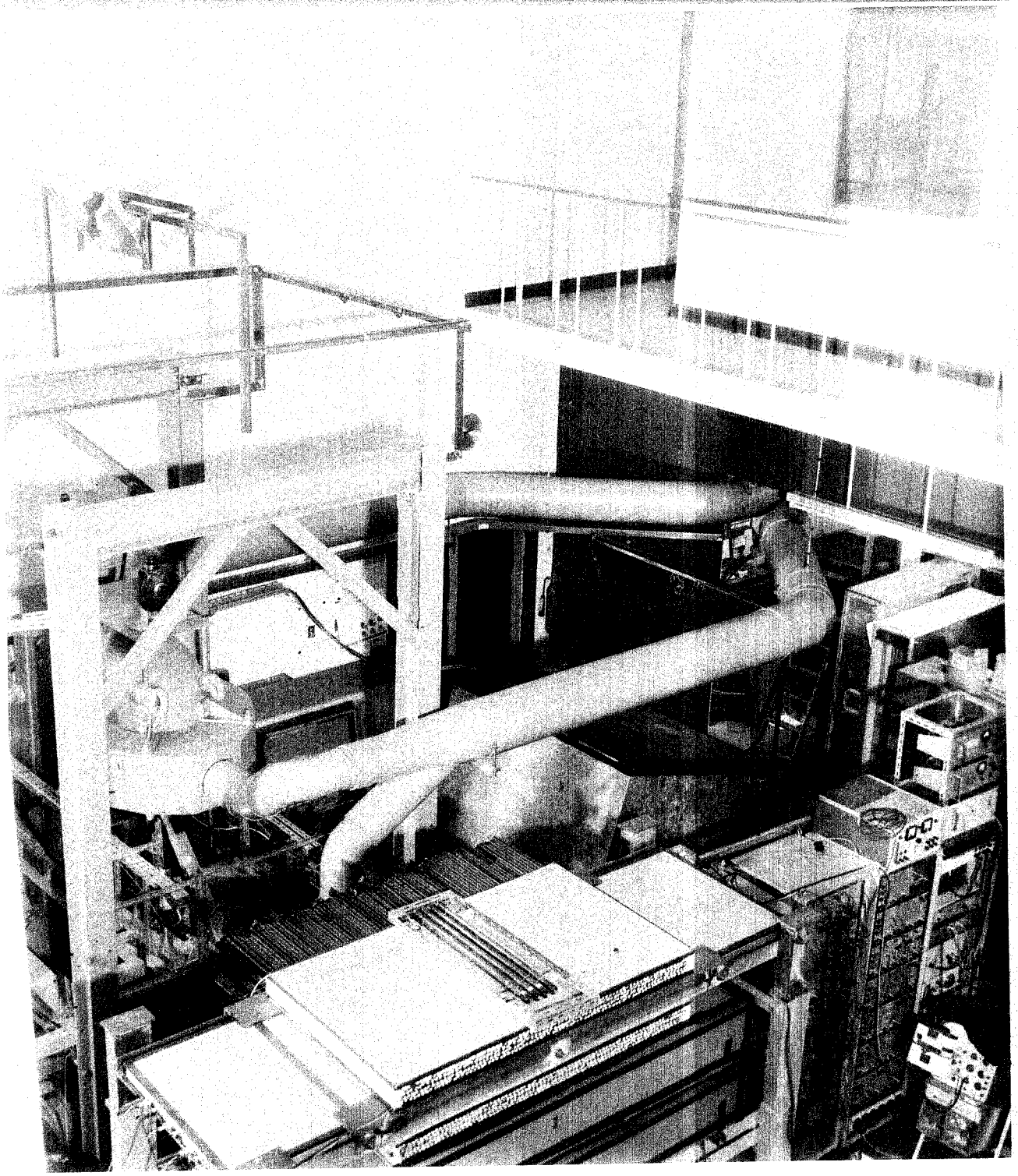

General view of a portion of the spectrograph(top)

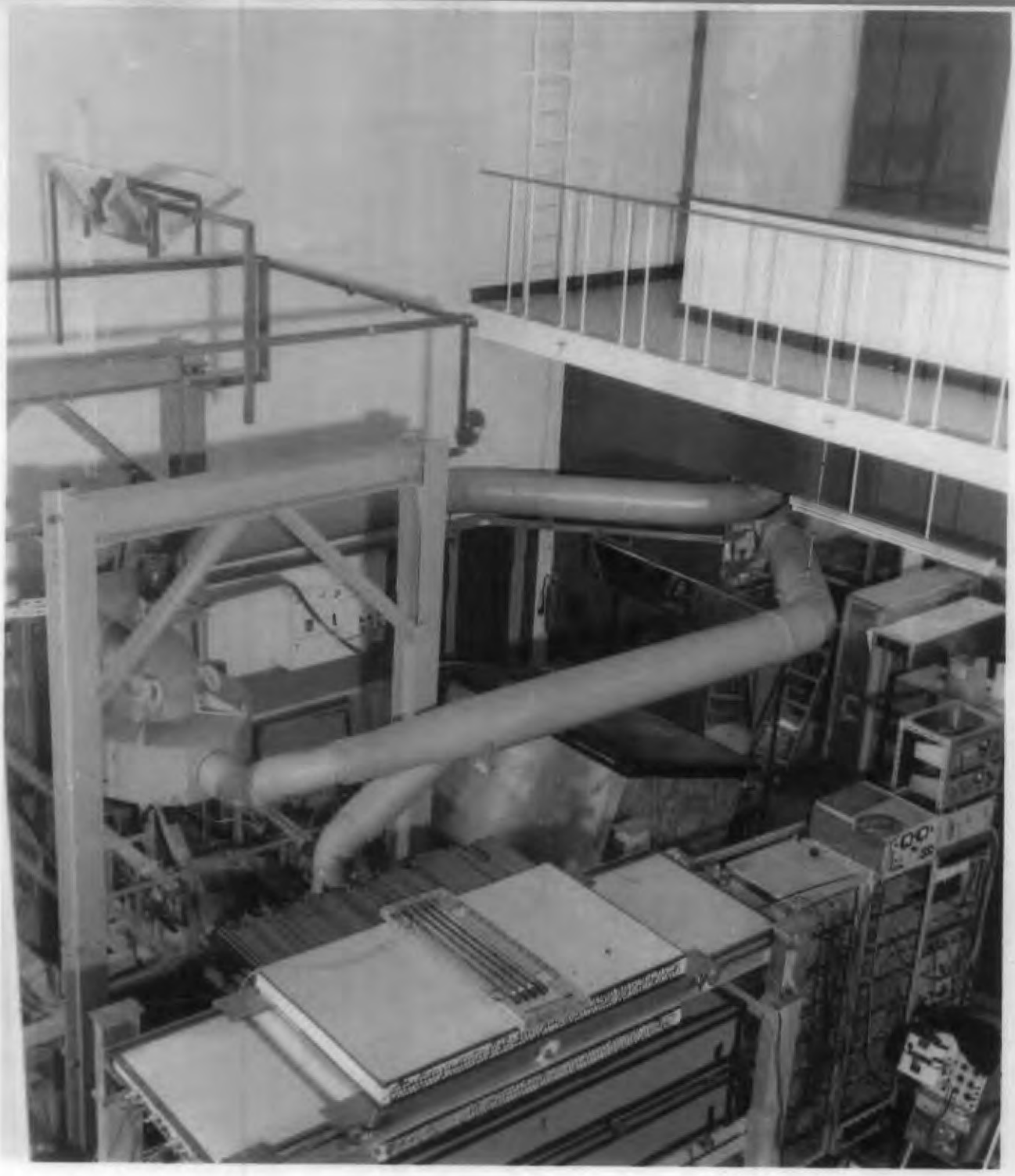

General view of a portion of the spectrograph(top)

CHAPTER 5.

THE SPECTROGRAPH:-

5.1 The General Features:-

A new horizontal magnetic spectrograph with the deflecting plane horizontal has been constructed for the measurement of particle momenta. A deflection plane view and a back plane view of the spectrograph are shown in figures 5.1 and 5.2, respectively. The spectrograph is positioned to select particles from a direction 27° East of geomagnetic North. The instrument consists of an air-cooled Blackett type electromagnet with plastic scintillation counters S1, S2, S3, S4, S5, S6 and S7. The counters S1 (or S7), S2, S3 and S4 are used to select particles which pass through the spectrograph. S5 and S6 are anticoincidence counters. A pulse from S1 (or S7), S2 and either S3 or S4, and no pulse from S5 and S6 would constitute an event that would trigger the spectrograph. There are four trays of neon flash tubes at levels A, B, C and D which determine the particle trajectories through the spectrograph.

5.2 a. The Electromagnet:-

The electromagnet of the present spectrograph is the one used in the original version of the Durham vertical spectro-

FIG. 5-1. DEFLECTION PLANE VIEW OF THE SPECTROGRAPH

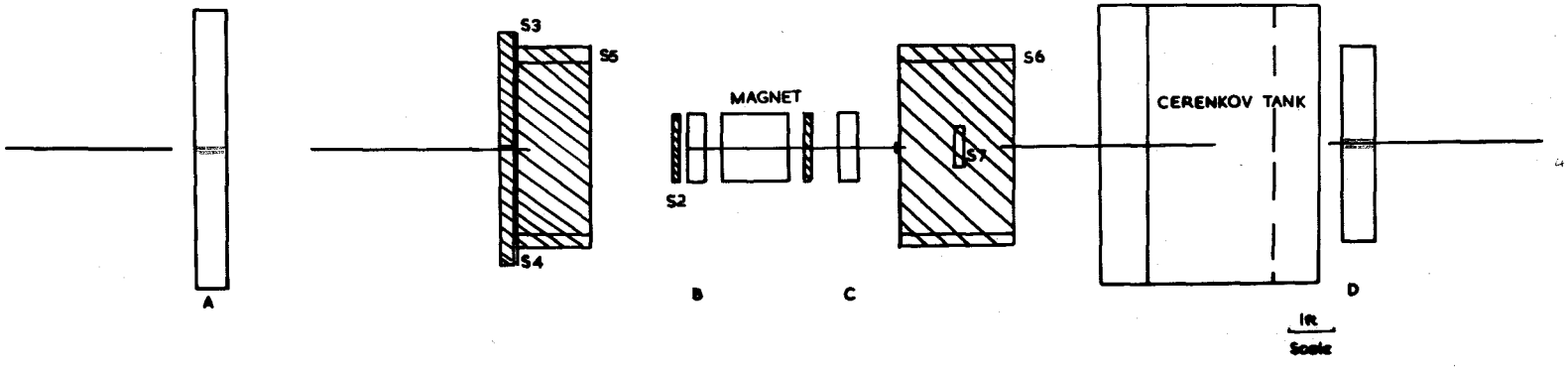

FIG.5·2. BACK PLANE VIEW OF THE SPECTROGRAPH

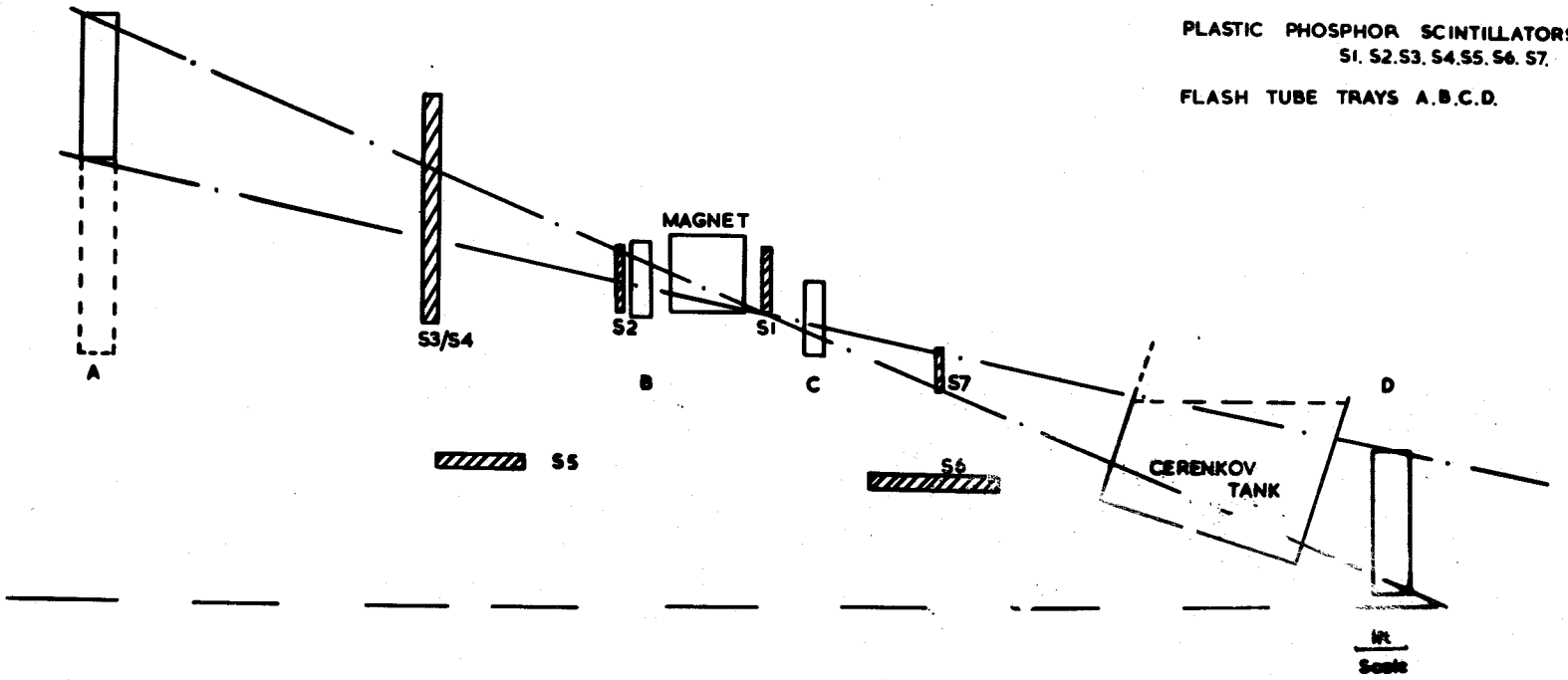

graph. At present, the electromagnet has an air-gap of 45 cm x 45 cm x 38 cm gap, the field being in the vertical direction.

5.2 b. Measurement of the Magnetic Field:-

The average magnetic induction B in the pole gap of the electromagnet was measured using a search coil of 100 turns and area 1.1 cm^2, rotating at a constant speed of 50 c/s. At first, the coil was calibrated with a Helmholtz type galvanometer by measuring the amplitudes of the wave-form induced on a C.R.O. In order to obtain a complete picture of the magnetic field between the pole pieces as well as outside it, the whole gap was divided into several regions, each 10 x 10 x 10 cm^3, as shown in figures 5.3 a and 5.3b. The rotating coil was placed at different levels. The pulses induced, at a mean excitation current of 41.0 amps. through the electromagnet were recorded on the C.R.O. The actual measurements are shown in fig. 5.3b. Again, in figures 5.4a and 5.4b, the lines of forces of the field in two central planes, the former (in fig. 5.4a) along the path of the particle, and the latter in the deflection plane, are shown. It can be seen from the above figures that the field is reasonably uniform between the pole pieces while it decreases very rapidly outside.

The maximum field strength in the pole gap at the

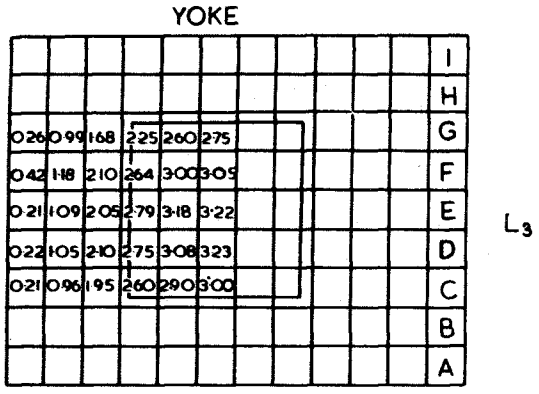

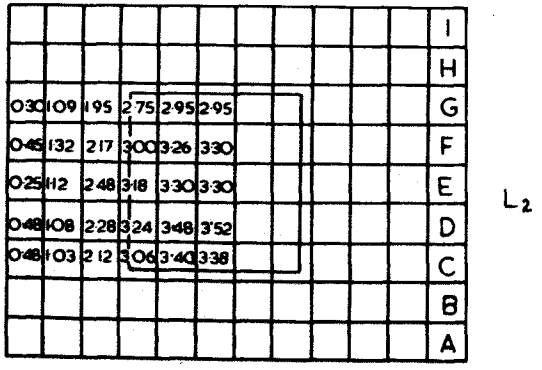

FIG. 5·3a Deflecting field in Kilo Gauss at levels L_1 L_2 & L_3.

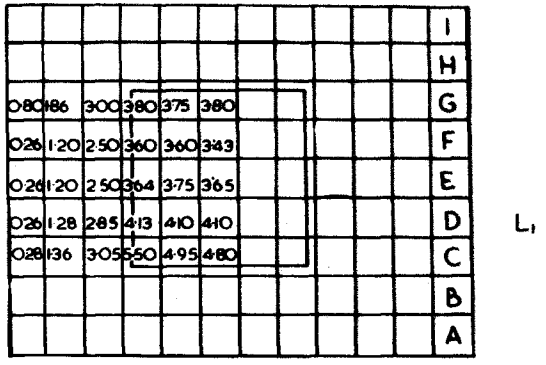

FIG. 5·3b Deflecting field in Kilo Gauss (horizontal section of the pole) at level L_1

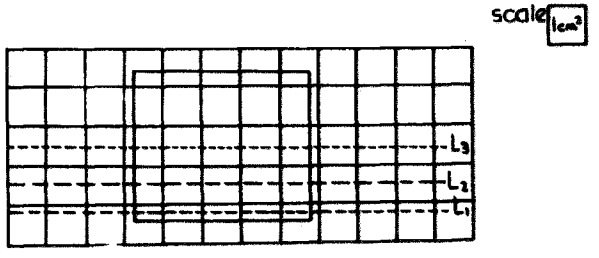

Vertical section of the pole showing levels L_1 L_2 & L_3.

FIG. 5·4a. Lines of force in the central plane along the trajectories of the particle.

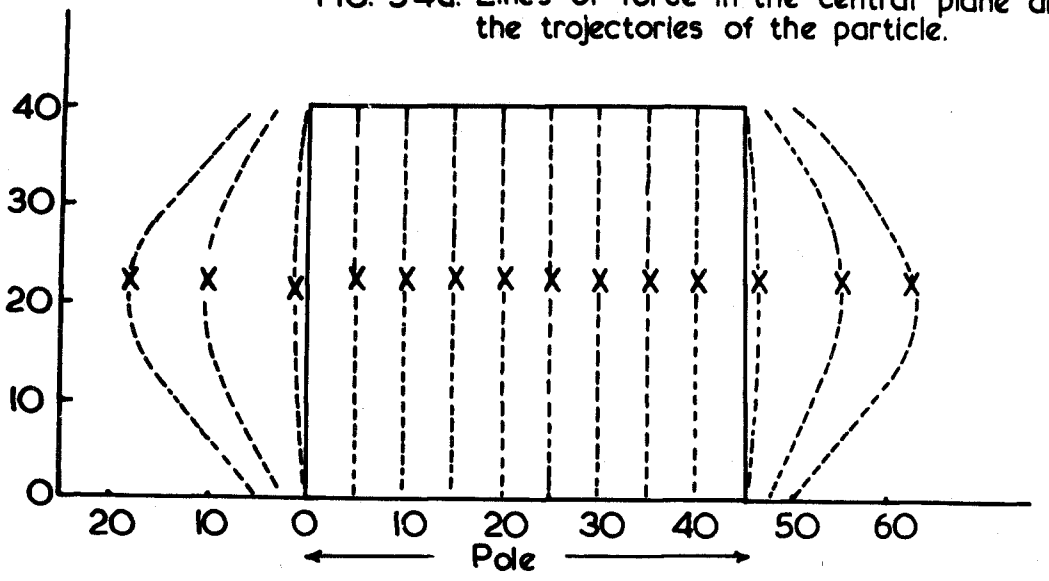

FIG. 5·4b. Lines of forces in the central deflection plane in the pole gap.

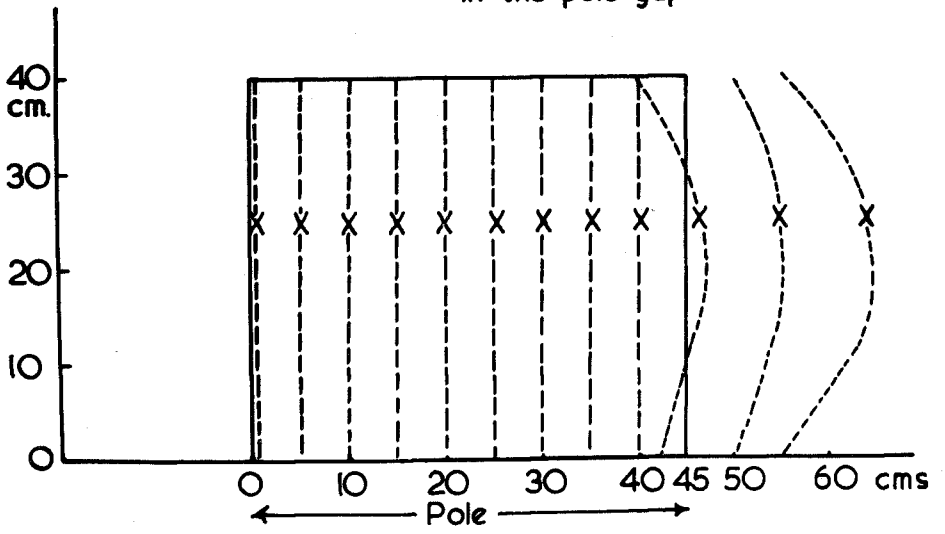

working mean current of 43.5 amps, 210 volts is about 4.0 Kilo gauss. Although the absolute field strength is not very high, the integral of the magnetic field along the trajectories of near horizontal particles, which governs the deflection, is reasonably high and is found to be (2.0 ± 0.1) 10^5 gauss cm.

5.3 The Scintillation Counters:-

5.3a. Introduction:-

A scintillation counter basically consists of a plastic phosphor, the light guide, and the photomultiplier tubes with their light tight mountings.

The action of a scintillation counter can be briefly summarised as follows: Whenever a charged particle (or photon) traverses a phosphor, it looses energy chiefly in ionizing and exciting the atoms of the phosphor. Most of the resulting excitation is quickly degraded into heat; the remaining part which is about 20% in the most efficient known phosphor (Breitenberger, 1961), is stored by fluorescence centres of metastable energy levels and eventually reappears in the form of light. Some of the light emitted is lost due to either reabsorption in the phosphor or trapping within the boundaries of the phosphor by total reflection. The remaining portion of the light escapes into the optical system which guides it towards the semi-transparent photo-

cathode of a photmultiplier tube. The photomultiplier is a sensitive detector of light in which the electron current, derived from the photo-electric emission at the photocathode, is amplified by successive stages of secondary emission. The resulting charge pulse is then proportional to the energy absorbed by the phosphor.

5.3b Description of the Scintillation Counters and their Installation.

A schematic diagram of a scintillation counter is shown in figure 5.5.

Each of the counters is made up of a polished block of plastic phosphor of type NE 102A manufactured by Nuclear Enterprises Ltd. The dimensions of the counters from S1 to S7 are given in the following table:-

Table 5.1

Counters	Length (cm)	Breadth (cm)	Thickness. (cm)
S1	43.7	37.6	5
S2	43.7	37.6	2.54
S3	133	75	5
S4	133	75	5
S5	155	55	3.8
S6	133	75	5
S7	22.86	22.86	2.54

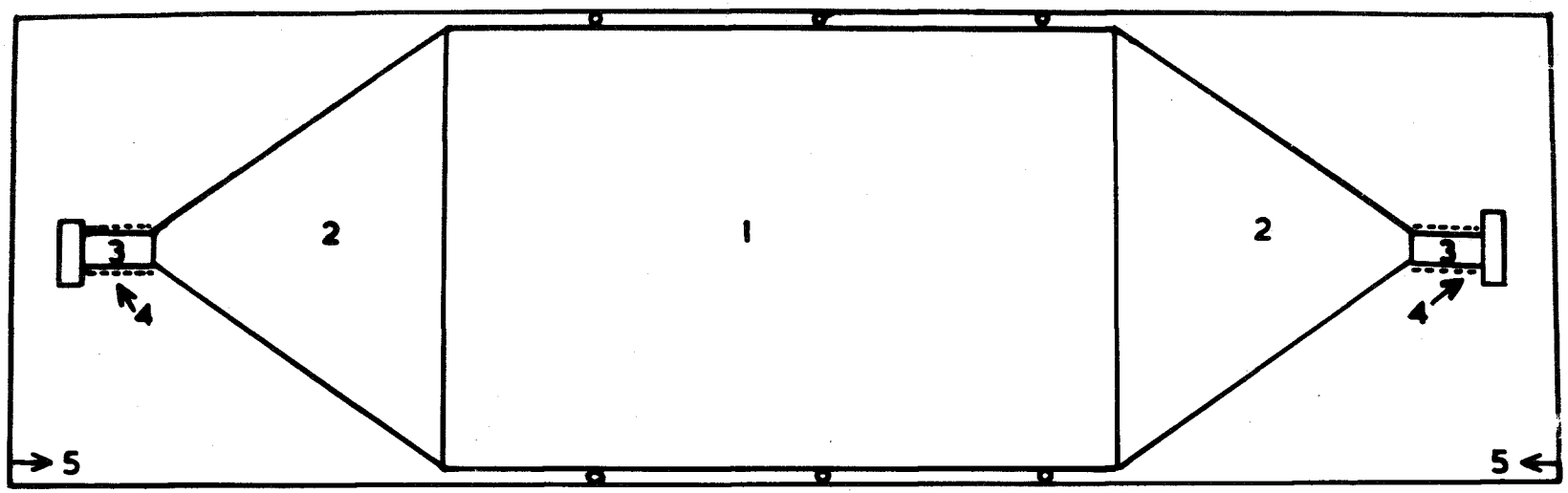

1. Phosphor.
2. Perspex light guide.
3. Photomultipliers.
4. Mu-metal shield.
5. Aluminium frame.

Fig. 5·5 Basic design of a Scintillation Counter.

Fig 5·5a Schematic Diagram of Plastic Scintillator S2.

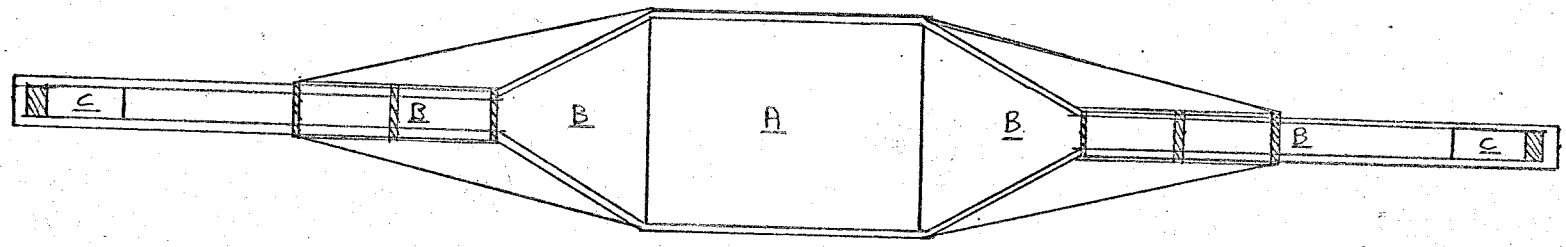

1'

A Phosphor

B Perspex Light Guides

C. 53 AVP Photomultipliers

The density of the phosphor is 1.032 gm cm^{-3}. The decay time of the fluorescence is quoted by the manufacturers as about 3 $n$sec. Other properties of the phosphor are listed in Appendix 1.

All the counters, except S7, were viewed by a pair of 53 AVP (Mullard) photomultiplier tubes. In S7, only one photomultiplier tube, (also 53 AVP), was used to collect the light. In addition to the normal light guides as shown in fig. 5.5, a perspex cylinder of diameter 2" and length 3 feet had to be used at each end of the two counters S1 and S2, to take the photomultipliers further away from the strong magnetic field. This was found essential as the two counters with their normal light guides (See fig. 5.5) stopped working altogether when the magnet was switched on. With the present set up, the counters were found to be unaffected by the stray magnetic field. The joints between the phosphor, light guides, and the photomultipliers were made by a transparent optical cement (type NE 580).

Each photomultiplier tube was screened from the strong field of the magnet by a mu-metal cylinder and a long soft concentric iron cylinder. The cylindrical light guides in the counters S1 and S2 were also enclosed within the soft-iron cylinders.

Each of the scintillation counters, along with their light guides and photomultiplier tubes, was mounted firmly

within a box made of a strong aluminium channel, the sides being covered with thin ($\simeq$ 0.022") aluminium sheets. The joints were covered by black 'Scotch' tape to make it completely light tight.

The positions of the different counters in the spectrograph are shown in figures 5.1 and 5.2. The counters S3 and S4 were held, by means of a rigid frame-work of steel, with the axes of the photomultiplier tubes vertical. On the other hand, the counters S1 and S2 were held within aluminium frames, the axes of their photomultiplier tubes horizontal, the counters standing on their narrow (2") side. The broad sides of each of the counters S1, S2, S3 and S4, and also of S7 , were at right angles to the path of a particle passing symmetrically through the spectrograph. The counter, S7, was kept vertical with its photomultiplier tube at the lower end. The anti coincidence counters S5 and S6 were in a horizontal plane.

5.3c The Electrical Connections:-

In figure 5.6, the dynode chains along with the head amplifier circuit are shown. The E.H.T. on each photomultiplier tube in a counter was adjusted so as to have equal gains from the two ends. This was done as follows. The pulse height from each photomultiplier tube was recorded on a P.H.A. (RIDL). The latter was triggered by a scint-

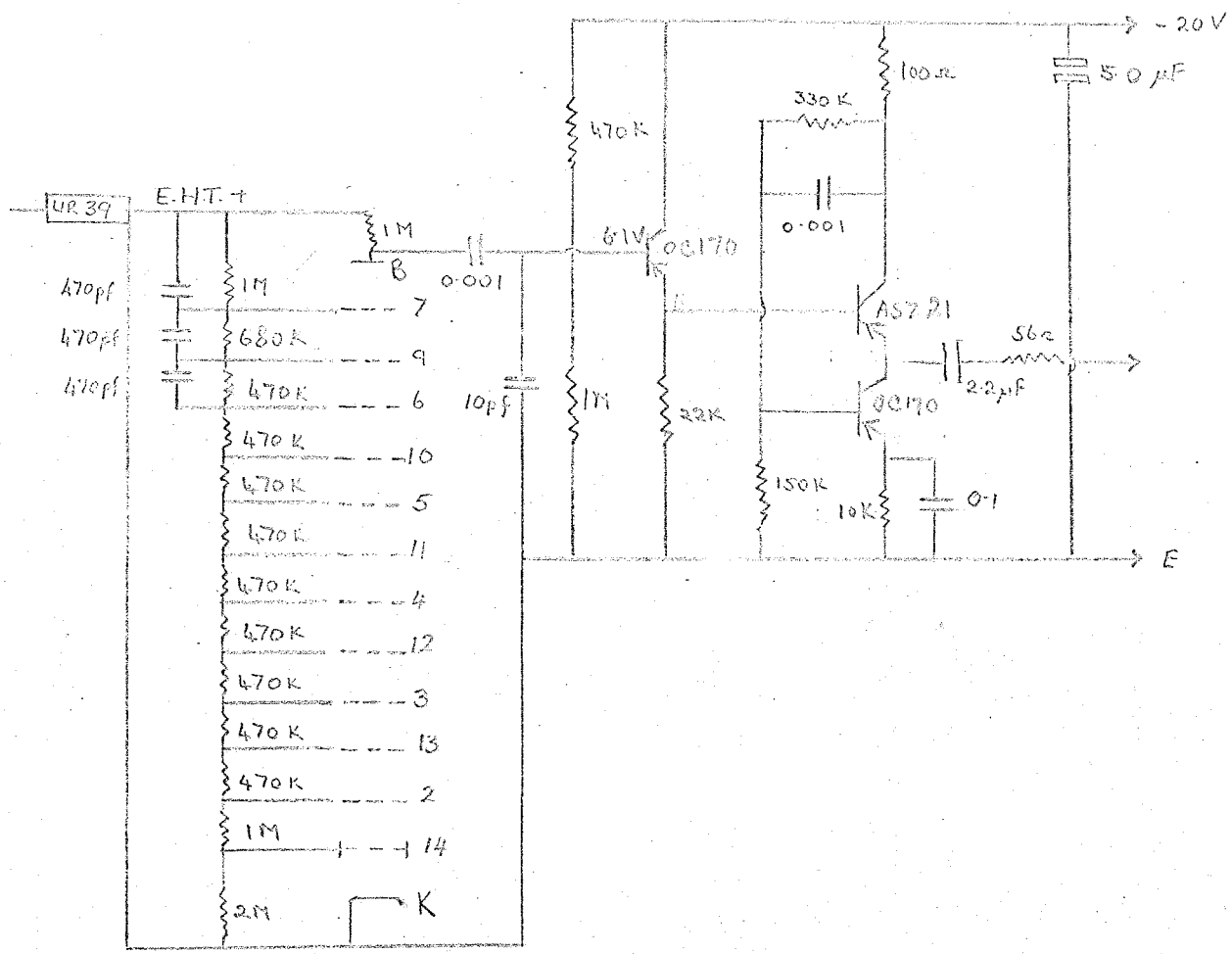

Fig 56 The PM Chain And Head Unit For Scintillation Counter.

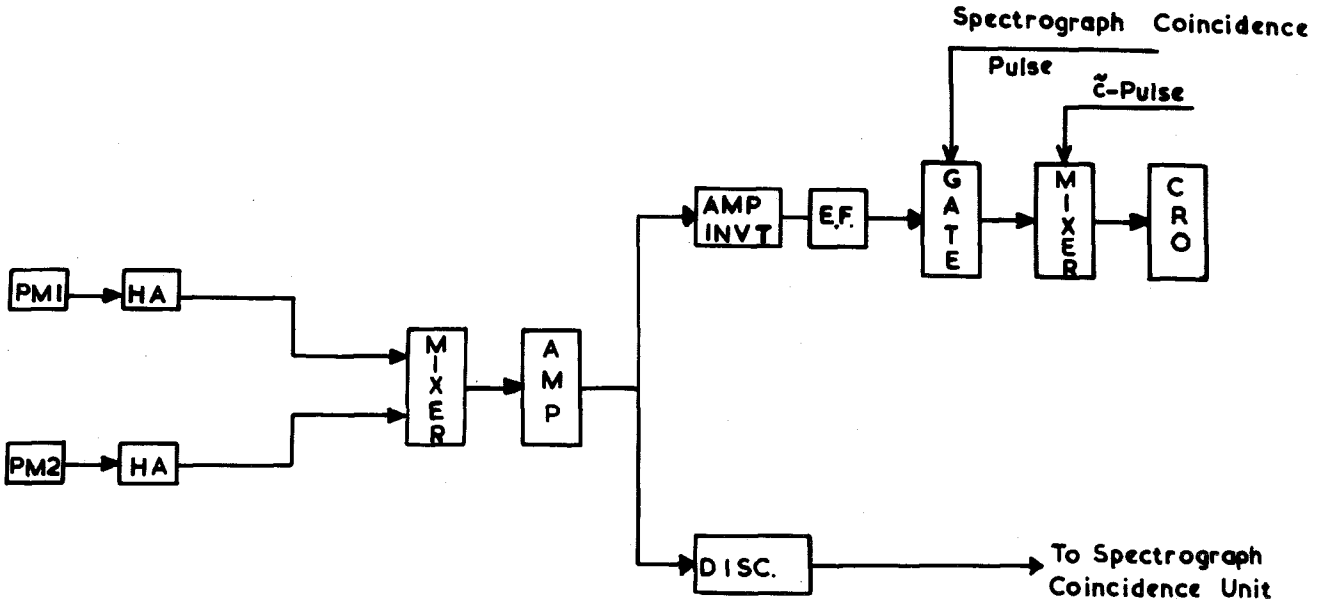

Fig. 5·7 Block diagram of electrical connections in a Scintillation Counter.

illation telescope selecting cosmic ray particles passing through the centre of the counter. The E.H.T. was adjusted till the most probable pulse height from each end was equal within $\pm$ 1.0%. The most probable pulse height for each counter was checked from time to time during the whole run of the experiment and the counters were found to be stable to within $\pm$ 3%.

A block diagram of the electrical connections for a scintillation counter is shown in fig. 5.7. The pulses from each of the photomultiplier tubes of a counter were immediately fed through a head amplifier of unit gain and then mixed resistively, and amplified. The pulses thus amplified were split into two channels as shown in the fig. 5.7. The pulses through one channel were discriminated at a level of about 250 mV and shaped to give a constant pulse height of 10V(matched). Then they were fed into the spectrograph coincidence unit. The pulses from the other channel were further amplified and then inverted. In the counter S2, the pulses from this channel were recorded in the energy loss experiment.

5.4 The Neon Flash Tubes:-

The neon flash tube, introduced by Conversi et al. (1955) and later developed by Gardener et al. (1957), consists of a glass tube filled with neon gas. If a high

voltage pulse is applied across the tube soon after the passage of an ionizing particle through it, there is high probability of a discharge taking place in the tube. The flash of light is intense enough to be photographed through the end of the tube.

5.4a Flash Tubes in Trays A and D:-

In the present spectrograph, flash tubes of two different types were used. In the trays A and D (fig. 5.2), the flash tubes were of the type described by Coxell (1961). In the tray A, the tubes were 2 metres long, where as in tray D, they were one metre. The reason for using 2 metre tubes in tray A is to use the spectrograph, in future, in conjunction with an E.A.S. experiment. The tubes in both trays were of mean internal diameter 1.55 cm and external diameter 1.75 cm and were made of soda glass, with a plane window at one end. They were filled with neon gas to a pressure of 60 cm. of Hg. In order to isolate the light from neighbouring tubes, each tube was separately covered with a black polythene sleeve.

Each of the trays A and D was made up of two separate small trays (see fig. 5.1), joined together. Both trays A and D contained eight rows of tubes, a row in tray A had 78 tubes whereas one in D, 58. The tubes in each small unit were supported in frame-works of slots accurately

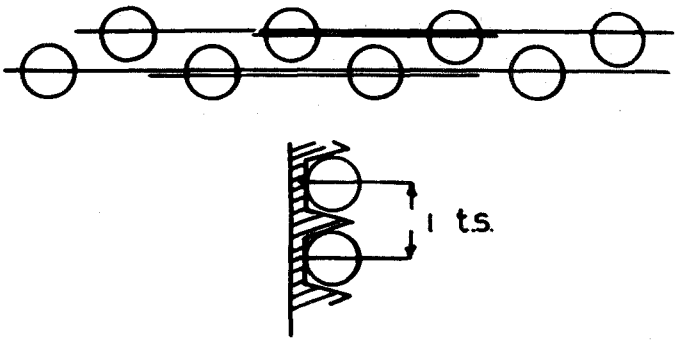

FIG. 5·8. The arrangement of the flash tubes in trays A & D.

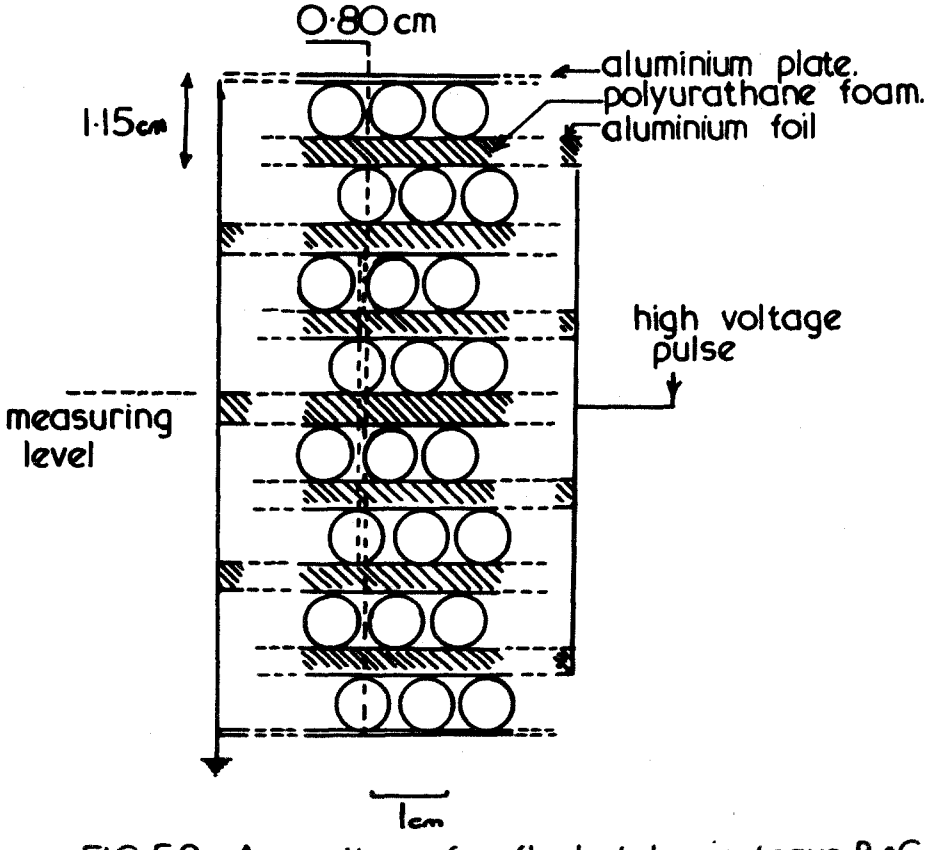

FIG. 5·9 A portion of a flash tube in trays B & C

milled in identical Tufnol rods (fig. 5.8) and were fastened tight with elastic bands. The vertical separation of adjacent slots was 1.905 $\pm$ 0.002 cm and the horizontal separation between rows was 2.80 cm. The two units in a tray were further supported together by another rigid steel frame. Each unit was fixed with adjustable screws. Each tray was held vertically in its steel frame, with the tube-window facing normally upwards. The rows were interleaved with thin aluminium electrodes, alternate ones being connected together, the outermost ones being earthed.

5.4b Flash Tubes in Trays B and C:-

The flash tubes in trays B and C were those used in the Durham Vertical spectrograph. (See Brooke (1964), and Aurela (1965)). They were 42 cm long with an external diameter 0.72 cm and internal diameter 0.59 cm. The tubes were painted black and had a plane window at one end. They were filled with commercial neon gas to a pressure of 2.3 atmospheres (Coxell and Wolfendale, 1960, Hayman and Wolfendale, 1962).

Each of the trays B and C consisted of 8 rows of flash tubes, a row in either of the trays containing 46 tubes. The tubes in both the trays were held vertically in accurately milled aluminium slots (See fig. 5.9) with window resting

downward on a thin sheet of transparent perspex. The electrods in the trays were thin sheets of polyurathene foam covered with aluminium foil. The trays were held firm in brass frames with adjustable screws. The vertical separation of the centres of the tubes in a row was 0.80 cm and the horizontal separation between the rows was 1.15 cm.

The individual rows in all the four trays were staggered relative to each other (see fig. 5.8 and 5.9) such that at least 4 tubes per tray were traversed by a particle; in majority of the cases, however, at least six tubes were observed to flash in a tray along the path of a particle. Each flash tube tray was fitted with two fiducial lights which were switched on whenever the spectrograph was triggered. The fiducials helped to locate the positions of the trays on the projection of the film.

5.4c The Flash Tube Pulsing System:-

In figure 5.10, the pulsing unit used for applying high voltage to the flash tube electrodes is shown. Whenever the spectrograph triggered, a preamplified pulse of about 20 volts from the spectrograph coincidence unit was fed into the first amplifier stage, consisting of two power pentodes (6 CH6 and EL 360) of the pulsing unit. An output pulse of $\simeq$ + 220V triggered the thyratron x H 16 with its anode at 3 KV. This in turn triggered the surge

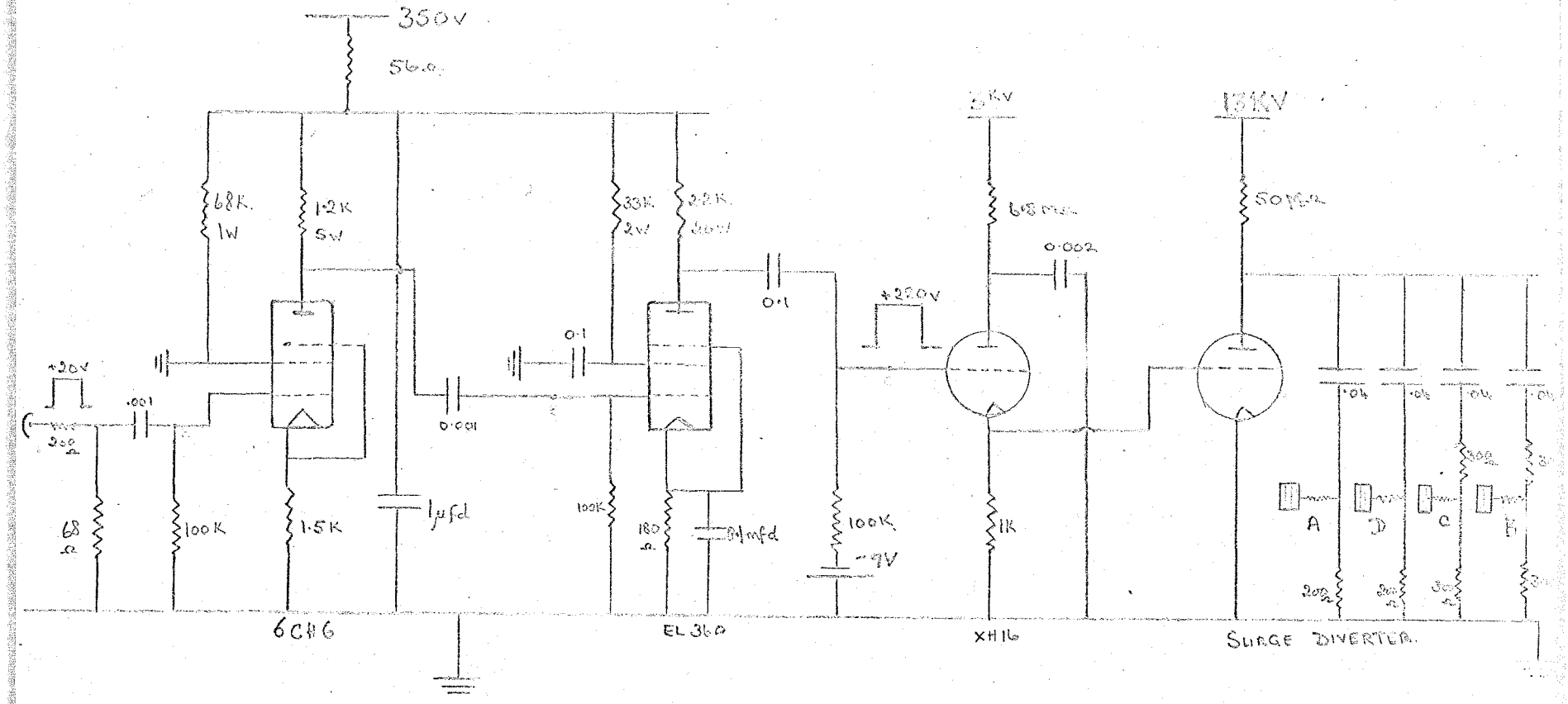

Fig 5·10 PULSING UNIT FOR THE SPECTROGRAPH FLASH TUBES.

diverter which is connected to the 13 K.V. EHT (Brandenburg). This discharged the four condensers previously charged to the 13 KV and which are connected to the electrodes of the four flash tube trays. The delay between the passage of the particle and the application of the high tension to the flash tube electrodes is only about 3 μ sec. As such, the high voltage pulse reaches the electrodes well within the sensitive time of the flash tubes, which is about 39 μ sec, after the passage of an ionizing particle through them. A typical output pulse has a rise time of about 0.8 μ sec to a maximum of about 13 KV, and a width of about 25 μ sec. This produces a field of about 4.64 KV cm^{-1} in trays A and D, and about 11.3 KV cm^{-1} in trays B and C. The field in trays B and C had to be made high in order to have flashes of reasonable brightness.

5.5 The General Electronics:-

A block diagram of the general electronic equipment is shown in fig. 5.11.

A particle passing through the spectrograph was detected by the counters S2, S3 or S4, and S7. The counter S1 was replaced by S7 to keep the counting rate at reasonable level. The counters S5 and S6 were used as anticoincidence counters to eliminate vertical showers. A block diagram of the spectrograph coincidence unit is shown in figure 5.12.

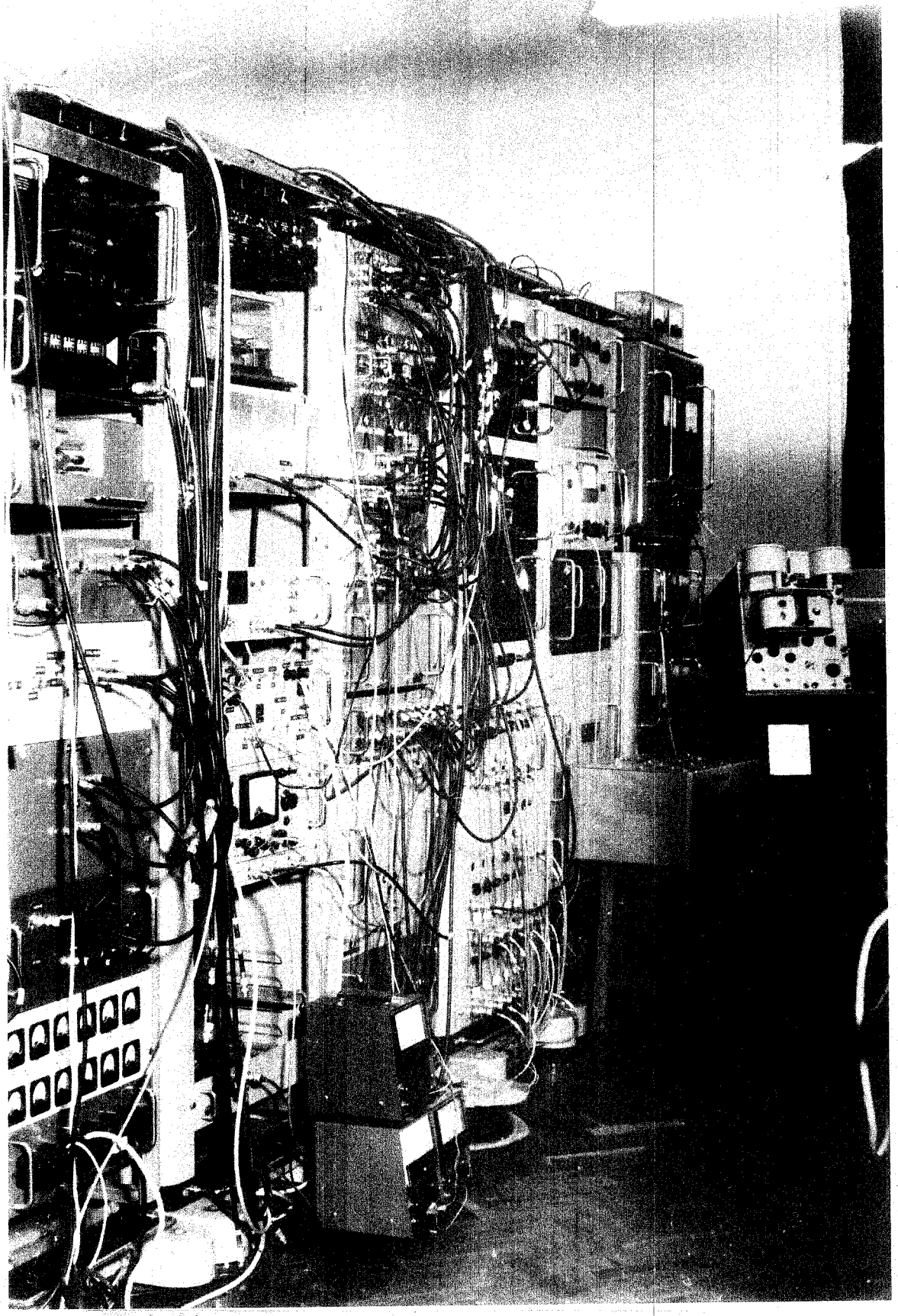

A view of the electronic equipments

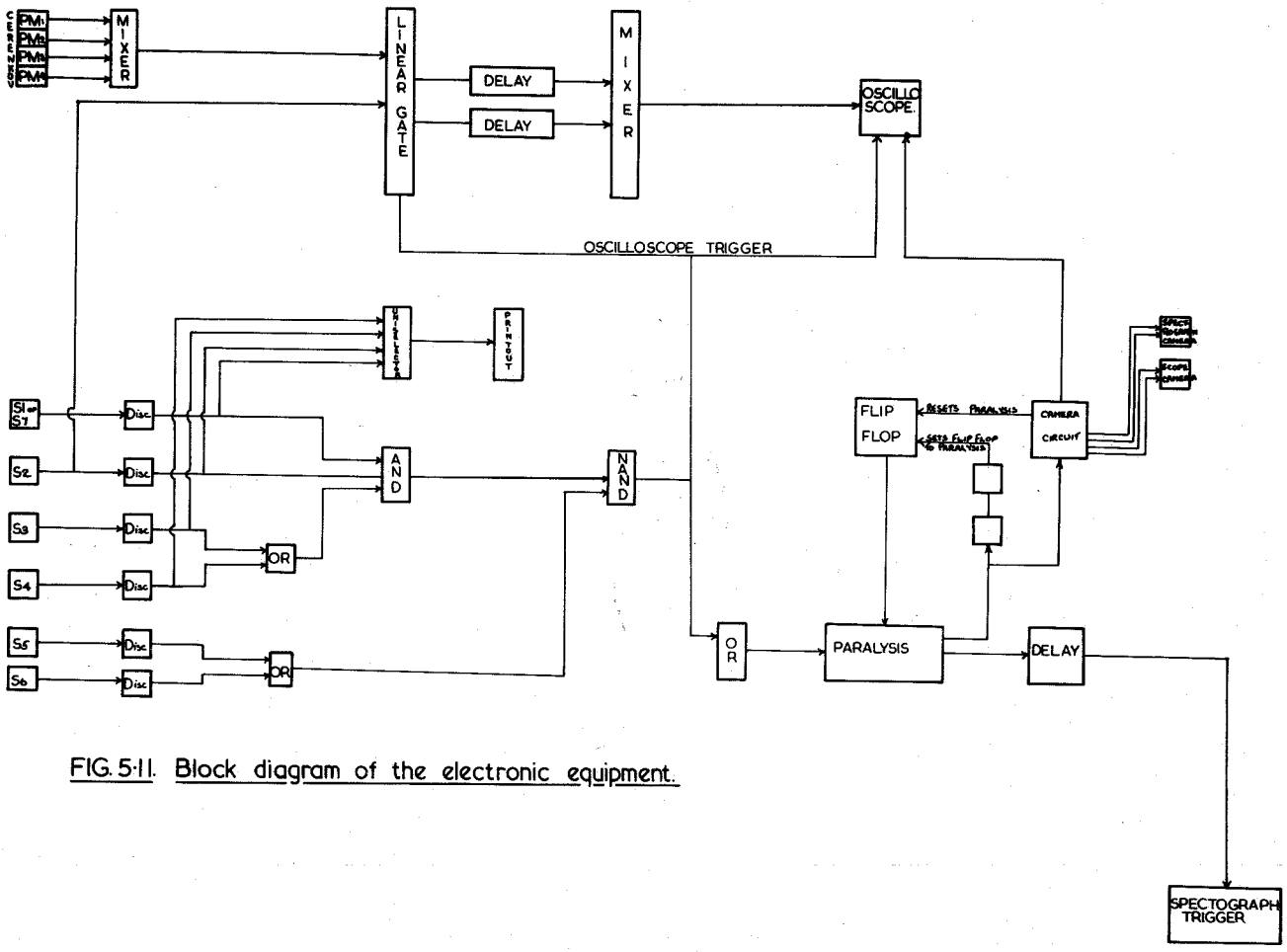

FIG. 5·11. Block diagram of the electronic equipment.

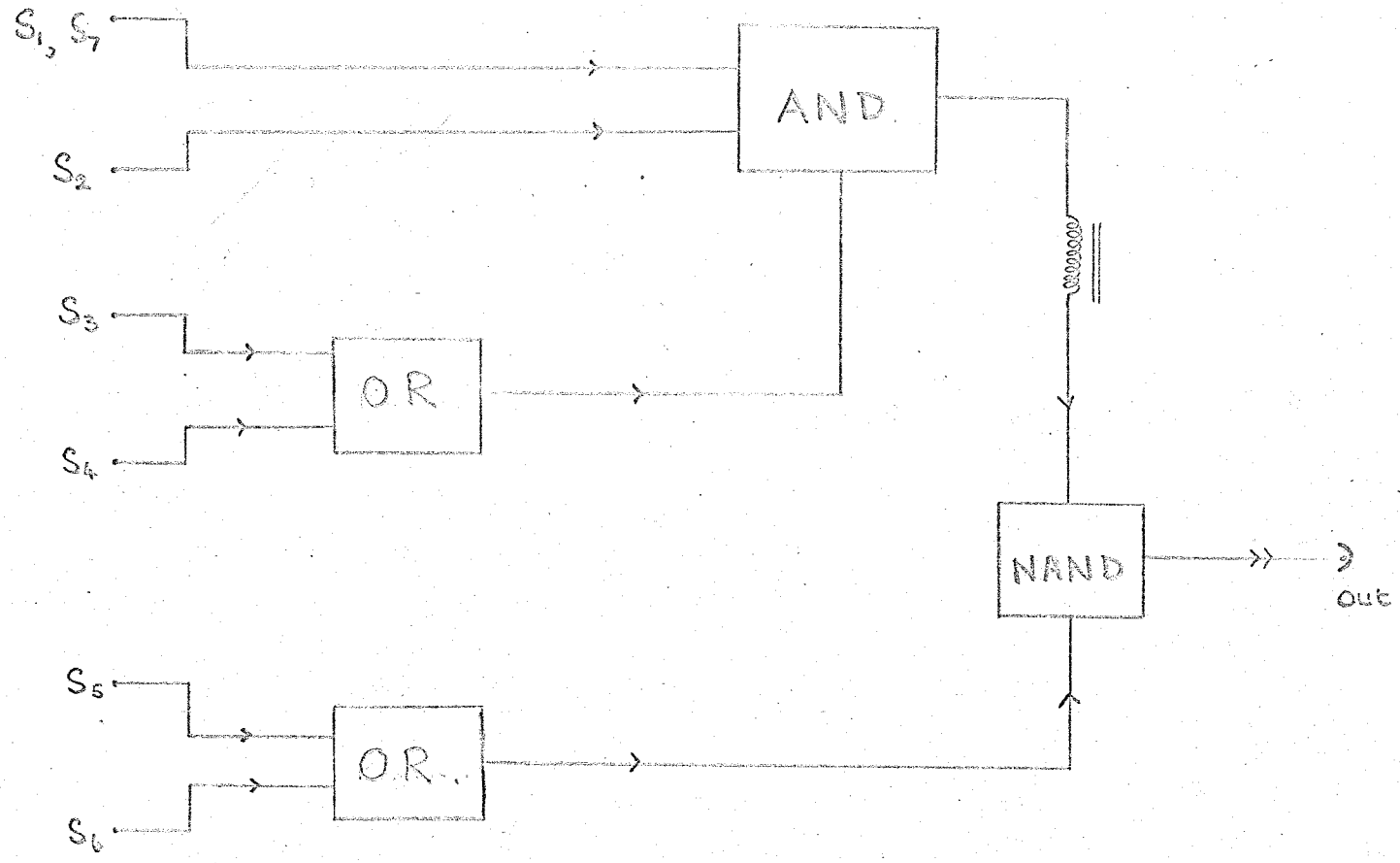

Fig. 5.12 BLOCK DIAGRAM FOR SPECTROGRAPH - COINCIDENCE UNIT

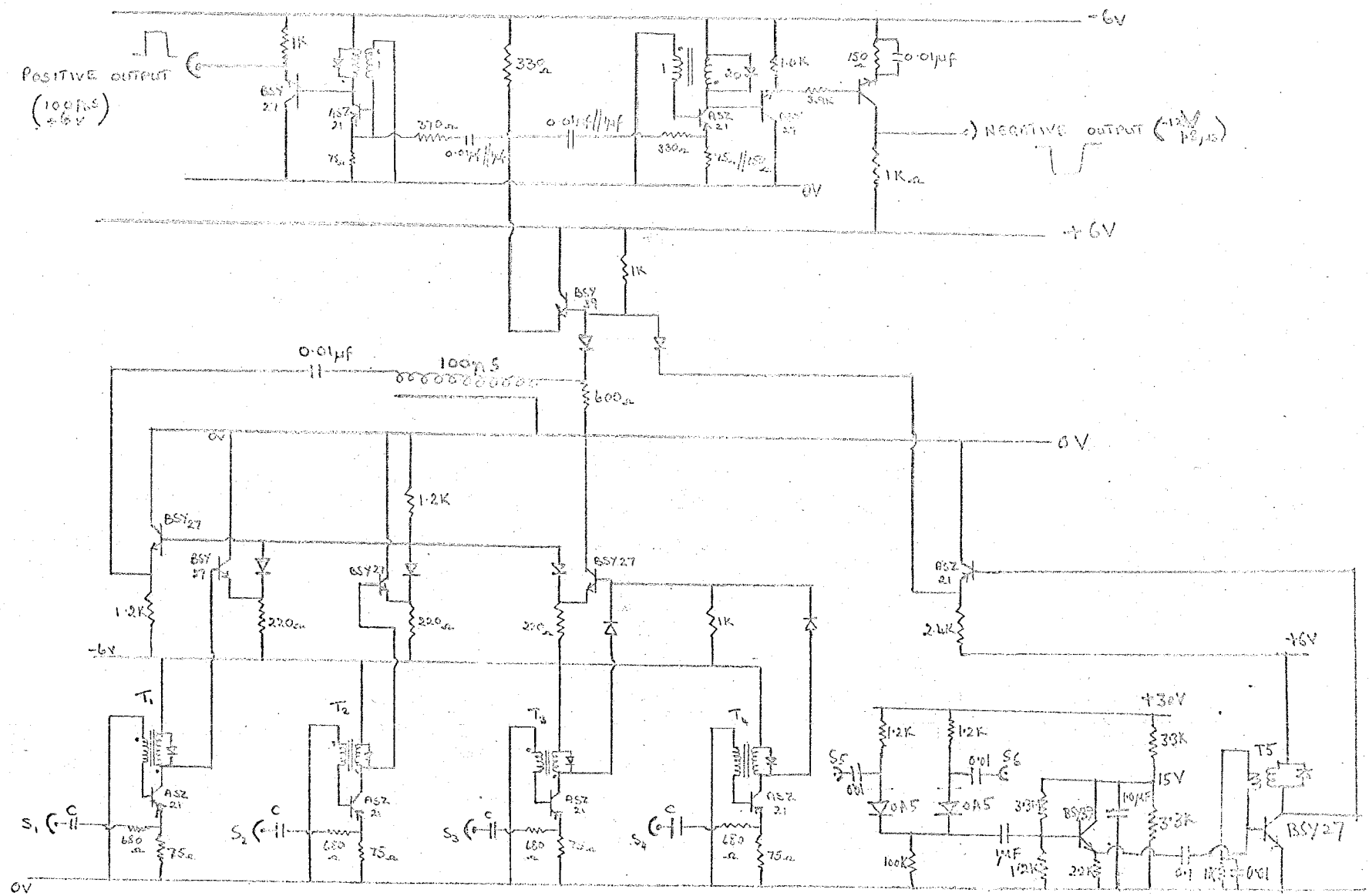

C - 500 pf
Diodes OA90
T_1, T_2, T_3, T_4 3 × 2236 RATIO S=1 P=10
T_5 3 × 2236 RATIO S=2 P=20

Fig 5.8 Spectrograph Coincidence Unit.

The coincidence unit itself is shown in figure 5.13. All other electrical circuits are given in appendix 2.

5.6 The Recording Systems:-

5.6a. The Recording System in the Spectrograph:-

Two cameras were used to record the flashes of the flash tubes. By means of systems of plane mirrors, one camera recorded the flashes in A and D, and the other, flashes in C and D. The flashes from the tubes in B and C could not be recorded satisfactorily beyond a distance of about 10 ft. So a complicated mirror system using six plane mirrors for each tray had to be used to get them in one camera. The cameras were used without shutters and the spectrograph could be run only in complete darkness. For every event, reference bulbs in the trays were illuminated and photographed. Two clocks were also photographed, one in each camera, to synchronise the frames on the films.

5.6b The Oscilloscope Pulse Recording System:-

The scintillator pulses from the counter S2, and the Cerenkov pulses from the Cerenkov counter (See chapter 6) were each gated by means of a master pulse from the spectrograph coincidence unit (see fig. 5.7). The Cerenkov pulse was then delayed by 110 n sec, while the scintillator pulse was delayed by 660 n sec. and they were then mixed. They

were photographed on a C.R.O. (Tektronix) triggered externally, also by means of the spectrograph coincidence pulse. The scintillator pulses, which were very much bigger than the Cerenkov pulses, were attenuated to a suitable size so as to accomodate both types of pulses in the same C.R.O. setting. The scope setting was 0.100 V/cm and 200 n sec/cm. Along with the pulses, the scope graticule and a clock indicating the time of the event were also illuminated and photographed.

Ilford HPS films were used in all the cameras.

5.7 The Sequence of Operations:-

Whenever the spectrograph triggered, a cycling system comprising a system of relays and relaxation circuits carried out the following sequence of operations.

(1) The coincidence circuit was paralysed.

(2) (A) Sequence of operations in the spectrographs:-

(i) High voltage pulse was applied to the flash tube trays and the flashes photographed, the cameras being open all the time;

(ii) The two clocks and the reference bulbs were illuminated and photographed;

(iii) The cameras were wound on;

(B) Sequence of operations in the oscilloscope:-

(i) The oscilloscope was triggered externally and the pulses were photographed;

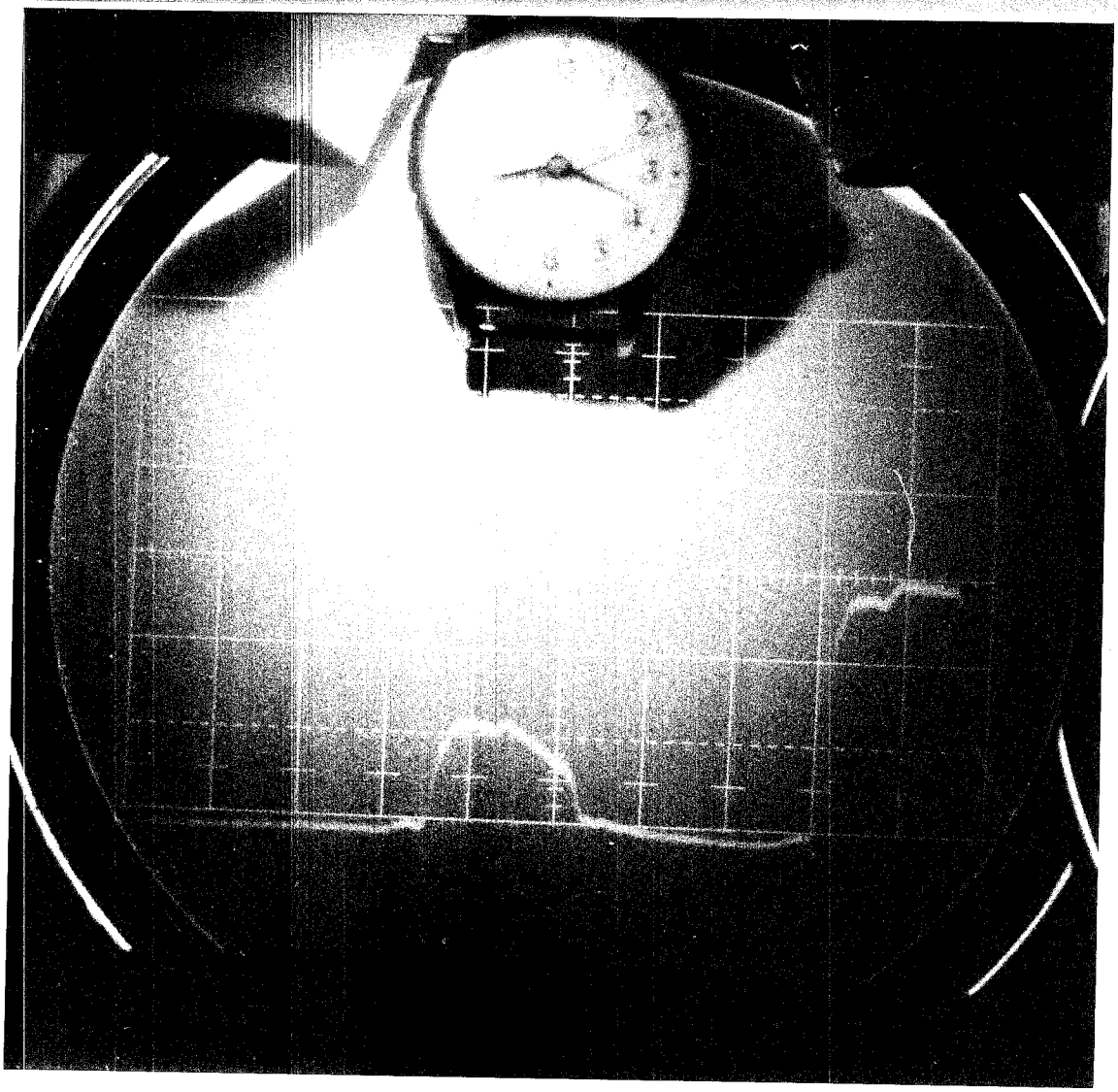

5.14 Typical pulses (a) Cerenkov,(b) Scintillation

(ii) The clock and the 'scope graticule were illuminated and photographed;

(iii) The camera was wound on.

(3) The paralysis was removed from the coincidence unit.

(4) The spectrograph and the 'scope were ready for the next event.

The whole sequence took about 6 seconds.

5.8 The Acceptance Functions:-

The acceptance of particles for different possible angles through the spectrograph is chiefly controlled by the coincidence counters. Since the particles are deflected in passing through the spectrograph, the acceptance is a function of the magnetic deflection, and hence of momentum, falling to zero at 'least detectable momentum'.

The calculation of an exact acceptance function for a spectrograph which is not symmetrical about the centre of the magnet is complicated and for the present experiment it is not essential. However, in order to have an idea of the rate of acceptance w.r.t. the zenith angle as well as the momentum of the particle, an approximate calculation for the acceptance function was made as follows.

The acceptance function for an ideal spectrograph may be defined as

$$N(\theta, P)\ d\Omega\ dp = No\ (\theta, P)\ F(\theta, P)\ d\Omega\ dp$$

Where No $(\theta, P)\, d\Omega\, dp$ is the number of particles incident on the spectrograph in an element of solid angle $d\Omega$ at an angle θ w.r.t. the horizontal direction having a momentum range p, and p + dp. $N(\theta, P)\, d\Omega\, dp$ is the number of above kind of particles detected by the spectrograph.

$F(\theta, P)$ may be written as $F(\theta, P) = A(\theta, P)\, S(\theta, P)$ where $A(\theta, P)$ is called the geometrical differential aperture and $S(\theta, P)$ is the scintillator efficiency function.

Using an analytical method and the momentum spectrum of cosmic ray muons at large zenith angles as given by Allen and Apostolakis (1961), a rough estimate of the accepted particles having a certain momentum has been made. The results are shown in fig. 5.15. Again the relative acceptance of the number of particles w.r.t. zenith angle had also been calculated geometrically. Fig. 5.16 shows the calculated results. It can be seen from fig. 5.16 that the angle of maximum acceptance was $73^{\circ} \pm 1^{\circ}$. This result had been utilised in installing the Cerenkov counter in the spectrograph.

The 'collecting power' of the present spectrograph can be compared with those of the earlier ones. The collecting power is defined as $\iint dA\, d\Omega$ where $d\Omega$ is the allowed solid angle of collection for an area dA. The integral is taken over the effective area at scintillator level S3 S4 and at the central plane of the magnet and is found to be 19.41 sterad cm^{-2}. A comparison with some previous spectrographs is shown in table 5.2.

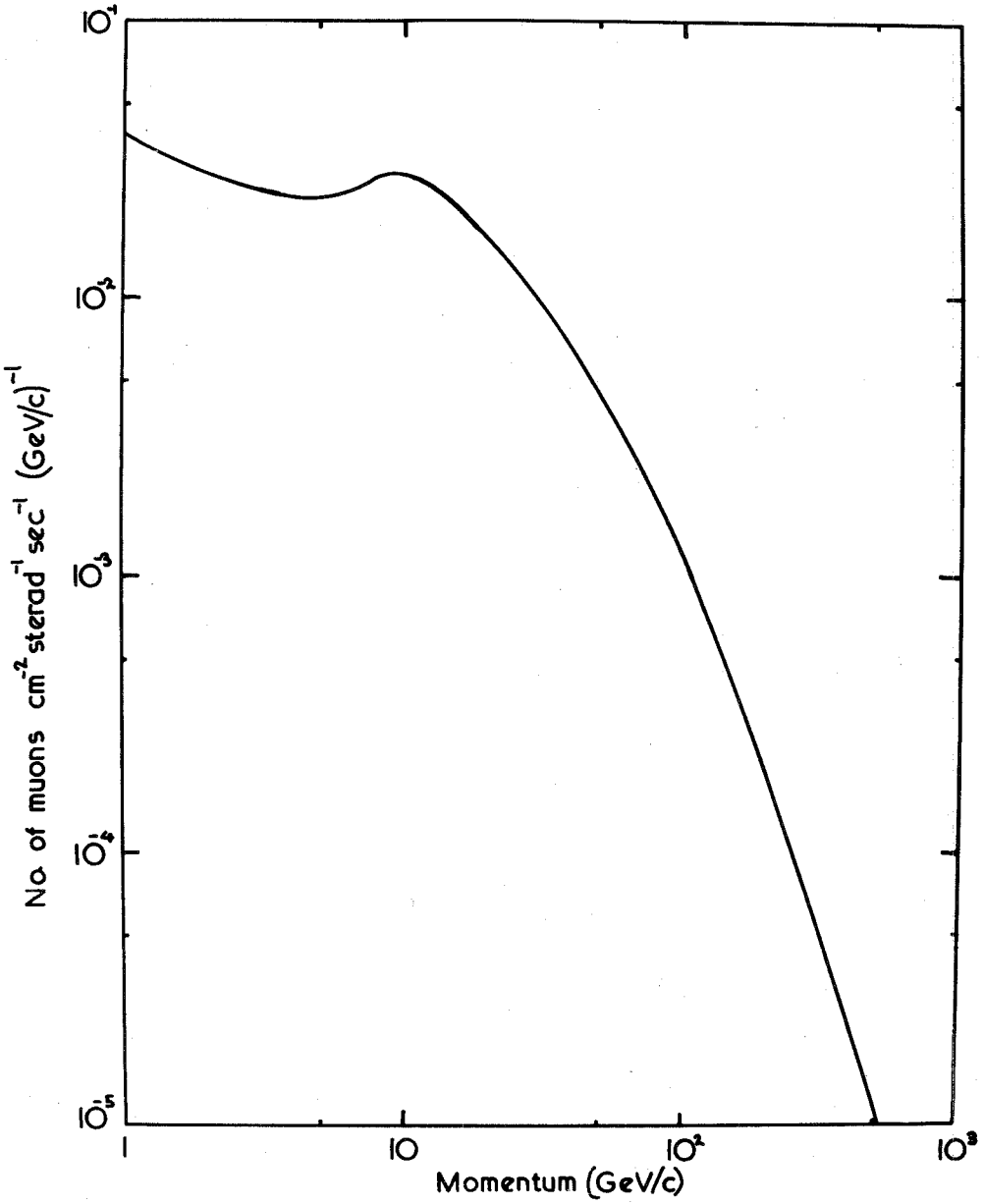

FIG.5.15 Differential acceptance rate of muons by the spectrograph

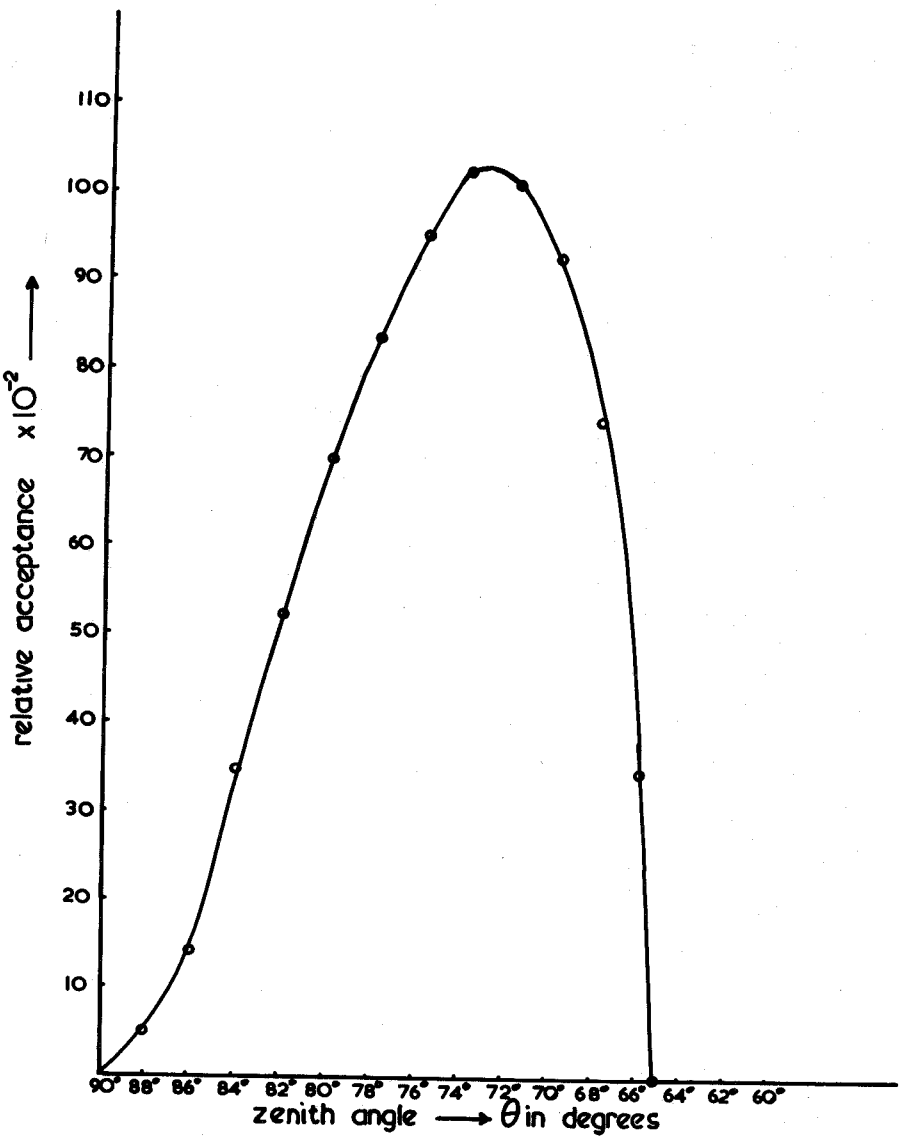

FIG 5·16 THE RELATIVE ACCEPTANCE OF NUMBERS OF MUONS BY THE SPECTOGRAPH w.r.t. THE ZENITH ANGLE θ

Table 5.2

Detectors	m.d.m. GeV/C	Collecting Power cm^2 sterad	Authors
Air gap	50	0.7	Caro et al.(1951)
Air gap S.C.	30	0.39	Allkofer (1959)
Air gap G.C. C.C.	260	7.9	Pine et al.(1959)
Air gap, Emulsion on glass plates.	300	small	Allen and Apostolakis (1961)
Air gap, G.C. F.T.	650	8.0	Hayman and Wolfendale (1962)
Solid Fe, F.T. G.C.	(300(MKI)) (1950(MK2))	(29.8(MKI) (9.61(MK2)	MacKeown (1965)
Air Gap, F.T. S.C.	116	19.41	Present work.

G.C. = Geiger Counter F.T. = Flash Tubes
S.C. = Spark Chamber S.C. = Scintillation Counter
C.C. = Cloud Chamber

5.9 Particle Rates:-

Without the magnetic field, the spectrograph coincidence rate with counter S1, S2 (S3 or S4) was 150 ± 2.5/hr.; with the anticoincidence counters, the rate (S1, S2, (S3 or S4) $\bar{S5}$, $\bar{S6}$) was (133 ± 2) hr^{-1}. This rate was too high and would create complications in analysing the data. As

such, the counter S1 was replaced by the counter S7 to cut down the rate and to select only those particles that went through all the flash tube trays. Thus in the present experiment, the spectrograph was run with counters S7, S2, (S3 or S4) $\bar{S}5$, $\bar{S}6$. The coincidence rate was $(40 \pm 2)hr^{-1}$ without magnetic field, and $(36 \pm 2)hr^{-1}$ with magnetic field.

The useful number of events in the films which satisfied the selection criteria to be described in sec 5.11, was only $(6 \pm 1)hr^{-1}$. This low efficiency of actual useful events was partly due to the weak images from the trays B and C, and partly due to the gaps between the units in each of the trays A and D. The number of events with tracks in all the 4 trays used in the present experiment is 20 37.

5.10 The Measurements of the Positions of the Particle Trajectories:

A system of two projectors had been constructed for analysing the two spectrograph films. The films were projected onto a movable board on a table. In order to obtain the positions of all the flash tubes in a tray, at first the photographs were taken using a δ-source to make the tubes flash and applying a succession of high voltage pulses. The reference bulbs were also illuminated. Then, circles, corresponding to the positions of the flash tubes in each tray were drawn on the boards. Each tube in a row in every tray was numbered serially with the origin at the

centre of the outermost tube on the north west side of the spectrograph. The frames in the two films were synchronised by the two clocks, and the time as shown by the clock in the trays A and D was recorded for synchronising with the oscilloscope films. The projected images of the flashes were positioned on the boards by means of the fiducial marks. The numbers of the tubes flashed in each tray were then recorded. A method similar to the "track simulator method" described by Hayman (1962) was used to find the position of the particle in each tray. For analysing tracks in trays A and D, exact scale diagrams of a section of each tray were drawn on papers. On the other hand, for trays B and C, scale diagrams magnified by a factor of 4, were used. Knowing the positions of the tubes from the projection board, the tracks were reconstructed on the simulator sheets. A scale, marked in units of one tube separation, was drawn, immediately below the 4th layer from the centre of the magnet, on the simulator sheet for each tray. The best estimate of a particle track through a flash tube tray was made by using a cursor to pass through all the tubes that had flashed and either miss, or pass as near to the edge as possible, tubes which had not flashed. The point of intersection of the cursor with the scale in each tray was recorded as the co-ordinate of the particle in a tray. It was known that there might be some latitude for adjusting the cursor as

the exact direction of a particle's path in a tray was not known. In order to check the errors in the co-ordinate measurements, a sample of events was reanalysed by three independent scanners and in majority of the cases, agreement was very good, i.e. within $\pm$ 0.05 tube space. The accuracy of track location using this method of co-ordinate measurements is 1 mm (r.m.s.) at levels A and D, and 0.5 mm (r.m.s.) at levels B and C.

5.11 Selection of Events:-

A track in any one of the trays was accepted initially as a possible one if there were at least three tubes flashed with appropriate configuration. An event was recorded if there were single tracks in all the 4 trays. Events were rejected for the following reasons:-

(a) If in any tray there were two adjacent flashes in two or more layers of flash tubes, due to knock-on electrons.

(b) If there were two particle tracks in any tray and it was not possible to decide, from their angles and the angle of the tracks in the other trays, which was the track produced by the particle that had passed through the other trays.

(c) If two or more tracks were observed in tray D.

5.12 Alignment of the Spectrograph:-

In order to make accurate measurements on track location, it is essential that all the flash tubes be accurately

parallel to each other throughout the instrument and that their relative positions be known. The tubes were, as has been mentioned earlier, held firmly in accurately milled slots. Thus, the tubes, inside a frame, were parallel to each other within $\pm$ 0.01 cm. The tubes were kept vertical by adjusting their supporting frames. The latter in each tray was provided with screws with the help of which the frames could be adjusted in three mutually perpendicular directions. The adjustments were carried by using spirit level, plumb lines and a cathetometer. After, thus having aligned the trays, the geometrical constants of the instrument were measured. The important ones were a_o, a'_o, b_o, c_o, do, and d'_o as shown in figure 5.17, these being the distances from a reference line to an arbitrary origin of co-ordinates in each tray. The origin of co-ordinates in all the trays was taken as the centre of the outermost tube from the north in the 4th row from the centre of the magnet. As shown in fig. 5.17, each unit in trays A and D was taken to have separate origin. This would eliminate the errors if the two units in either of the trays A and D were not parallel. Since the measuring levels in the trays were at different heights above the floor, a vertical plane parallel to the central line of symmetry of the spectrograph and defined by a system of plumb lines, was taken as the reference line For this, a tensioned monofilament (0.2 mm diameter) nylon thread was stretched along the length of the spectrograph.

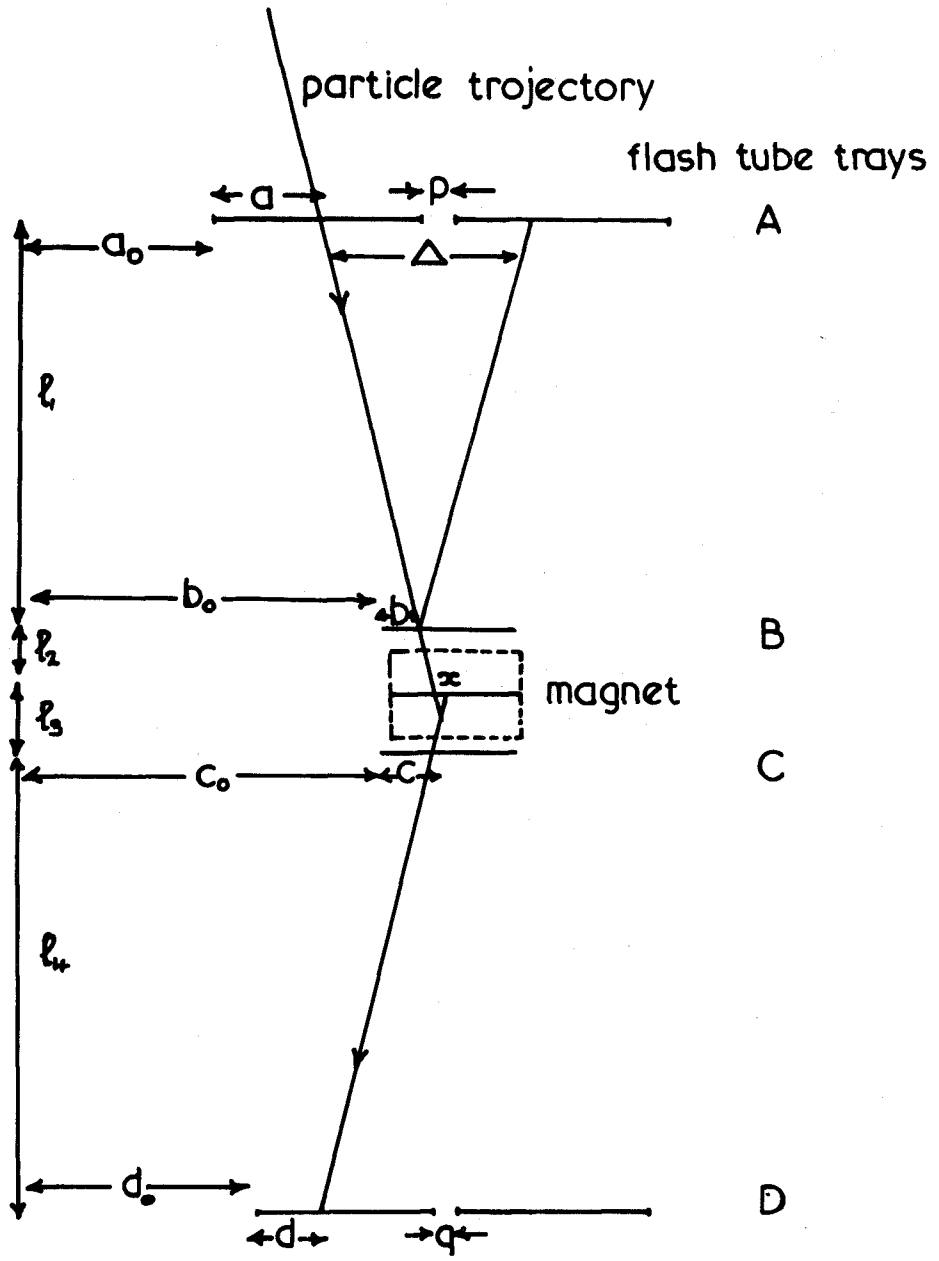

FIG. 5·17. Schematic diagram of the spectograph and a particle trojectory.

The thread was made parallel to the central line of symmetry of the spectograph, with the help of two plumb lines suspended at equal distances from the central plane of the magnet, in the north. Four other plumb lines, also of nylon thread, were hung from this thread. Each of these latter plumb lines was set parallel to the measuring row of a particular tray by means of a cathetometer. The distances of these plumb lines from the origins of their respective measuring levels were measured by the cathetometer. The separation of the trays, also determined from the same measuring level in a tray, were found using an accurate steel measuring tape. The measurements were carried out by two independent observers. The accepted values for the geometrical constants are shown in table 5.3:-

Table 5.3

Adopted Values of the Geometrical Constants:-

Dimension	cm.
a_o	41.26 ± 0.002
$a_o^1 = (a_o + p) =$	64.55 ± 0.004
b_o	114.52 ± 0.003
c_o	112.62 ± 0.003
d_o	68.64 ± 0.002
$d_o^1 = (d_o + q) =$	87.38 ± 0.005
l_1	317.50 ± 0.05
l_2	43.75 ± 0.03
l_3	59.35 ± 0.03
l_4	368.38 ± 0.06
$\bar{x}$	$+0.0075 \pm 0.0068$

l.t.s. in A and D tray = 1.905 cm.

l.t.s. in B and C tray = 0.80 cm.

The accuracy of the above constants was tested by having a run of the spectrograph without a magnetic field as described in section 5.14.

5.13 Calculation of the Particle Momentum:-

If a particle of charge e, on moving transversely through a magnetic field of strength H over a distance $d\ell$, suffers a deflection, $d\phi$, then, it can be shown that

$$e.H.d\ell = m\,v\,d\phi = P\,d\phi \quad \ldots \quad \ldots \quad \ldots \quad 1$$

where m is the mass of the particle, v its velocity, and mv = P = particle momentum.

Integrating equation (1), one gets

$$P\phi = e \int H d\ell$$

$$\text{or, } P = 300 \frac{\int H d\ell}{\phi} \quad .. \quad .. \quad .. \quad .. \quad 2$$

with P in units of eV/c, $\int H d\ell$ in gauss-cm, and ϕ in radians.

For a given value of the magnetic current, $\int H d\ell$ is constant, and so equation (2) can be written as

$$P = \frac{\text{constant}}{\phi}$$

Since the angles involved are small, ϕ can be evaluated by finding the displacement, Δ, of the trajectory over a given arm of the spectograph, fig. (5.17).

If a, b, c and d are the co-ordinates of a trajectory measured with respect to origins in trays A, B, C, and D respectively, and a_o, b_o, c_o, and d_o are the distances of the origins from the vertical reference planes, the displacement, Δ, over the arm l_1, for four tray instrument is given by

$$\Delta = (a + a_o) - (b + b_o) - \frac{l_1}{l_4}\left((c + c_o) - (d + d_o)\right)$$

or $$\Delta = (a - b) - 0.868\,(c - d) + \Delta_o \quad \ldots\ldots\ 3$$

It is, however, possible to calculate, Δ, from the measured co-ordinates in A, B, and C only. If Δ be measured over the arm $(l_1 + l_2)$ (see fig. 5.17), then for 3 chamber arrangement, it can be shown that

$$\Delta = \frac{l_1 + l_2}{l_3}\left(\frac{l_2 + l_3}{l_1}(a + a_o) - \frac{l_1 + l_2 + l_3}{l_1}(b + b_o) - (c + c_o)\right) \quad \ldots\ldots\ 4$$

If a, b, c and d are measured in units of tube space, and expressed in cm, then for 4 chamber measurement, equation (3) becomes,

$$\Delta_4 = 1.905\,a - 0.8\,b - 0.695\,c + 1.655\,d + (\Delta_{01}, \Delta_{02}, \Delta_{03}, \Delta_{04}) \quad \ldots\ 5$$

where

Δ_{01} = - 87.55 cm for a $\geq$ 39 t.s, d $\leq$ 30 t.s.

Δ_{02} = - 95.43 cm for a $\leq$ 38 t.s , d $\geq$ 30 t.s.

Δ_{03} = -110.84 cm for a $\leq$ 38 t.s., d $\leq$ 29 t.s.

Δ_{04} = - 72.14 cm for a $\geq$ 38 t.s., d $\geq$ 29 t.s.

And, for 3 chamber measurement, equation (4) becomes.

$$\Delta_3 = 3.77a - 6.45\ b + 4.87\ c + (\Delta_o^{I}, \Delta_o^{II}) \ldots . \quad 6$$

where

Δ_o^{I} = -156.5 cm for a $\leq$ 38 t.s.

Δ_o^{II} = -110.42 cm for a $\geq$ 39 t.s.

The deflections Δ_3 and Δ_4 bear the following relationship

$$\Delta_3 = \frac{l_1 + l_2}{l_1} \quad \Delta_4 = 1.138 \quad \Delta_4 \ldots \ldots \quad 7$$

If l is the distance over which the deflection ϕ is measured, then $l\phi = \Delta$, and from equation (2) one gets.

$$P\Delta = C, \text{ where } C = 300\ l \int B\, dl.$$

For $\int B\, dl = 2.0 \times 10^5$ Gauss cm., $l = l_1 + l_2 =$

$= 361.25$ cm,

$$P\Delta = 21.68 \text{ GeV/c cm.} \ldots \ldots \ldots \quad 8$$

5.14 Accuracy of Measurement:-

The accuracy of measurement of the displacement depends not only on the accurate values of the co-ordinates a, b, c and d but also on an accurate estimate for the constants in the equations (5) and (6). The accuracy of the constants obtained by direct measurements (see table 5.3) are tested by running the spectrograph with zero magnetic field. Frequency distributions of Δ_3 as well as Δ_4 from this zero field run are plotted and shown in figures 5.18 a and 5.18 b. From these distributions, it is seen that the mean values of Δ_3 = 0.184 ± 0.14 cm, and for Δ_4, the mean is equal to - 0.127 ± 0.05 cm. These mean values are within the limit of accuracy of the measurements in track location which indicates that the accepted constants are quite reliable.

A test for the measured co-ordinates can be obtained from a quantity, X, which shows (fig. 5.17) the discrepancy at the centre of the field. This discrepancy arises mainly due to three reasons:

(1) errors in location at the measuring levels and uncertainties in the position of the tubes,

(2) multiple coulomb scattering in the instrument,

and (3) possible inaccuracy in the geometrical constants.

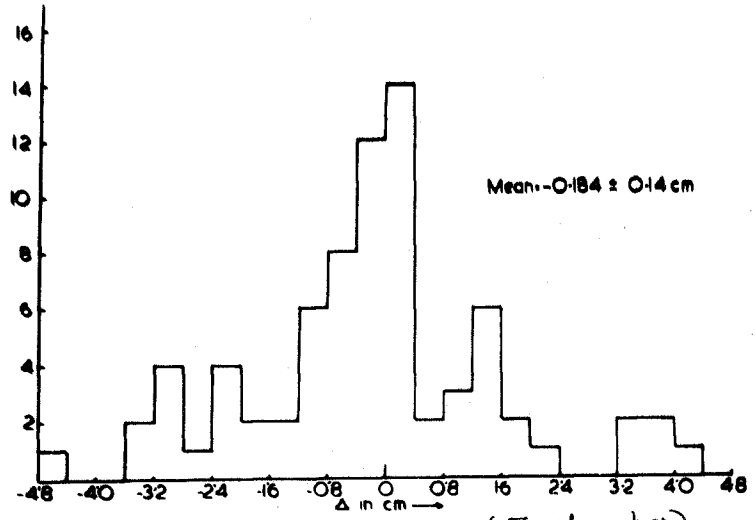

FIG 5.18a Δ — Distribution for zero field run (3 chamber)

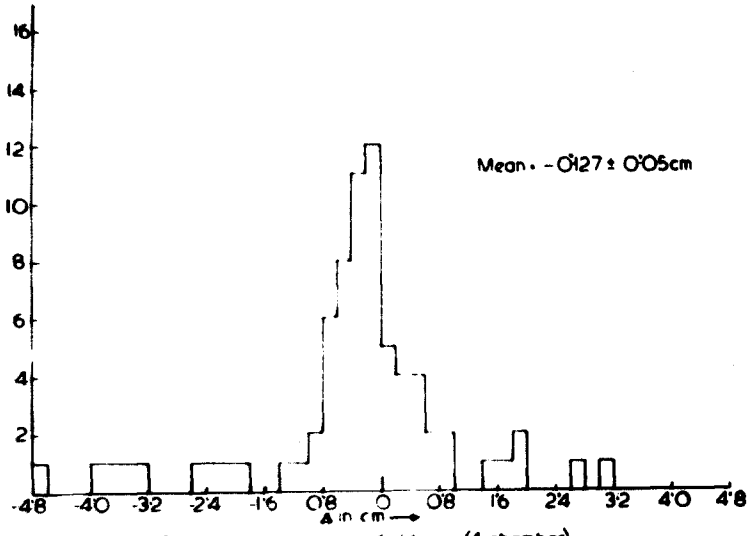

FIG 5.18b Δ — Distributions for zero field run (4 chamber)

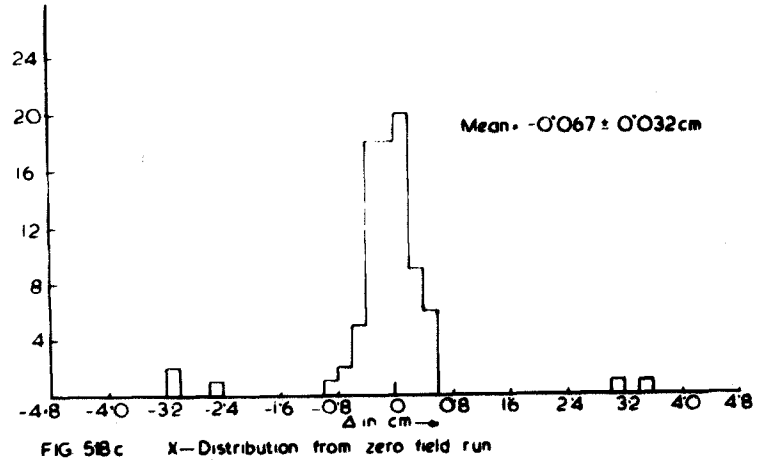

FIG 5.18c X — Distribution from zero field run

The discrepancy, X, can be shown to be given by

$$X = X^1 + X_o = (b + b_o) - (c + c_o) - \frac{\ell_2}{\ell_1}\left\{(a + a_o) - (b + b_o)\right\} + \frac{\ell_3}{\ell_4}\left\{(d + d_o) - (c + c_o)\right\} \quad \ldots\ldots \quad 9$$

where $X_o = \left(1 + \frac{\ell_2}{\ell_1}\right) b_o - \frac{\ell_2}{\ell_1} a_o - \left(1 + \frac{\ell_3}{\ell_4}\right) c_o + \frac{\ell_3}{\ell_4} d_o$. $\quad \ldots\ldots \quad 10$

Using the measured values of ℓ_1, ℓ_2, etc.

$$X = 0.91\, b - 0.263\, a - 0.929\, c + 0.307 d + (X_{01}, X_{02}, X_{03}, X_{04}) \quad \ldots\ldots \quad 11$$

where $X_{01} = 4.93$ cm for $a \leq 38$ $\quad d \leq 29$

$X_{02} = 7.95$ cm for $a \leq 38$ $\quad d \geqslant 30$

$X_{03} = 4.73$ cm for $a \geqslant 39$ $\quad d \geqslant 30$

$X_{04} = 1.71$ cm for $a \geqslant 39$ $\quad d \leq 29$.

In fig. 5.18 C, the X - distribution for the zero field run is shown. The mean of this distribution is equal to -0.067 ± 0.032 cm, which is close to zero. This again

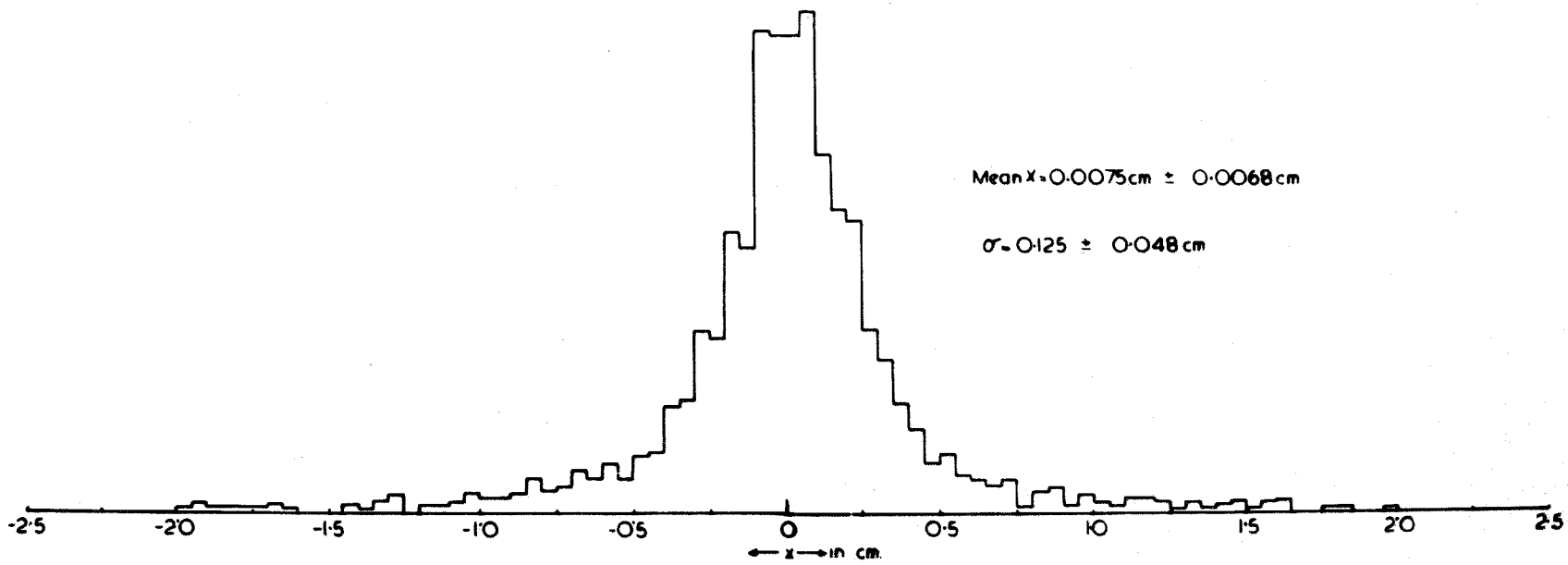

FIG. 5·19 The X-distribution for all accepted particles

supports the accuracy of the geometrical constants used.

The frequency distribution of X, for all the accepted particles in the actual experiment, with field on, is shown in fig. 5.19. The standard deviation is $\sigma_x = 0.125 \pm 0.048$ cm. The spread of the distribution, as mentioned earlier, is due partly to errors of measurement. The occasional high values of X($>$ 1 cm) are largely due to cases where two unassociated particles traverse the spectrograph and in the experiment, all events with $X > 1$ have been omitted. For high momentum particles, the scattering will be small and the spread of the above distribution can be used to find the error in Δ due to measuring errors.

The error in the deflection Δ may be used to define a quantity known as the maximum detectable momentum (m.d.m.) of the spectrograph, which is that momentum corresponding to which a deflection equals to the most probable error in deflection.

$$P \text{ m.d.m.} = \frac{21.68}{\sigma_\Delta} = \frac{21.68}{1.5\sigma_x} = 115.6 \text{ GeV/c.}$$

A particle passing through the spectrograph has to traverse, besides the scintillators and flash tube trays, about 4 feet of water in the Cerenkov tank (see section 5.15). As such, a low momentum particle will suffer large coulomb scattering which may give rise to large location error in tray D. To minimise this error, three chamber calculations

using levels A, B and C have been made for all particles having $\Delta > 2.0$ cm. For particles of momenta above $\simeq$ 10 GeV/c, error in measured values of Δ ($\simeq$ 17.8%) using three chambers becomes equal to that due to scattering in water. So for $\Delta \leq 2.0$ cm, four chamber calculations have been used.

5.15 Operation of the Spectrograph:-

Before every run, the counting rates of all the scintillators were checked. The magnet was switched on at least 3 hours ahead of the actual starting of the spectrograph. This was found necessary since the magnet current showed a high reading every time it was switched on and took about two hours to settle down to its normal working mean current of 43.5 ± 0.5 amp. The direction of the magnetic field was reversed daily to reduce the effect of any sources of bias slowly varying with time. The oscilloscope gain as well as the shape of the Cerenkov and scintillator pulses were also checked daily.

5.16 Installation of the Cerenkov Counter in the Spectrograph:-

A water Cerenkov counter to be described fully in the next chapter was installed in the spectrograph between the trays C and D. The exact position and orientation of the counter in the spectrograph have been shown in the figures 5.1 and 5.2. From fig. 5.16, it is seen that the rate of

acceptance of muons by the spectrograph is maximum around 17° to the horizontal direction. In order to make full use of the spectrograph, the Cerenkov tank was tilted to the same angle (17°) to the horizontal direction such that all the detected particles had to traverse the whole depth of water in the tank. Further, the tray D was so placed that any particle passing through the four trays A, B, C and D, had to traverse the Cerenkov counter as well.

CHAPTER 6.

THE CERENKOV COUNTER

In the construction of a Cerenkov counter two main factors are to be taken into consideration: (i) Photon economy, and (ii) the cost. The main aim always should be to get maximum number of useful photons per particle traversing the counter at the minimum cost of production. To achieve this, it is best to use a less expensive medium having minimum absorption and the refractive index $n \gg 1$, over the useful spectral range. Again, to have output electrical pulses of useful sizes from the photomultiplier tubes, the optical collection efficiency with which the Cerenkov photons are directed to the photocathodes should be pushed to the highest possible value. So as to make the counter a truly directional one, the back reflection should be avoided. The side walls of the container should be good reflectors.

Taking the above factors into consideration, a directional but non-focusing type of water Cerenkov counter has been constructed. Given below is a detailed description of this counter.

6.1 (a) Description of the Counter:-

The Cerenkov counter consists of:

(i) a galvanised steel tank of inside dimensions 6 ft. x 4 ft. x 4 ft, containing water, a metre deep;

(ii) four light collectors, each viewed by a 53 AVP (Mullard) photomultiplier tube and filled up with a solution of liquid paraffin and dimethyl popop.

The tank is so placed at the rear part of the spectrograph (fig. 5.1) that its 6 ft. sides are symmetrical in the deflection plane of the spectrograph. Further, it has been kept at an angle of 17° with the horizontal direction along which the relative acceptance of the spectrograph is maximum (fig. 5.16). Thus the situation of the tank is such that a cosmic ray particle of infinite momentum, after passing symmetrically through the spectrograph, will also traverse the tank symmetrically through the 6 ft. sides.

The light collectors are kept in such a manner that for a symmetrically passing particle the path length in water is one metre. The two inside surfaces (each 4 ft. long) as well as the inside bottom of the tank are fitted with good plane mirrors. Since the angle of emission of the Cerenkov radiation in water is about 42°, the Cerenkov light striking the air-water boundary at the top surface is internally reflected into the water. The tank along with the light collectors is made light tight by covering the top with an aluminium lid fixed with black Scotch tape.

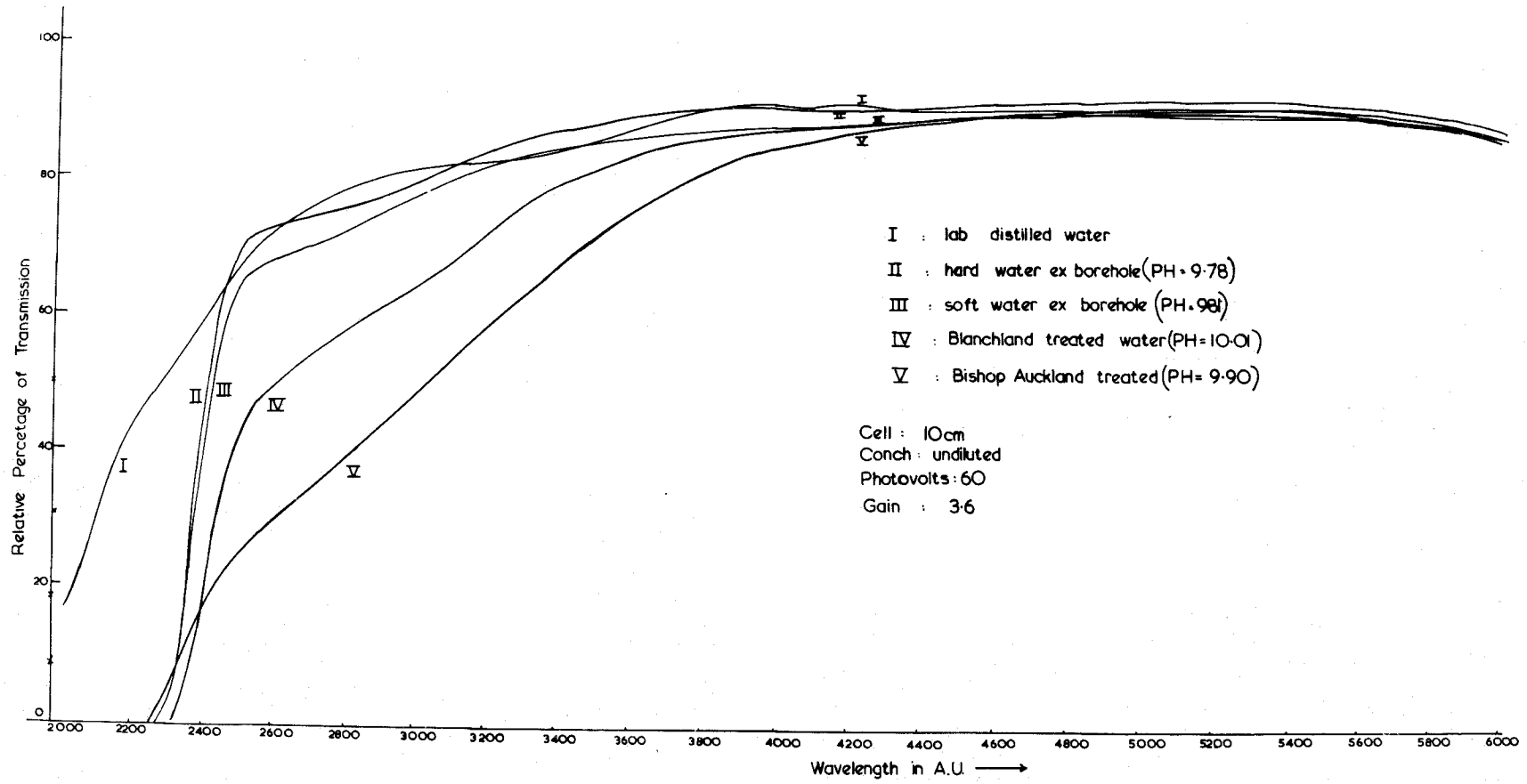

FIG 6·1: Transmission characteristics of different samples of water.

6.1 b. Selection of Water:-

The number of useful photons arriving at the light collectors surface would depend on the absorption characteristic of the water used. In order to select a sample of water having minimum absorption, the transmission characteristics of several samples of water are studied using a spectral photometer. The results are shown in fig. 6.1. It is seen that over the useful spectral range (3000 to 5000 ÅU), the transmission characteristics of the water from exbore hole are similar to those of laboratory distilled water. The former, being less expensive and easily available, is used in the present experiment.

6.2 The Light Collectors.

6.2 a. Description of the Light Collectors:-

The light collectors used in this experiment are similar in principle to those developed by Bergeson et al. (1965).

Each of the light collectors is a one metre long quartz tube of internal diameter 5.0 cm. and wall-thickness $\simeq$ 0.32 cm. The lower end of each tube is tightly fitted with a rubber bung and carries a mirror for reflecting the light up. At the upper end of the tube a short glass cylinder (10 cm long and 7 cm in diameter) is sealed with fibre glass

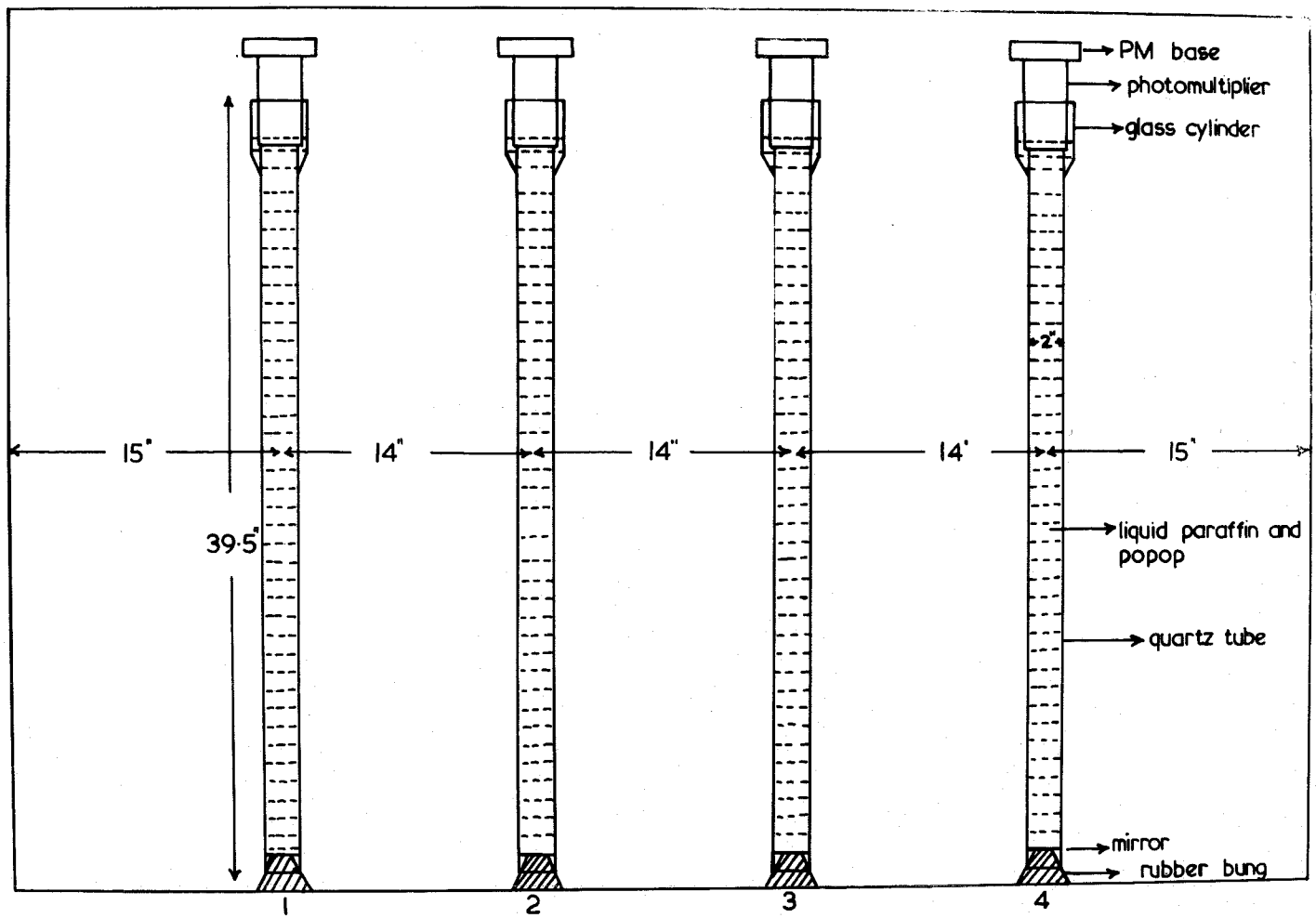

FIG 6·2 LIGHT COLLECTORS WITH PHOTOMULTIPLIERS

so that the photomultiplier together with the mu-metal cylinder can rest inside the cylinder safely. Each of the tubes is filled with a solution of liquid paraffin and dimethyl popop, the concentration of the latter being 5 mgm per litre of paraffin. The photocathode of each photomultiplier tube is in optical contact, being dipped into the solution. The light collectors are fixed 14 inches, centre to centre, apart in an aluminium 'handy-angle' rack (fig.6.2) standing normally on the bottom of the tank.

The reasons of using quartz tubes, liquid paraffin and dimethyl popop in a light collector are explained below.

Quartz tubes, although they are more expensive compared to those of perspex, have been used because of their excellent ultraviolet transmission properties. The Cerenkov light, being predominantly of shorter wavelengths, is easily transmitted through the quartz wall of a tube and thus can be trapped inside the latter.

The absorption and emission spectra of dimethyl popop in paraffin is shown in fig 6.3. Since the emission spectrum closely matches the spectral response of the photocathode of a 53 AVP tube, the dimethyl popop has been used as the wavelength shifter. It may be mentioned here that by using a similar type of light collector, Hilton et al.(1966) observed that the collecting efficiency does not depend critically on the concentration of popop in the range from

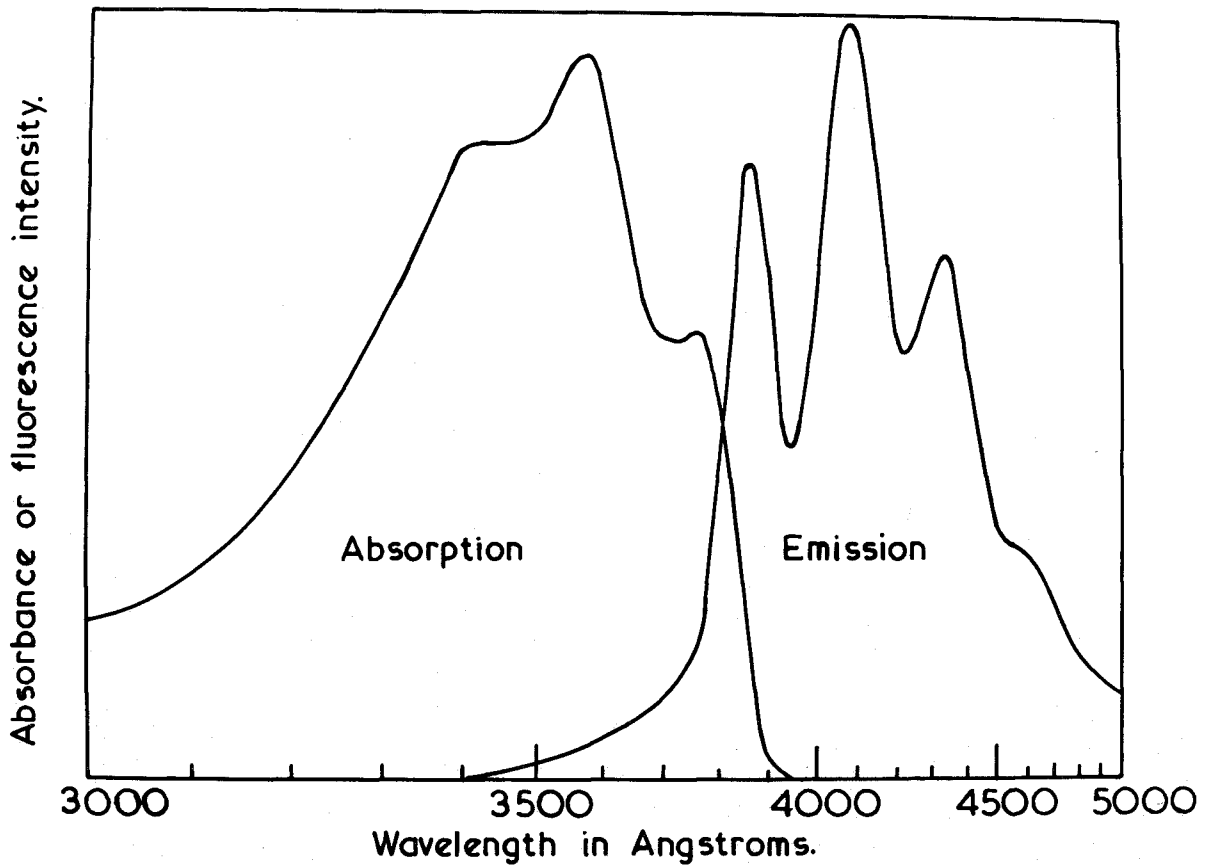

Fig.6·3. Absorption & emission spectra for POPOP in cyclohexane. The emission spectrum is for an extremely dilute solution & is uncorrected for the response of the spectrometer (Swank).

0.01 gm to 0.02 gm/litre. But in the present experiment, the popop concentration is kept to a minimum (about 0.005 gm per litre) to avoid possible scintillation effect within the light collectors.

6.2 b. Action of a Light Collector:-

Whenever a relativistic cosmic ray muon traverses the water in the tank, it produces a forward cone of Cerenkov light. The latter is partially intercepted by the quartz (refractive index = 1.55) light collectors filled up with liquid paraffin (r.i. = 1.48). The ultraviolet Cerenkov light penetrating the light collectors is shifted to the higher wavelengths by the popop and is isotropically re-radiated. A fraction of this light is trapped by total internal reflection and reaches the photocathode of the photomultiplier.

6.2 c Efficiency of the Light Collecting System:-

The photon collection efficiency depends very much on the area covered by the collecting system. Ideally the latter should cover the whole surface over which the Cerenkov light spread. It may be mentioned here that at the beginning of the present experiment, an attempt was made to cover the whole back surface of the tank by means of a 1/2" thick perspex sheet coated in front by a thin (1/8") layer of

popop and resin. Four 56 AVP photomultiplier tubes were fitted at the four corners for viewing the light trapped in the perspex. But unfortunately the system, particularly the popop and resin layer, deteriorated very fast in water and hence it was necessary to try the alternative method of the collection described here.

In the present arrangement the four collecting elements cover only about 8.3% of the available area. Obviously the light collection efficiency of the system is low. Theoretical calculations show that each tube traps about 14% of the reradiated light. Further it can be shown that the four light collecting elements together trap only about 1.7% of the Cerenkov radiation emitted by the passage of a fast muon through the tank.

6.3 Calculation of the Expected Number of Photoelectrons:-

A theoretical estimate for the number of photoelectrons to be produced at the photocathode of the 4 photomultiplier tubes, taken together, when a relativistic muon passes symmetrically through the tank, can be made in the following way.

The number of photoelectrons, Ne, produced at the photocathode depends on several factors and may be written empirically as:

$$Ne = N_0 . \alpha . G . \eta . \eta$$

where

N_o = total number of photons produced by the passage of a fast muon through the tank, at the detector level,

α = transmission co-efficient in water,

G = geometrical collection factor,

$\mathcal{R}$ = reflectivity of the mirror system,

and η = mean photocathode efficiency of the photo-multipliers.

An analytical method of calculating Ne has been used here.

First, the number of photons per cm path of the muon in water has been calculated by using the following equation (3.8).

$$\frac{dN}{dx} = \frac{2\pi}{137} \int \left\{ 1 - \frac{1}{\beta^2 n^2} \right\} \frac{d\lambda}{\lambda^2}$$

If $\beta \simeq 1$, and $\bar{n}$ is the average refractive index of water over the two wavelengths λ_1 and λ_2, we get,

$$\frac{dN}{dx} = \frac{2\pi}{137} \left(1 - \frac{1}{\bar{n}^2}\right) \left(\frac{\lambda_2 - \lambda_1}{\lambda_1 \lambda_2} \right) \text{ photons/cm.}$$

Fig. 6.5 shows the differential distribution of the number of photons per cm path of the muons in water; the

FIG. 6·4 Variation of refractive index n, with the wavelength of light λ.

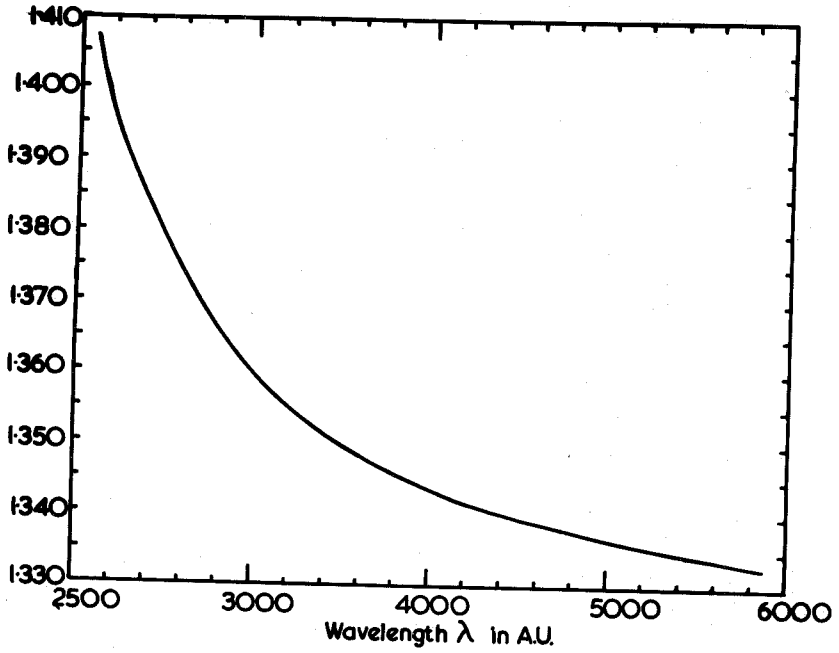

FIG. 6·5 Differential distribution of no. of Cerenkov photons/unit wavelength cm.

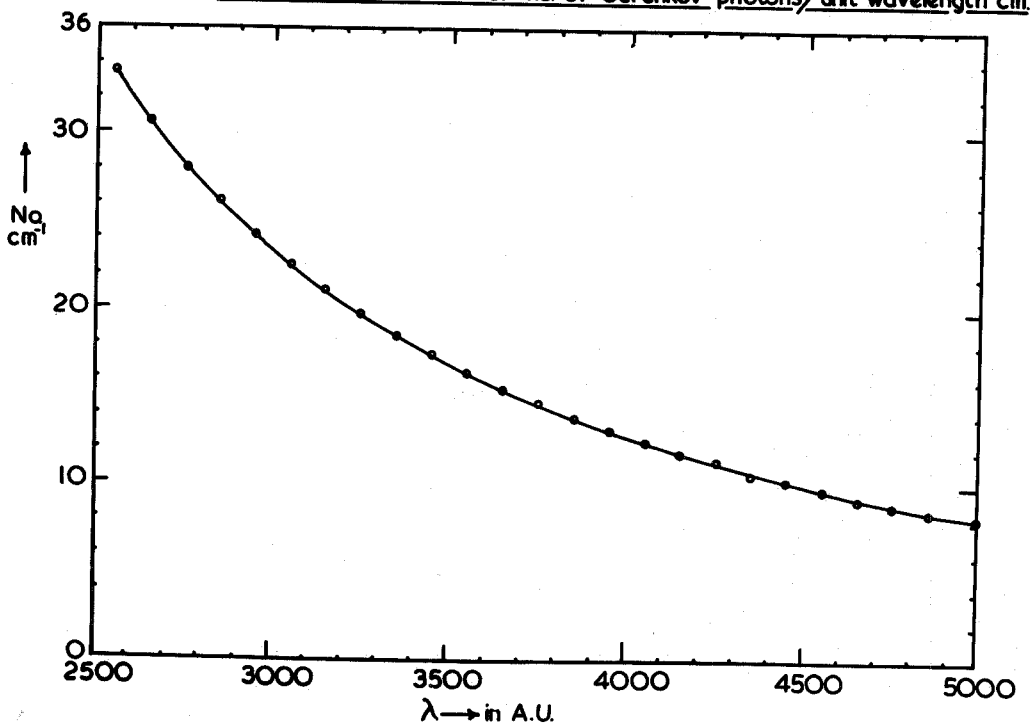

FIG. 6·6 No. of photons from unit cm path of the particle arriving at the detector as a function of the wavelength

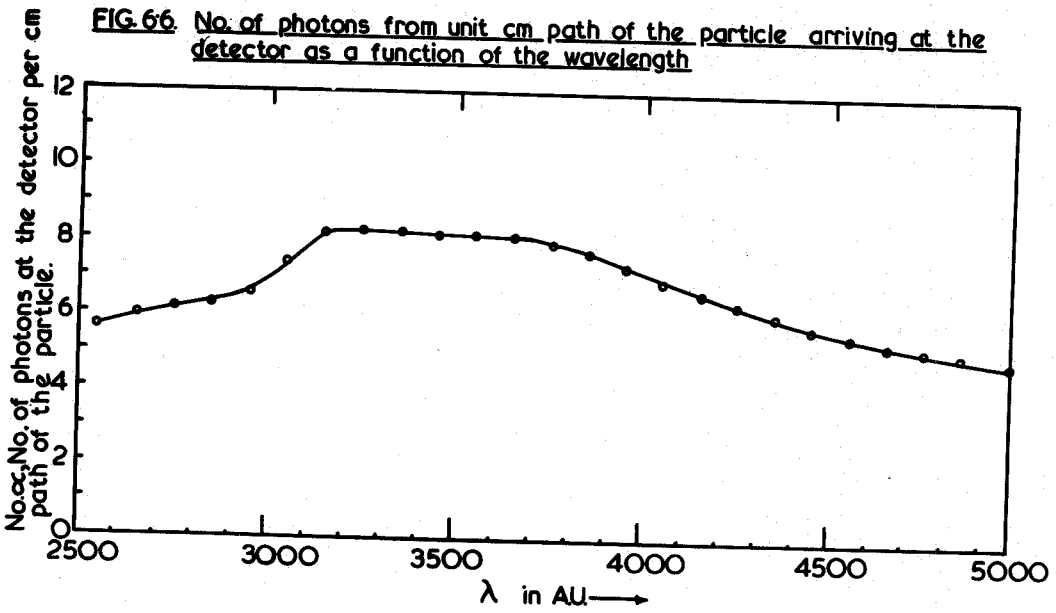

FIG. 6·7 No of photons per unit path of the particle, observed by the popop at the detector level.

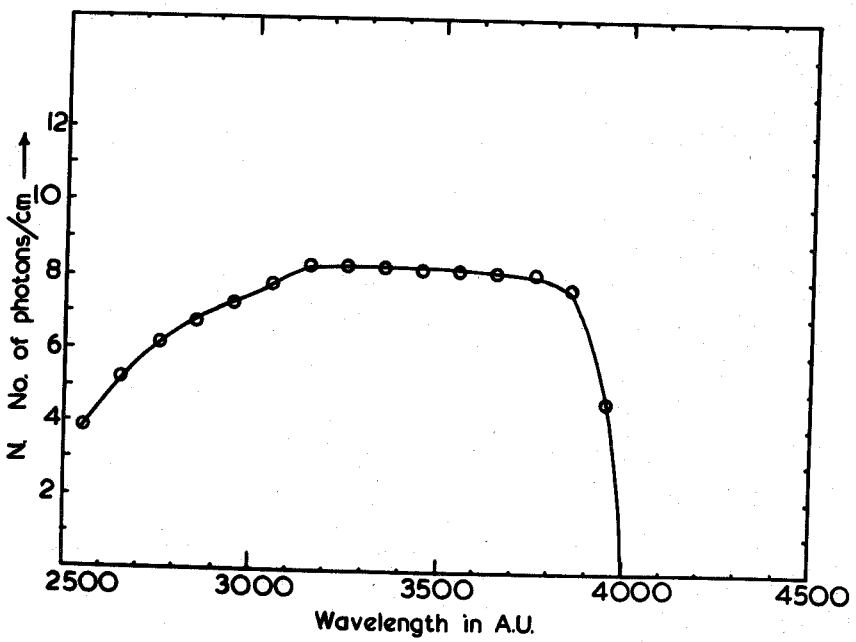

average value, $\bar{n}$, of the refractive index for any wavelength interval ($\lambda_2 - \lambda_1$) has been obtained from the graph 6.4.

From figure 6.1, which shows the transmission characteristic of the water used, the transmission coefficient has been found for each wavelength interval, and $N_0 \alpha$, the number of photons per cm at the detectors level has been calculated. The result has been shown in fig. 6.6.

Utilising the graph 6.3, which shows the absorption characteristic of popop, the number of photons absorbed by 4 cm path in the solution has been calculated .. The results are shown in fig. 6.7. Although the internal diameters of the tubes are 5.0 cm each, an average value of 4 cm has been assumed as the absorption path in the popop solution, as most of the rays will not pass diametrically through the tubes.

Then, on integration of the curve 6.7 in the wavelength interval λ_1 = 2500 to λ_2 = 4000 ÅU, one gets 108 photons per cm arriving at the detector level. Therefore, for a fast muon having 100 cm path in water, $N_0 \alpha = 108 \times 10^2$ photons. But, since the geometrical collection factor i.e. the fraction absorbed and collected by the 4 light collectors is 1.7% the total photons falling at the detector, the number of Cerenkov photons seen by the 4 light collectors is

$$N_0 \alpha \quad G = (108 \times 10^2) \times 0.017 \quad = 184.$$

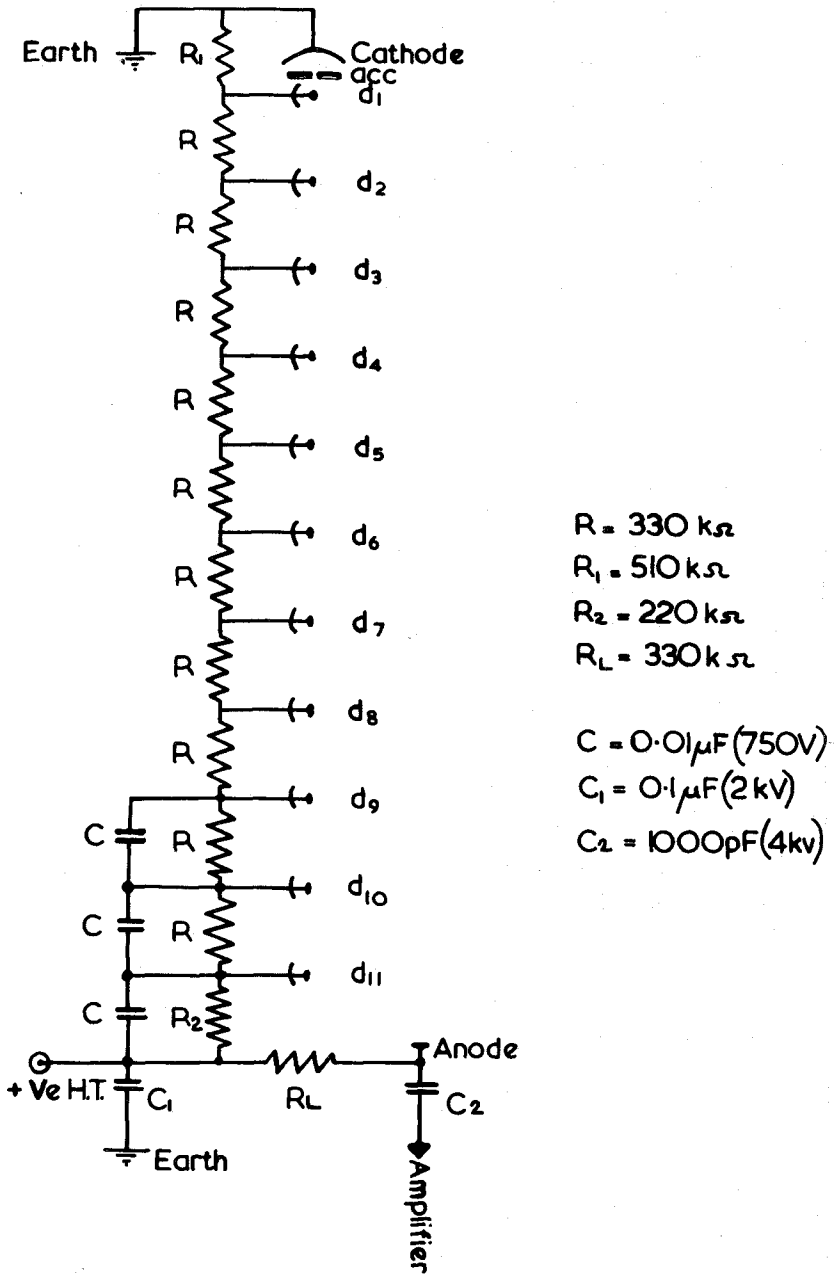

FIG.6·8. DYNODE CHAINS FOR 53 AVP PHOTOMULTIPLIERS

Again, for a muon passing symmetrically through the tank, the Cerenkov cone reaches the detector level without undergoing any reflection. So we assume here the reflectivity factor $\mathcal{R} = 1$.

Assuming η, the mean photocathode efficiency as 10%, the number of photoelectrons per muon is

$$Ne = N_0 \cdot \alpha \cdot a \cdot \mathcal{R} \cdot \eta$$

$$\simeq 18$$

For muons passing in a direction other than the one described above, the expected number of photoelectrons may be different due mainly to two reasons: (1) the change in actual path length in water, and (2) the change caused by the reflections in the mirrors.

6.4 The Electronics:-

(a) General Features:-

The type of the dynode resistor chains for each photomultiplier tube is shown in figure 6.8. The output pulses are taken from the anode of each photomultiplier tube.

A block diagram of the electronics for the Cerenkov counter is given in fig. 6.9. The output pulses from the anodes of the four photomultiplier tubes, after being immediately fed through emitter followers, are first resistively mixed, and then inverted. After that, they are amplified to a factor of 15. A typical unamplified pulse

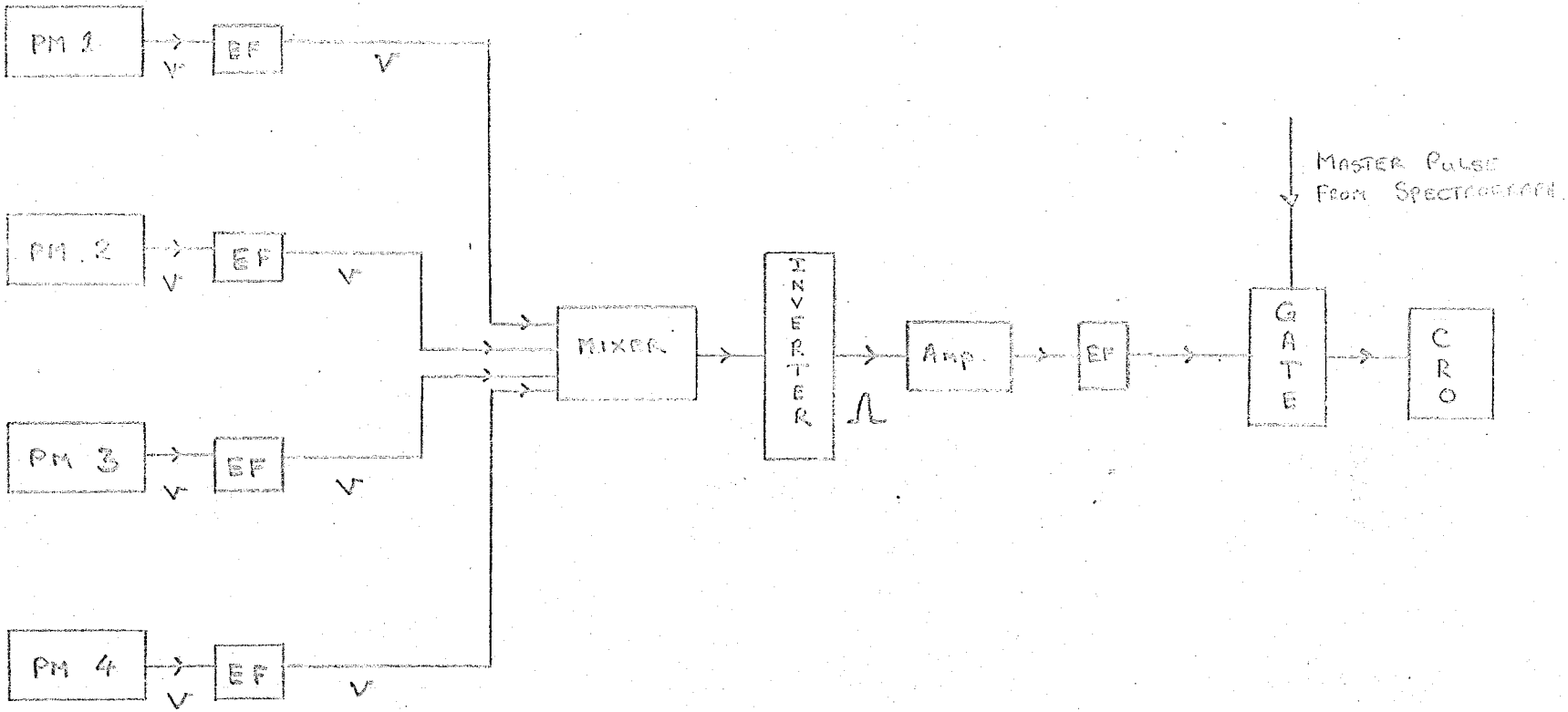

Fig. 6.9 BLOCK DIAGRAM FOR CERENKOV COUNTER CIRCUITS.

has a half-width of ~300 n sec, and rise time about 20 n sec. The emitter followers and the other electronic components are kept outside the tank. The finally amplified pulses were gated (see fig. 5.14) and delayed by 110 n sec and then displayed in a C.R.O. (Tektronix) along with the scintillator pulse. A typical photograph of the pulses are shown in fig. 5.14. The circuit diagrams for emitter follower, mixture, inverter and the amplifier are given at the appendix 2.

6.4 b <u>The Variations of the Most Probable Pulse Height with High Tension Voltages</u>:-

In order to fix the operating voltages on each photo-multiplier so that all may have the same gain, the variation of the most probable pulse height with high tension voltages for each tube was studied using a standard light flasher. The latter was a mercury-wetted relay switch. The source of light was the arc between two contacts which had a potential difference of 300 V D.C. (stabilised). One of the contacts could oscillate and cause a make and break with the other one. The oscillations were generated by an electromagnet oscillating at mains frequency. The oscillations of the moving contact were steadied by a small permanent magnet held at one side. The stability of the light flasher was checked by testing the same tube at different time and was found to be stable within $\pm$ 1%.

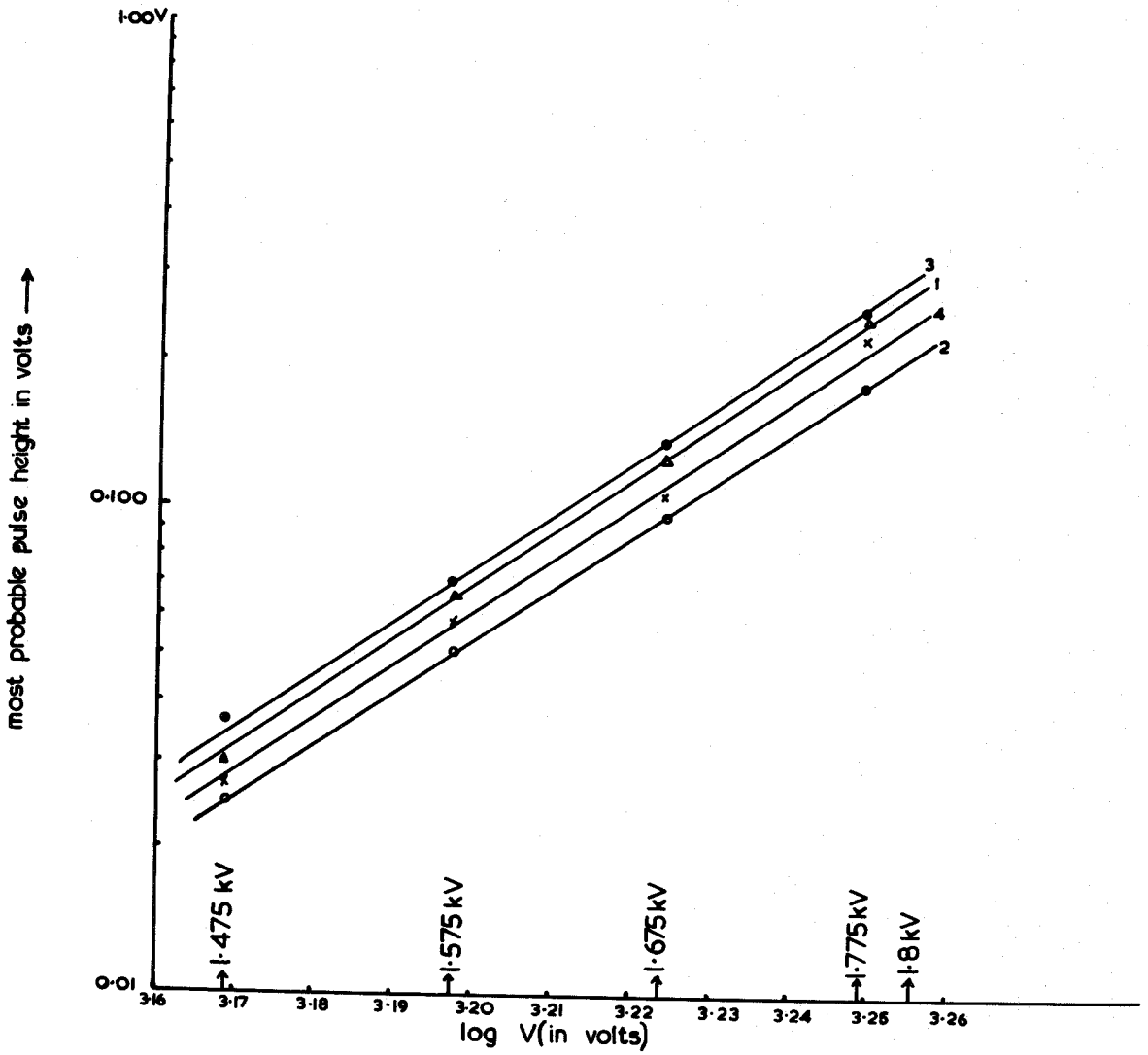

FIG.6·10. VARIATIONS OF THE MOST PROBABLE PULSE HEIGHT WITH VOLTAGE ON THE PHOTOMULTIPLIERS (1,2,3,4) (ALL 53 AVP)

The relay switch and the photomultipliers, one at a time, were kept at fixed positions, the photocathode viewing the flasher, inside a light-tight box. Then, the variations of the most probable pulse height with E.H.T. were studied by recording the photomultiplier pulses in an oscilloscope (tektronix). The results are shown in fig. 6.10. It is seen that although the tubes are of same make, there are differences in their gain. The E.H.T. values of the four tubes are fixed at (1) 1.660 KV, (2) 1.700 KV, (3) 1.650 KV, and (4) 1.675 KV respectively.

From the fig 6.10, an idea of the total gain as a function of the voltage across dynode chains can be derived as follows. Gain, G, with voltage, V, can be described by a power law as $G \propto V^m$. The exponent m has been calculated for each tube from the curve 6.10, and has the following values;

$m = 10.99 \pm 0.2$, 10.96 ± 0.20, 10.94 ± 0.2, and 10.93 ± 0.2 respectively for the tubes (1), (2), (3), and (4).

Because of the high power relationship, the voltage supply to the photomultiplier must be extremely stable. The stability of the E.H.T. supply unit (I.D.L. type 532/D) was tested over several days and was found to be constant to within 0.01%.

6.4 c The Linearity of the Amplifier Circuits:

A test for the linearity of the amplifier circuits was

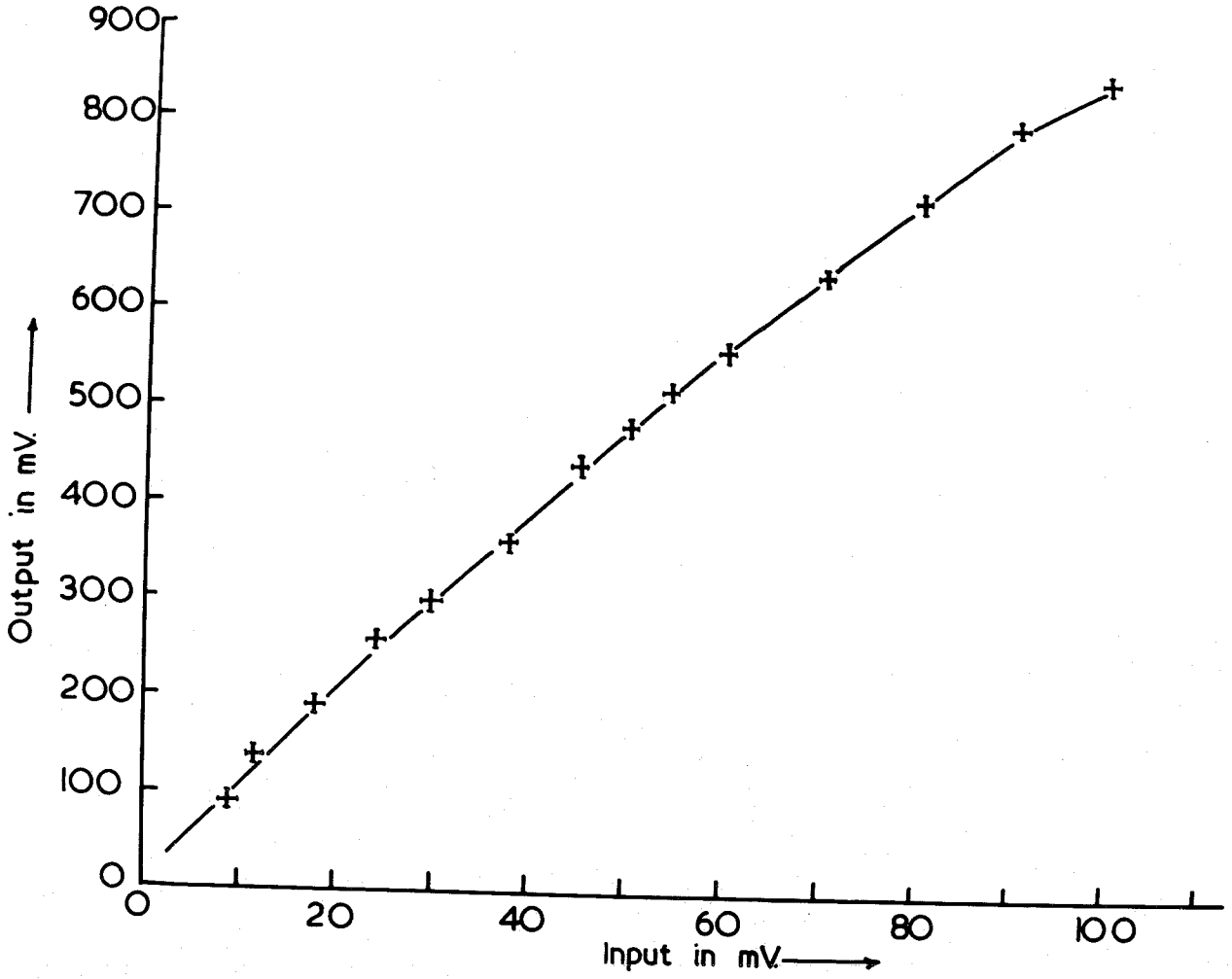

Fig.6·11. Curve showing the linearity of amplifier circuit.

made by using pulses from a pulse generator. Four input pulses from the pulse generator were fed into the four channel of the mixing and amplifier circuits, and the resultant output pulses were recorded in the Tektronix C.R.O. The results are shown graphically in the fig. 6.11. It is seen that the mixing and the amplifier circuits are quite linear up to an input pulse of 100 mV in each of the four channels.

6.5 Response of the Cerenkov Counter:-

The response of the Cerenkov counter was tested by using a plastic scintillator coincidence telescope. The latter was placed at the back of the tank in such a manner that it selected cosmic ray particles traversing the tank in the forward direction i.e. coming from the spectrograph side.

The telescope was first set to select particles passing symmetrically. The output pulses from each tube were recorded separately in the P.H.A. (RIDL) triggered by the telescope coincidence pulses. The results are shown in the fig. 6.12 (a, b, c and d). Later on, the mixed output pulses from the four tubes were also recorded in the similar way. Fig. 6.13 shows the results of this run. It is found that the most probable pulses in the two outer tubes (tubes 1 and 4) are respectively 9.82 ± 2 mV and 10.80 ± 3.5 mV whereas the most probable pulses from the two inner tubes

FIG. 6·12 a.

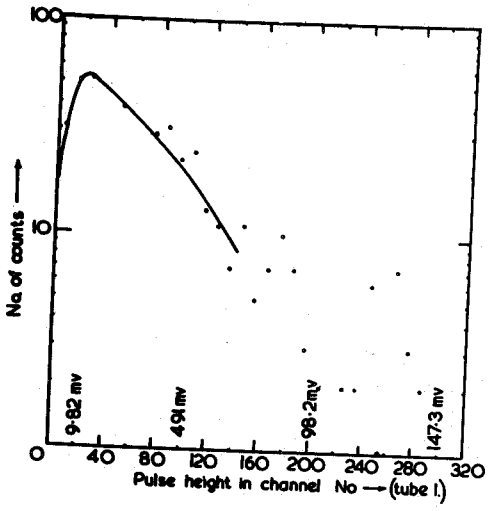

FIG. 6·12 b.

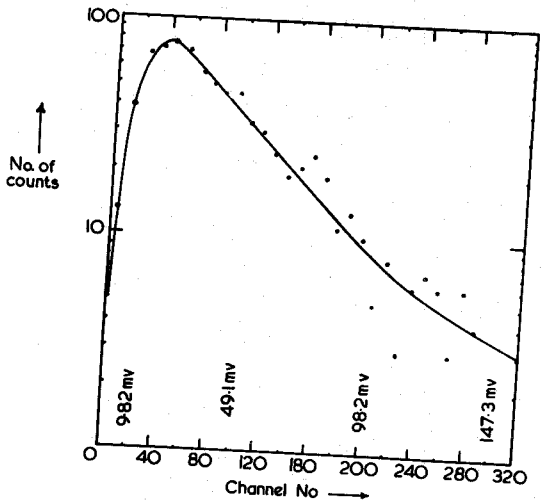

FIG. 6·12 c.

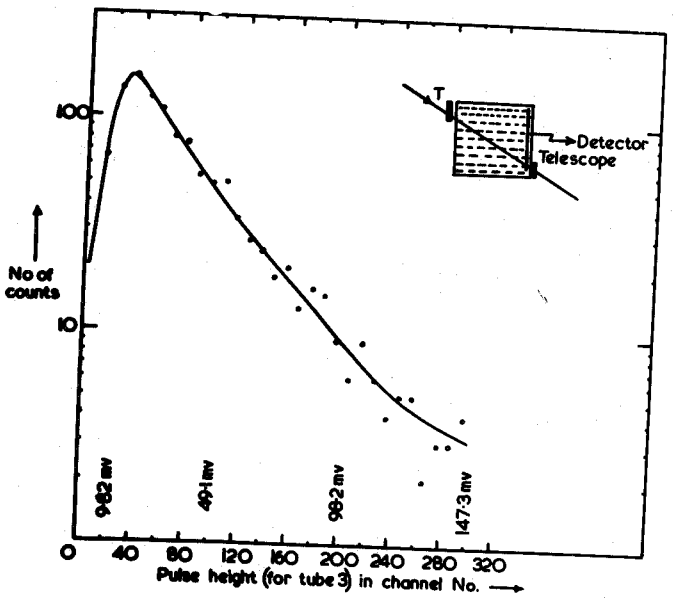

FIG. 6·12 d.

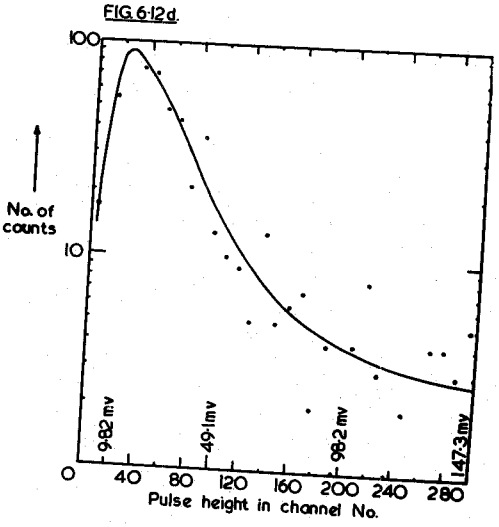

FIG. 6·12 a, b, c, d.: Pulse height distribution from tubes 1 2 3 & 4 respectively.

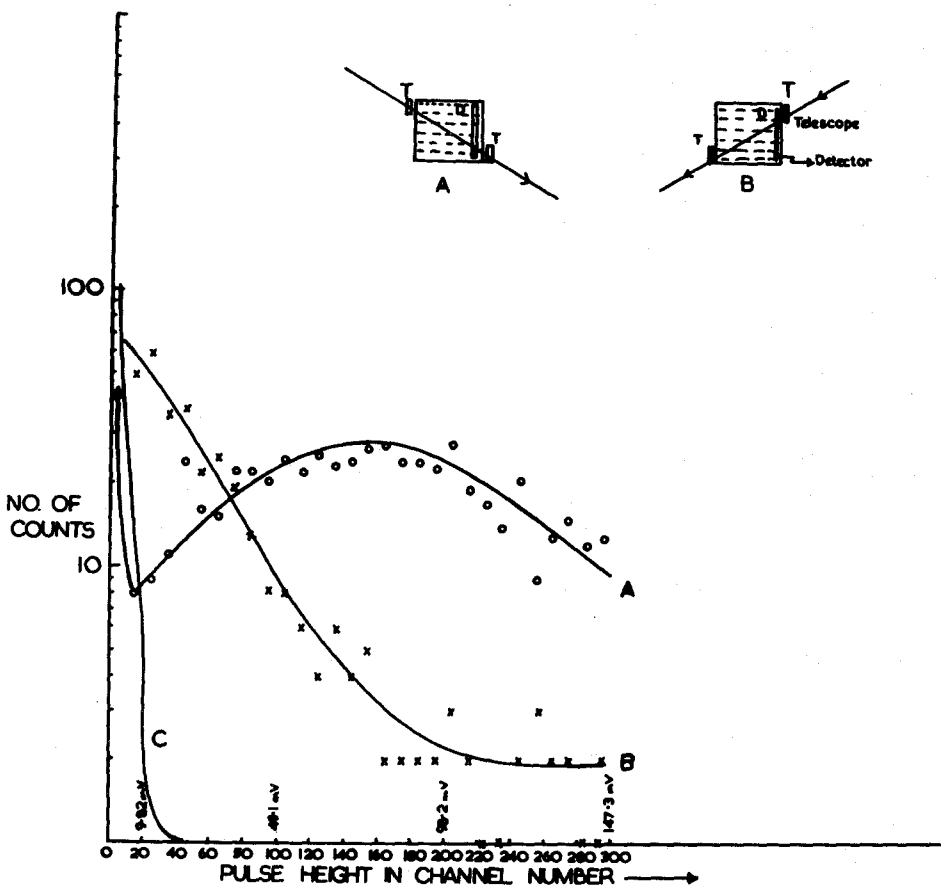

A→ MIXED CERENKOV PULSES FROM THE 4 LIGHT COLLECTORS IN POSITION A OF THE TELESCOPE.

FIG.6·13. B→ MIXED CERENKOV PULSES FROM THE 4 LIGHT COLLECTORS IN POSITION B OF THE TELESCOPE.

C→ NOISE DISTRIBUTION.

*[CURVES ARE FOR EQUAL NO. OF TRIGGERINGS]

(tubes 2 and 3) are found to be 19.64 ± 3.5 mV and 18.66 ± 3.5 mV respectively. The most probable value from the four mixed pulses is 68.7 ± 5 mV.

A theoretical estimate for the relative photon collection efficiency of the 4 tubes for Cerenkov radiation from a symmetrically passing fast muon showed that the collection efficiency of the two outer tubes (tube 1 and 4) should be about 48.5% of that of the two inner tubes. The observed value of this ratio is about 53.9%. Thus, within experimental error, the observed proportion of the most probable values for the 4 tubes are in good agreement with the expected results.

Next, the telescope was set so as to cover one of the tubes. Thus, some of the muons passing through the telescope would also traverse the tube. The output pulses were recorded in an oscilloscope (Tektronix) triggered by the telescope. The histogram in fig. 6.14 shows the experimental results. In addition to the first peak due to Cerenkov radiation, the distribution indicates a second peak around 200 mV. Considering the area covered by the tube inside the telescope, and the proportion of the number of pulses in the second peak with respect to the total number of pulses, it is quite reasonable to attribute the second peak to the particles passing directly through the tube. It was not possible to carry this run with the PHA since the latter added up all pulses above 300th channel-

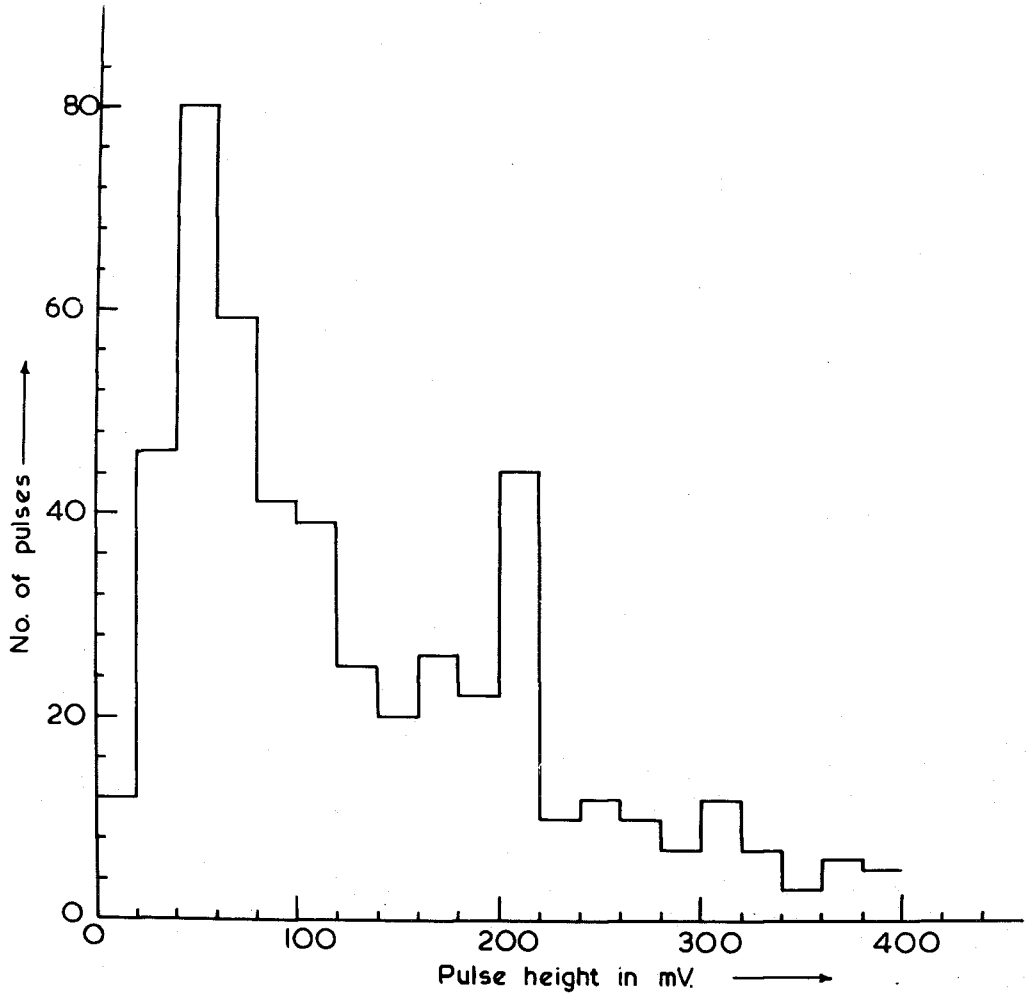

Fig.6·14. Cerenkov pulse height distribution in C.R.O. from a single light collector triggered with telescope in position A.

making the interpretation very difficult. So as to eliminate any personal bias, this series of observation was repeated by another worker, and was found to substantiate the previous results.

Next, the telescope was set so as to select muons traversing the tank in different angles i.e. having different path lengths in water. The added pulses were recorded in the PHA. The following table shows the variation of the added most probable pulse height from the 4 tubes with direction of motion of the muons in the tank.

Angle with the line of symmetry	Most probable pulse height.
0^{o}	68.0 ± 5 mV
14^{o}	69.5 ± 5 mV
26^{o}	71.5 ± 5 mV
36^{o}	70.2 ± 5 mV

From the above table, it is seen that although the path of a muon in water increases with inclination with respect to the line of symmetry, the overall most probable value does not change very much. That is to say, the effective number of photons remain the same within 5% of those due to a symmetrically passing particle. This apparently contradictory result may be interpreted as follows.

For a fast muon traversing the tank in an angle with the central line of symmetry, the path length inside the tank would be longer than that of a muon passing symmetrically. As such, for a fast muon having a longer path in water, one would naturally expect a greater number of photons at the detector level, and consequently a higher value of the most probable pulse height. But the Cerenkov radiation from an inclined muon will undergo reflections at the side mirrors. Moreover, increase in path length also involves increase in absorption of the emitted Cerenkov photons. These two factors will reduce the apparently expected increase in the number of photons. So the number of useful photons will not change very much - for muons having slightly varying path length inside the tank.

6.6 Directional Properties of the Counter:-

The directional property of the counter was tested by using the telescope and cosmic ray muons. The telescope was set in order to detect muons from two different directions. First, (say position A) to select only particles in the forward direction so that the Cerenkov cone is directed towards the collector system. Secondly, (say position B) the telescope was set to select particles going in the opposite direction so that the Cerenkov cone diverges away from the collector system.

The four mixed Cerenkov pulses in the two positions of the telescope were recorded in the PHA, the latter being triggered by the telescope coincidence pulses. The mixed pulses, when the PHA was triggered randomly, were also recorded for comparison.

The results are shown in fig. 6.13. It can be seen from the above figure that only in position A of the telescope, the graph shows a definite peak, indicating thereby that the counter is acting as a directional one. The graph in the position B is much higher than that in random coincidences. This means that some Cerenkov photons in the position B are also detected by the collecting system - probably due to the reflections inside the tank. Nevertheless, its directional property is well-preserved.

6.7 Conclusion:-

From the above analytical description of the working of the counter, it can be reasonably concluded that the counter constructed has the desired directional property. The response of the counter for particles of slightly varying path lengths in water is uniform within 5%. The accuracy may be improved further if the actual direction of the particle through the tank is known.

The counter, as it stands, should be quite suitable to investigate the relative Cerenkov radiation loss of cosmic

ray particles with an accuracy of better than 5%, if the direction of the particle is precisely known.

CHAPTER 7

THE EXPERIMENTAL RESULTS

7A Results on the Ionization Loss of Muons in a Plastic Scintillator:

7A (a) The Scintillation Counter.

The scintillation counter S2 (see fig. 5.5a) was used for investigating the ionization loss of cosmic ray muons in a phosphor. The dimensions of the counter are given in table 5.1. The response of the counter and its other details will be given elsewhere. (I.S. Jones, M Sc. thesis, Durham, 1967 or 1968). Only a brief description of this part of the experiment along with the main results will therefore be given here.

The electrical connections of the counter are described earlier in chapter 5 section 3C. The scintillation pulses were properly attenuated so as to accommodate both the scintillator as well as Cerenkov pulses on the same screen of the oscilloscope. The stability of the electronics was further checked by dividing the whole set of data into five successive groups in time, each containing approximately equal numbers of events. The median pulse heights among the groups were found to agree to within $\pm$ 3%.

Since the counter S2 was very near the magnet, the

photomultiplier response for the two polarities of the magnet was checked several times during the whole run of the experiment. For this, the counting rates of the two photomultipliers were examined for different field directions, positive, negative, zero, and then reverse direction again, for the same magnet current. The rate with zero field was slightly higher than those with the field on. There was no significant difference in the counting rates for positive and negative field directions.

7A (b) The Experimental Data:-

As mentioned earlier in chapter 5, section 6b, the pulses from the scintillation and Cerenkov counters were recorded simultaneously on the oscilloscope film. For measuring the pulses, the film was projected on to a drawing of the oscilloscope graticule and the heights of pulses in millivolts were recorded. The frames on the oscilloscope film were correlated with the corresponding frames on the spectrograph film by means of the clocks on the films.

Of the total 2037 events recorded from the spectrograph films, only 1822 events were finally selected and used in the ionization loss experiment. In table 7.1, the pulse heights of all the selected particles are reproduced. The frequency distribution of pulse heights for particles of all momenta is shown in fig. 7.1.

Table 7.1

Frequency of Pulse Heights for Different Momentum Cells

Cell	Mid Value of Scintillator Pulse Height, in mV.													
	25	35	45	55	65	75	85	95	105	115	125	135	145	155
80 - 42	0	1	4	5	2	11	2	6	7	2	1	5	0	3
42 - 18	0	3	3	10	18	18	18	15	17	7	8	12	7	6
18 - 12	0	3	3	7	10	17	9	17	11	14	15	4	5	3
12 - 8	1	5	2	17	18	15	18	28	8	10	11	6	5	5
8 - 6	0	2	3	6	5	19	17	22	16	8	11	10	5	6
6 - 4	0	2	8	15	16	21	29	33	8	20	9	8	5	7
4 - 2	0	9	18	27	36	45	42	39	26	27	15	12	9	11
2 - 1	0	7	9	21	31	31	38	42	22	12	12	7	8	9
1 - 0.5	2	3	4	11	10	10	14	20	15	13	7	5	1	4
< 0.5	0	2	6	14	11	16	12	17	7	6	3	5	2	5

Table 7.1 (Continued)

Frequency of Pulse Heights for Different Momentum Cells

Momentum Cell (GeV/c)	Mid Value of Scintillator Pulse Height, in mV.													
	165	175	185	195	205	215	225	235	245	255	265	275	285	295
80 - 42	1	3	2	0	0	1	0	2	0	0	0	0	0	0
42 - 18	2	4	3	2	3	3	1	1	1	1	1	1	0	2
18 - 12	1	0	2	1	0	1	1	1	2	1	1	1	0	0
12 - 8	1	1	1	1	1	2	1	2	2	0	1	0	0	2
8 - 6	3	2	1	3	2	1	3	1	1	0	1	1	1	2
6 - 4	10	2	4	2	3	3	1	0	2	1	0	0	0	1
4 - 2	5	6	6	4	2	5	2	1	0	4	2	2	0	0
2 - 1	7	15	5	2	1	4	2	1	2	4	0	3	1	1
1 - 0.5	1	5	2	2	1	3	0	1	1	2	2	1	0	0
<0.5	2	2	0	1	1	0	0	1	0	0	0	0	0	0

Table 7.1 (Continued)

Frequency of Pulse Heights for Different Momentum Cells

Mid Value of Scintillator Pulse Height, in mV.

	305	315	325	335	345	355	365	375	385	395	400
80 - 42	0	1	0	0	0	0	0	0	0	0	0
42 - 18	0	0	0	0	0	0	0	0	0	0	1
18 - 12	1	2	0	0	0	0	0	0	0	0	0
12 - 8	0	0	0	1	0	0	0	0	0	0	1
8 - 6	0	0	0	0	0	1	0	1	0	0	2
6 - 4	0	1	0	2	1	0	0	0	0	0	0
4 - 2	0	1	1	0	1	1	0	0	1	0	1
2 - 1	0	1	0	0	0	0	0	0	1	1	1
1 - 0.5	0	0	0	0	0	0	0	0	1	0	3
< 0.5	0	0	0	0	0	0	0	0	0	0	0

Fig 71 Frequency distribution of pulse heights for particles of 11 MeV/n (Scintillator).

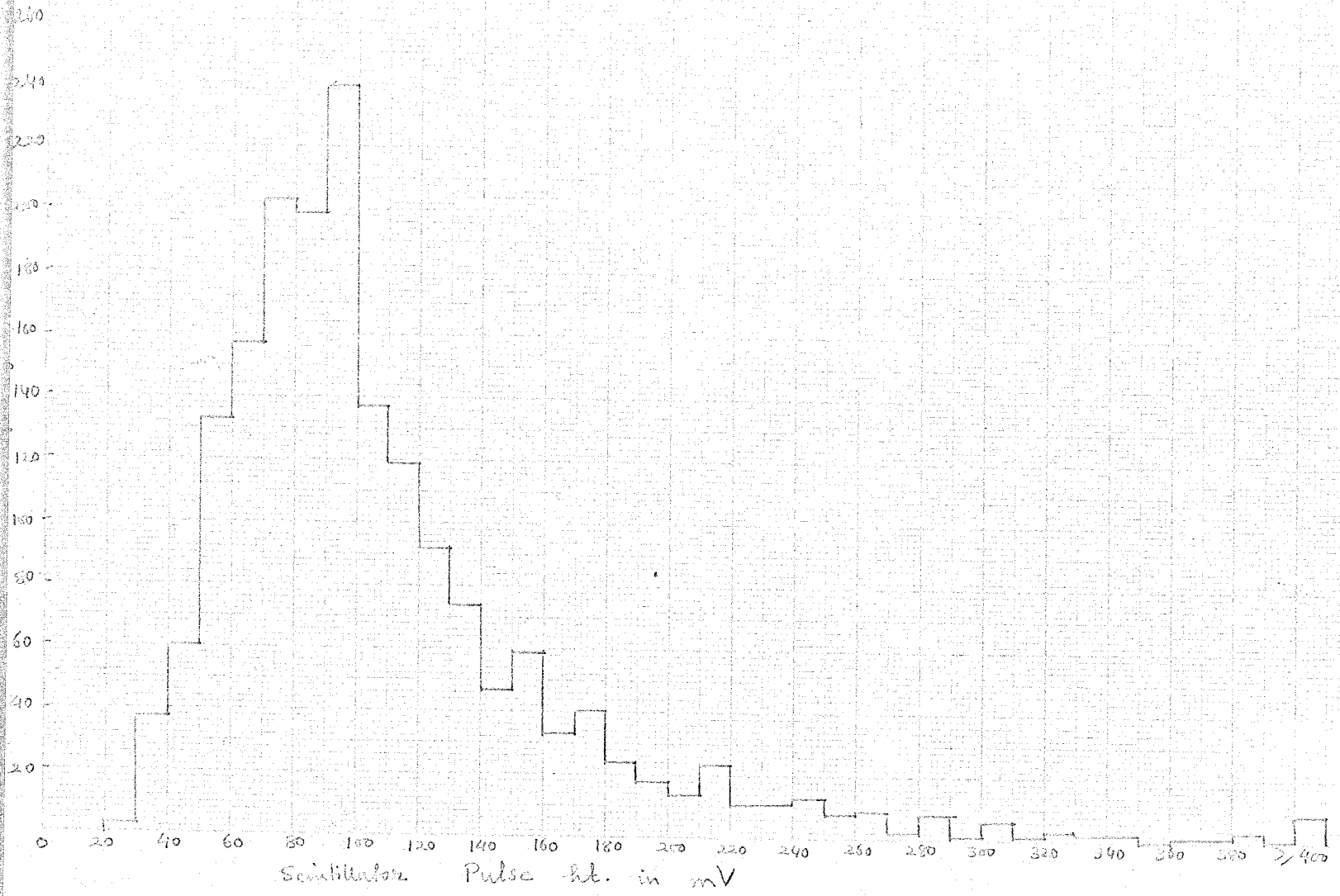

7A (c) The Resolution of the Peak of the Pulse Height Distributions:

If dh is the width at half-amplitude (fig. 7.1) and h is the pulse height corresponding to the peak position of the curve, the resolution R may be defined as $\frac{dh}{h} \times 100\%$.

The finite width comes from (a) the Landau effect, due to the statistical variations in the energy absorbed from the traversing particle by the phosphor,

(b) the statistical variation in the number of photo-electrons ejected from the photocathodes, and the variation in the number of electrons emitted from the various dynodes,

(c) the variation of the proportion of light collected from different regions of the phosphor,

(d) momentum distribution of the muons, (if indeed there is a momentum dependence) and

(e) the variation in the path length of the muons through the counter.

of these, the first two i.e. the Landau effect and the photomultiplier effect are the two main contributors to the resolution.

It can be shown that in a phosphor of thickness equal to that of the counter S2, the resolution due to the Landau effect is $\simeq$ 19%. Again, for an energy loss (mean value) equal to 4.5 MeV, the resolution due to the photomultiplier effect is $\simeq$ 20%. (The geometrical collection factor in

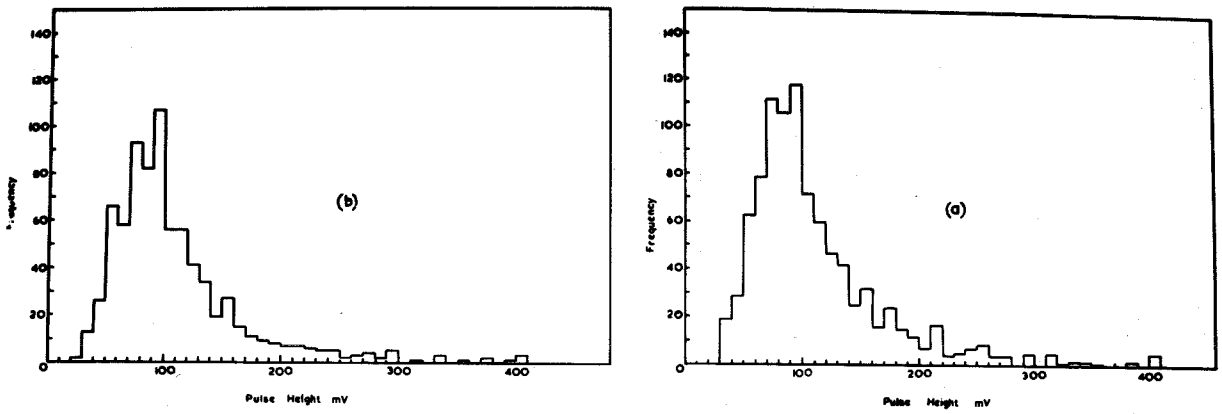

Fig 7·2 Scintillator pulse height distributions for (a) positive muons.
(b) negative muons

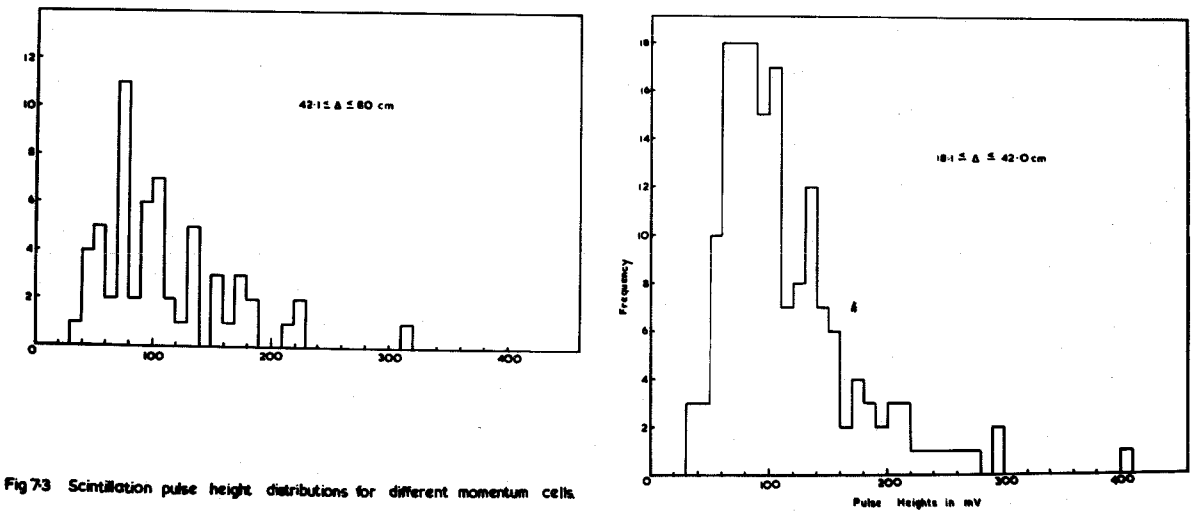

Fig 7·3 Scintillation pulse height distributions for different momentum cells

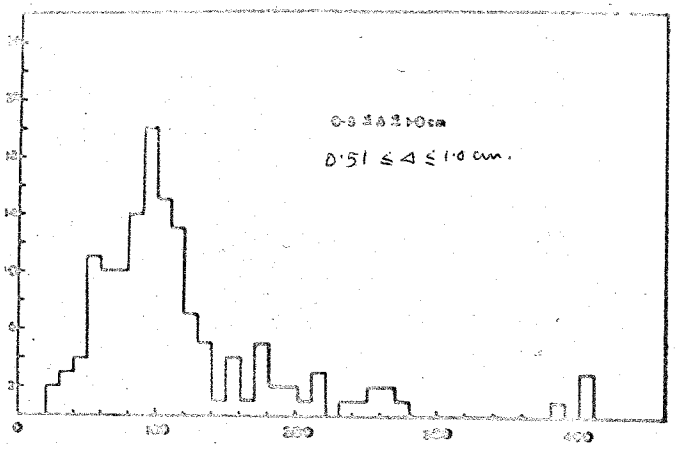

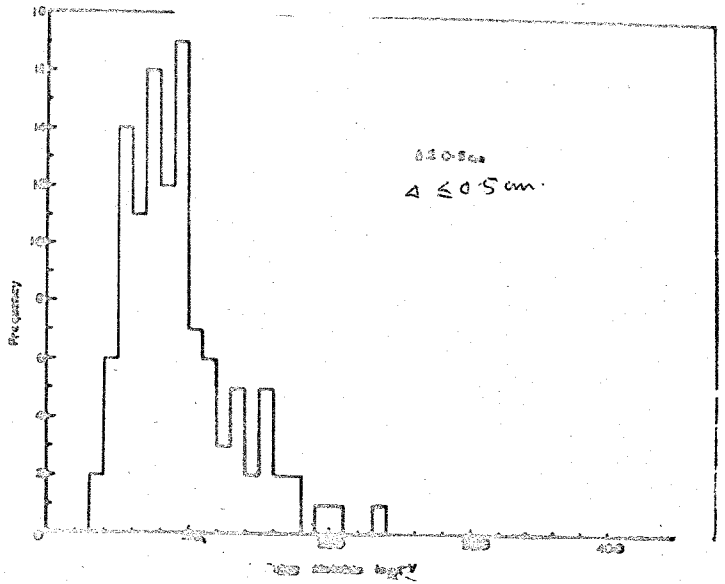

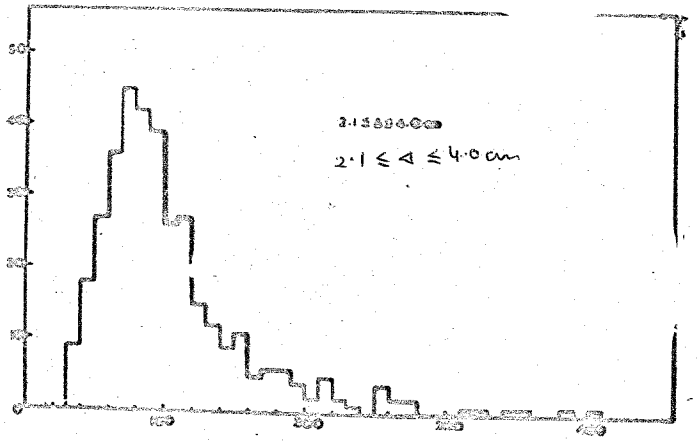

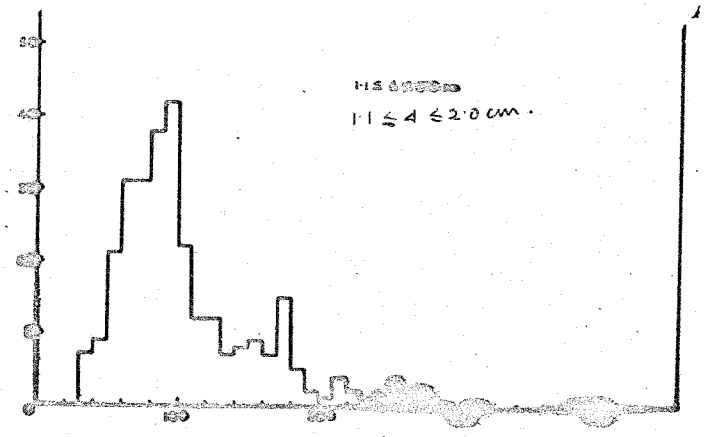

Fig 7.3 Scintillator pulse ht distributions for different momentum cells.

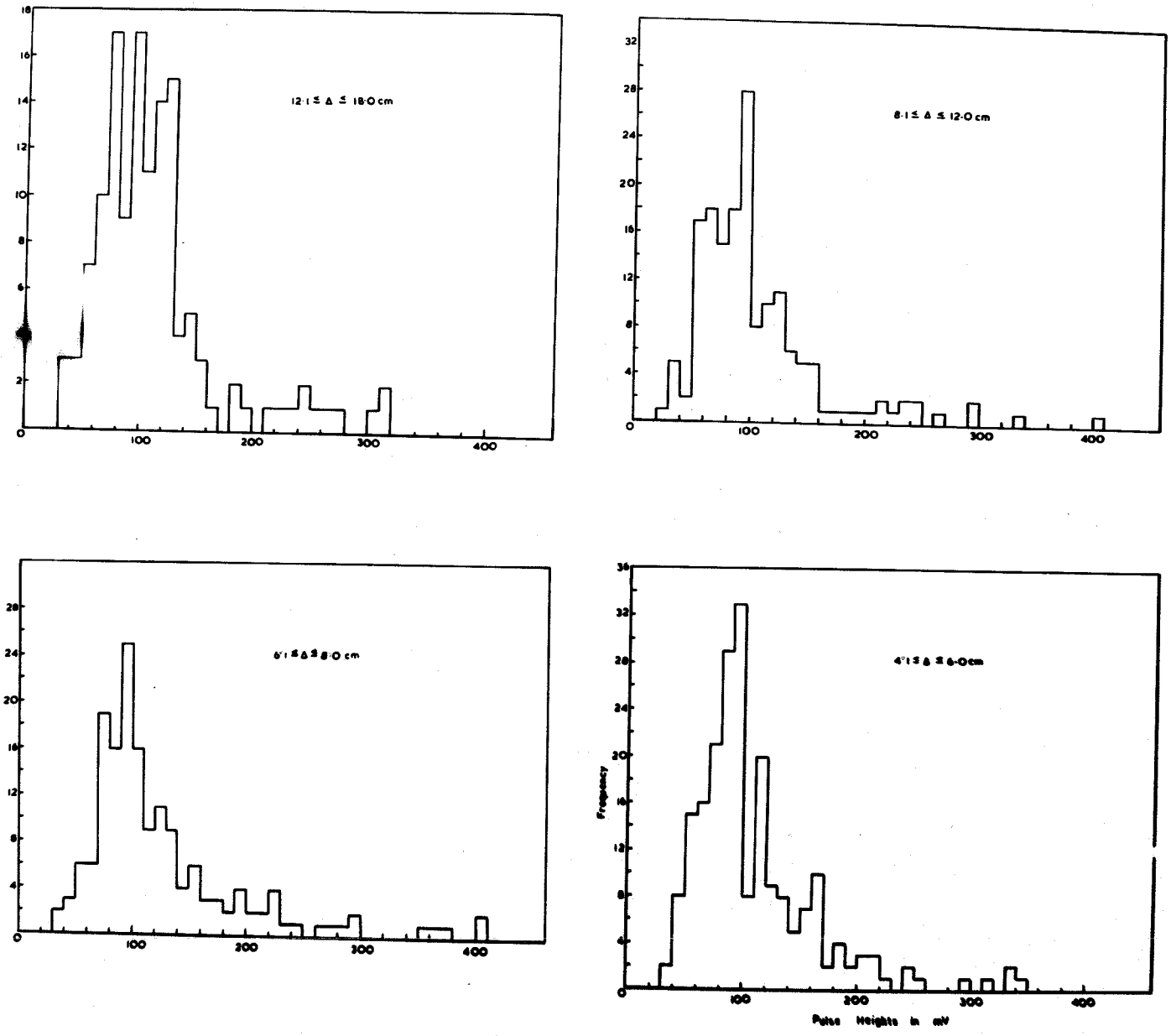

Fig 7·3 Scintillation pulse height distributions for different momentum cells

S2 $\simeq$ 0.08). The variation in response over the phosphor is $\simeq$ 8%.

Thus for a monoenergetic particle, the total resolution can be found by adding quadratically the above independent contributions and is equal to $\simeq$ 29%. The observed resolution is $35 \pm 3\%$ i.e. a value close to expectation.

7A (d) Pulse Height Distributions for μ^+ and μ^- Particles:

In fig 7.2, the pulse height distributions for positive and negative muons are shown. The most probable pulse heights of the two distributions have been calculated and will be discussed later.

7A (e) Grouping of the Data:

The pulses were grouped in momentum cells as shown in table 7.2. The frequency distribution of pulse heights for different momentum cell is shown in fig. 7.3.

Table 7.2:

Momentum Cells for Grouping of the Scintillator Pulses:

Cell Limits (cm)	Mean Momentum in the Cell (GeV/c)	No. of Particles
$42 < \Delta \leq 80$	0.355	59
$18 < \Delta \leq 42$	0.723	168
$12 < \Delta \leq 18$	1.50	133
$8 < \Delta \leq 12$	2.32	166
$6 < \Delta \leq 8$	3.18	163
$4 < \Delta \leq 6$	4.56	214
$2 < \Delta \leq 4$	8.04	361
$1 < \Delta \leq 2$	15.19	301
$0.5 < \Delta \leq 1$	30.48	144
$\Delta \leq 0.5$	98.6	113

7A (f) Analysis of the Data:-

The mode i.e. the most probable value of each distribution is the quantity of greatest physical interest. This is because in a skew distribution the most probable value, unlike the mean and the median, is insensitive to the infrequent high energy losses which give rise to the tail of the distribution. As such, the mode of a skew

distribution is a very useful parameter for assessing the relative magnitudes of energy loss for particles of different momentum groups, and has been used in the present experiment. Three different methods were used to calculate the peak positions of the distributions:

(a) The Subjective Method:

In this method a histogram of the frequency of pulse heights for each momentum cell was plotted against the logarithm of the pulse height and a smooth curve was fitted to each of the log-normal distributions. Comparing the curves for all the distributions, a master curve was drawn and the peak position was marked. Then, the distributions were submitted to ten independent observers, each of whom found the peak position in each distribution by fitting the master curve. The mean of these ten values for each distribution was accepted as the peak position of that distribution.

(b) The Reciprocal Method:

In this method, the cumulative percentage frequencies (i.e. the number of pulses of height less than the middle value of each interval in a distribution expressed as a percentage of the total number of pulses with a cut off at 200 mV) were plotted on "arithmatical probability" paper

against the reciprocals of the mid-points of the pulse height intervals for each distribution. A straight line was drawn using the method of least squares, which gave reasonable fitting between 10% and 90%. The peak of the distribution was given by the pulse height corresponding to the ordinate 50. (Barnaby 1961)

(c) The Area Method:

The peak position of each distribution was also estimated by measuring with a planimeter the areas on each side of the maximum ordinate. For this, a master histogram was drawn combining all the data. The tail of the distribution was artificially cut-off at 200 mV. The area on the cut-off portion was $\simeq 8\%$ of the total area under the curve. The maximum ordinate divided the remaining areas in the ratio 1 : 1.42. Barnaby (1961) found that the method was insensitive to the position of the cut-off provided the area removed was not more than 20% of the total area.

The peak position of each distribution was then found by applying the same cut-off and estimating the ordinate which divided the remaining area in the proportion 1: 1.42, by the method of successive approximations.

The results obtained from the three methods are tabulated in table 7.3. The errors on the most probable

Table 7.3

The Mean, the Median, and the Mode of the Scintillator Pulse Height Distrubtions:

Cell in cm	Mean in mV	Median in mV	Mode in mV by			Normalised Mode in MeV
			Reciprocal method	Subjective Method	Area Method	
$42 < \Delta \leq 80$	99.55 ± 5.5	94.2 ± 5.5	92.5 ± 3.4	80.86 ± 3.4	84.0 ± 3.4	4.41 ± 0.19
$18 < \Delta \leq 42$	100.62 ± 4.9	94.3 ± 4.9	90.5 ± 2.5	86.0 ± 2.5	88 ± 2.5	4.70 ± 0.14
$12 < \Delta \leq 18$	97.38 ± 4.1	97.4 ± 4.1	88.5 ± 2.5	84.88 ± 2.5	89 ± 2.5	4.67 ± 0.14
$8 < \Delta \leq 12$	92.19 ± 3.9	90.2 ± 3.9	84.5 ± 2.2	81.88 ± 2.2	83 ± 2.2	4.5 ± 0.12
$6 < \Delta \leq 8$	103.7 ± 4.2	97.9 ± 4.2	93.33 ± 2.1	90.33 ± 2.1	92 ± 2.1	4.93 ± 0.12
$4 < \Delta \leq 6$	99.27 ± 3.2	92.6 ± 3.2	86.0 ± 1.8	83.35 ± 1.8	86 ± 1.8	4.53 ± 0.10
$2 < \Delta \leq 4$	94.08 ± 2.5	87.97 ± 2.5	85.0 ± 1.3	78.22 ± 1.3	81 ± 1.3	4.30 ± 0.07
$1 < \Delta \leq 2$	101.0 ± 5.0	90.6 ± 5.0	84.5 ± 1.6	81.22 ± 1.6	84 ± 1.6	4.46 ± 0.09
$0.5 < \Delta \leq 1$	97.8 ± 5.04	95.3 ± 5.04	84.5 ± 2.2	83.44 ± 2.2	89 ± 2.2	4.59 ± 0.12
$\Delta \leq 0.5$	88.4 ± 3.6	85.4 ± 3.6	81.0 ± 2.8	76.4 ± 2.8	79 ± 2.8	4.20 ± 0.15

Table 7.3 (Continued)

	Mode in mV by		
	Reciprocal method	Subjective method	Area Method
μ^+	83.37 ±2.2	83.0 ±2.2	86 ±2.2
μ^-	81.87 ±2.8	81.80 ±2.8	86 ±2.8

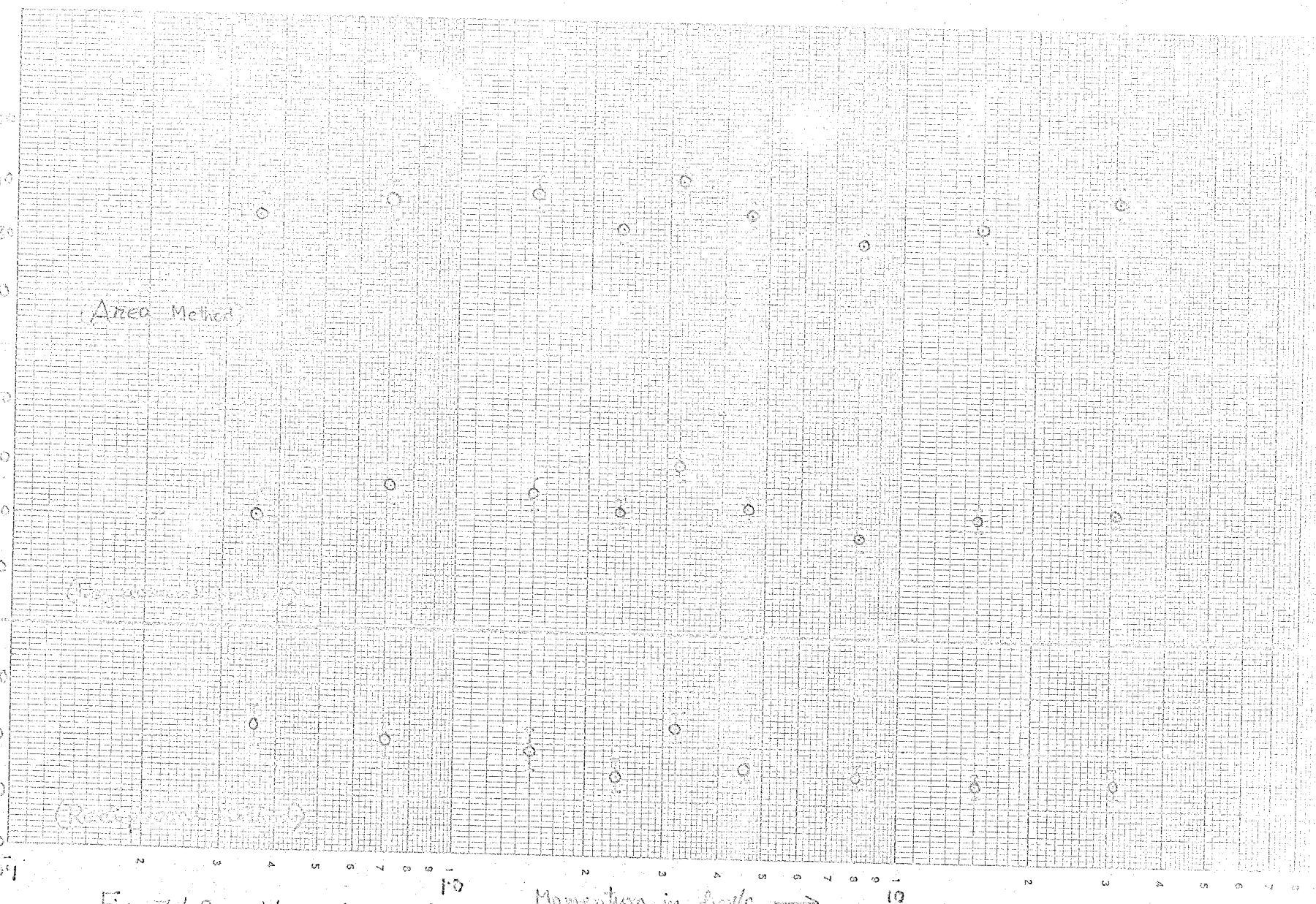

Fig 7.4a. Variation of the modes of Scintillator pulse height distribution vs. momen

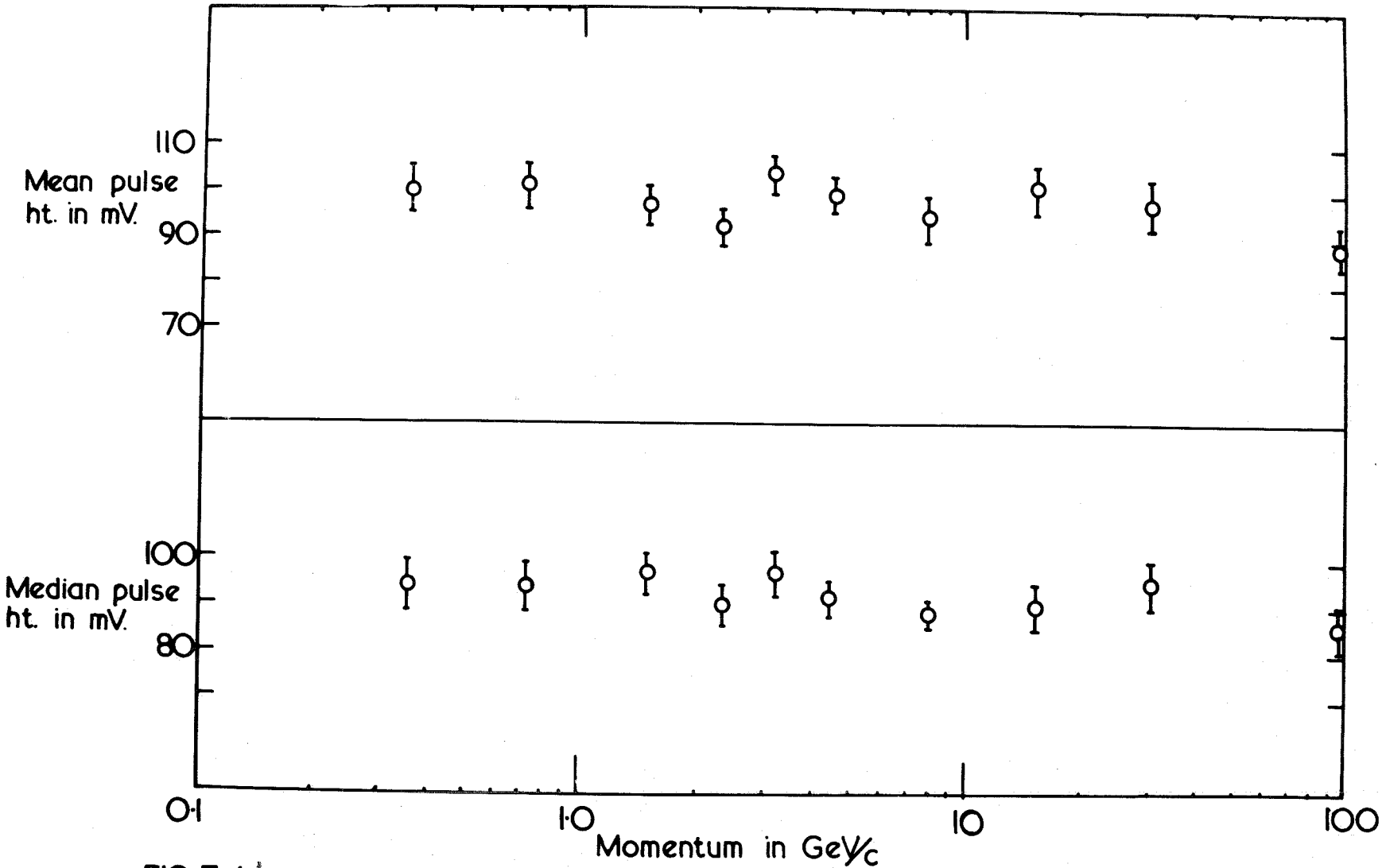

FIG. 7·4.b Variations of mean & median of the scintillator pulse ht. distributions as a function of muon momentum.

pulse heights were estimated by assuming that they would be similar to the error on the mean of a normal distribution. The error on the mean $= \frac{\text{full width at half-height}}{2.4\sqrt{N}}$,

where N is the number of events in the distribution (up to 200 mV). (West, 1962).

7A (g) The Results

The arithmetic mean, and the median have also been calculated for each distribution and the results for all three are shown in fig. 7.4 a and b. The nature of the variation with momentum for all the three parameters i.e. mean, median, and mode, is seen to be similar. (fig. 7.4 a and b).

The values of the modes obtained by the three methods are not equal, and as such they have not been combined together, although all are given in table 7.3. Only the results obtained by the subjective method (which seemed to have less error, being observed by ten people) are used for comparison with the theoretical prediction.

In fig 7.5, the observed values normalised to the mean value of the theoretical curve in the momentum range 1 - 100 Gev/c, given by Sternheimer for ionization loss in plastic scintillator of thickness 2.58 gm cm^{-2} are shown.

Above 1 GeV/c i.e. from about the onset of the density effect, the slope of the experimental curve was calculated

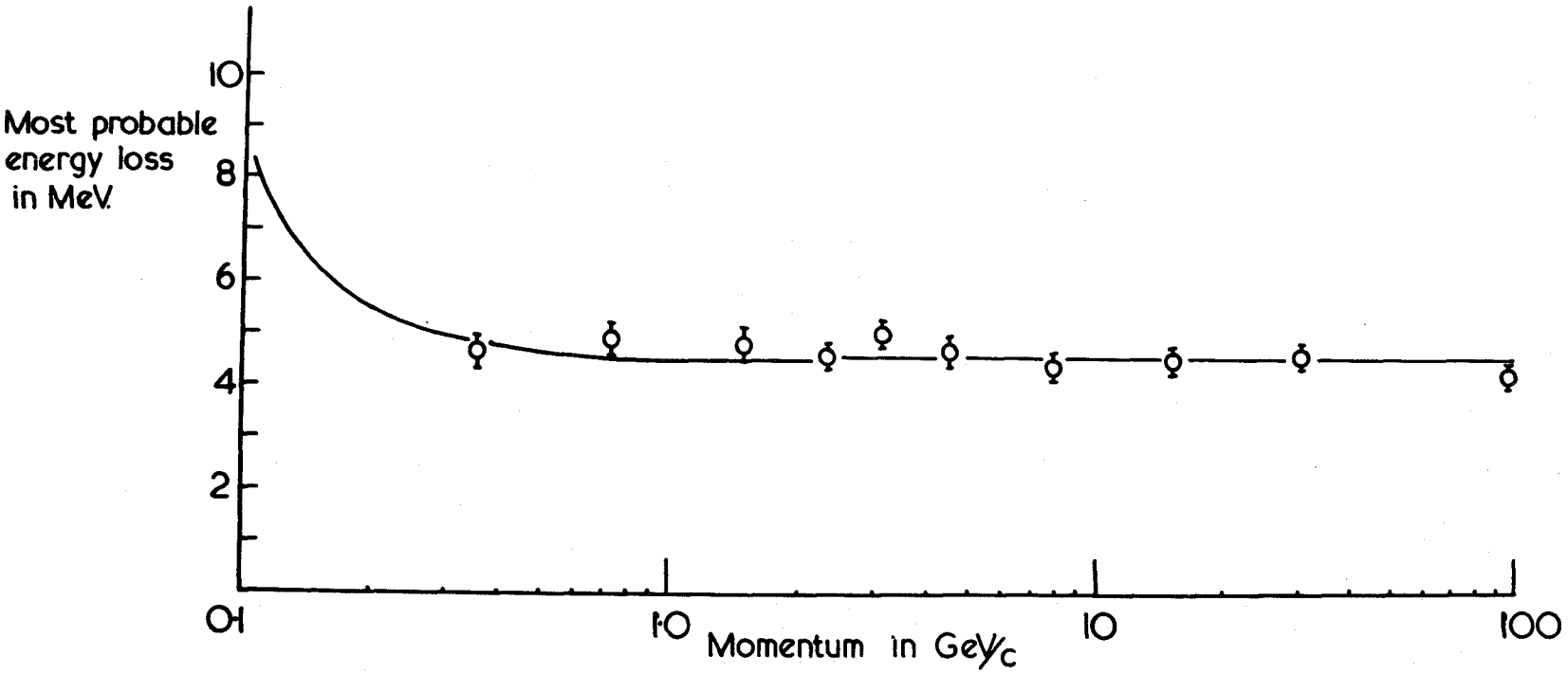

FIG. 7.5. The most probable energy loss due to ionization as a function of muon momentum.

by fitting a straight line by the method of Least squares through all experimental points above 1.5 GeV/c. The resultant curve has a slope of - 0.648 ± 0.38, giving an overall decrease of

(3.6 ± 1.8) % per decade of momentum

in the theoretically predicted plateau region. The slope for the points above 8 GeV/c was also calculated separately and a decrease of about (2.7 ± 1.7) % was found.

The most probable pulse heights for positive and negative muons were also calculated by the three methods and are shown in table 7.3. The ratios of the most probable pulse heights as obtained by the three methods are 1.018 ± 0.035, 1.015 ± 0.035 and 1.00 ± 0.035 respectively, the mean being 1.011 ± 0.035. Thus there is no significant difference in the ionizing capacity of the particles of the two kinds.

7A ($\hbar$) Discussion.

The main aim of the present experiment was to test the Tsytovich prediction according to which there should be a decrease in ionization loss at high energy ($\gamma > 100$) by about 7 to 10% below the Fermi plateau. As such the present discussion will be mainly confined to the results in the momentum range 10 GeV/c ($\gamma \simeq 100$) to 100 GeV/c ($\gamma \simeq 1000$).

The results of the present experiment show a decrease of 2.7% ± 1.7% of the energy loss over the momentum range

10 - 100 GeV/c. This decrease ($\simeq$ 2.7%) is not significant and is certainly much less than that predicted by Tsytovich. In other words, our results do not support the Tsytovich prediction. Rather, the present result is not inconsistent with Sternheimer's theory according to which the ionization loss should show a plateau value above a momentum of 10 GeV/c (see chapter 2, section 6).

The only other comparable measurements at high energy in a plastic scintillator are those of Crispin and Hayman (1964). These workers, using cosmic ray muons, found an indication of a small increase ($\approx$ 3% $\pm$ 1%) of the most probable energy loss at high energy ($\simeq$ 100 GeV/c).

It is valid to take a mean of the values in the two experiments in view of the fact that the type of scintillator used was identical and the instrument and method of analysis was very similar. The result is that the relative increase above 10 GeV/c is 0.15 $\pm$ 2.3%, a value even more clearly in agreement with Sternheimer expectation.

Recently Aston et al. (1965) studied the ionization loss of cosmic ray muons using a liquid scintillator. Their results also confirm the existence of density effect up to the highest momentum ($\simeq$ 250 GeV/c) measured. They too did not find any evidence for a decrease of energy loss at high energy as suggested by Tsytovich.

7B The Results on the Cerenkov Radiation Loss:

7B (a) Stability of the Electronics:

Before analysing the final data, a further test for the stability of the counter electronics was carried out. For this, the events were divided into five groups A, B, C, D and E, in sequence of running time of the spectrograph, each group having approximately equal number of events. Then, the median of the pulse height distributions for each group was calculated with a cut off at 400 mV. The results are tabulated below.

Table 7.4 Median Values of Pulse Heights in Different Groups:

Group	Median in mV
A	103.8 $\pm$ 5.5
B	103.1 $\pm$ 5.2
C	102.2 $\pm$ 5.7
D	100.2 $\pm$ 5.7
E	99.0 $\pm$ 5.9

It is found that there is a small systematic decrease of pulse height with time. This is probably due to the ageing of the transistors. Since the particles of all momenta are included in each day's run, this decrease should not affect the actual energy loss values relative to each

other. As such no correction was applied to the basic data.

The pedastal from the amplifier and gate circuit was checked by taking photographs on the oscilloscope and simulating the actual working condition of the spectrograph but without any Cerenkov or scintillator input pulse. The analysis of the film showed that the pedastal was negligibly small (less than 5 mV).

7B (b) The Experimental Data:

The methods of recording and the measurement of the Cerenkov pulses have been described already.

Altogether 1765 events were found useful for this part of the experiment. In table 7.5, the pulse height of all the selected particles are tabulated. The frequency distribution of particles of all momenta is shown in fig.7.6.

7B (c) The Resolution and Shape of the Cerenkov Pulse Height Distribution:

The finite width of the Cerenkov pulse height distribution (fig. 7.6) arises due to

(a) the photomultiplier effect,

(b) the variation in the path length of muons in water in the counter and variation of position of the tracks with respect to the quartz tubes,

and (c) a possible component due to the momentum distribution of muons.

Table 7.5

Frequency of Cerenkov Pulse Heights for Different Momentum Cells.

Cells in cm.	Mid-value of Pulse Height in mV.												
	10	30	50	70	90	110	130	150	170	190	210	230	250
$80 \geq \Delta > 42$	0	5	8	5	14	5	3	4	3	2	1	2	2
$42 \geq \Delta > 18$	0	22	27	24	17	16	10	9	3	7	6	7	9
$18 \geq \Delta > 12$	0	5	23	11	20	12	11	6	6	7	3	7	5
$12 \geq \Delta > 8$	0	16	26	20	10	12	13	13	10	6	3	3	3
$8 \geq \Delta > 6$	0	20	24	23	15	19	8	12	7	6	10	4	2
$6 \geq \Delta > 4$	2	15	37	23	14	13	13	13	9	8	10	2	4
$4 \geq \Delta > 2$	1	27	47	36	30	23	22	20	11	13	12	11	11
$2 \geq \Delta > 1$	0	21	57	32	31	22	21	31	6	10	10	7	8
$1 \geq \Delta > 0.5$	0	15	28	13	10	13	9	6	6	5	2	3	6
$\Delta \leq 0.5$	0	4	18	11	8	8	10	7	2	5	4	2	2

Table 7.5 (Continued)

Frequency of Cerenkov Pulse Heights for Different Momentum Cells.

Cells in cm	Mid-value of Pulse Height in mV.											
	270	290	310	330	350	370	390	410	430	450	470	490
$80 \geqslant \Delta > 42$	0	0	1	1	0	0	0	0	0	0	0	4
$42 \geqslant \Delta > 18$	4	1	2	3	0	3	1	1	1	1	0	7
$18 \geqslant \Delta > 12$	1	0	2	0	1	1	1	0	0	0	0	5
$12 \geqslant \Delta > 8$	3	6	1	1	0	0	0	0	1	2	0	5
$8 \geqslant \Delta > 6$	3	2	0	2	3	3	1	0	0	1	0	5
$6 \geqslant \Delta > 4$	6	5	7	2	5	7	2	3	0	3	2	8
$4 \geqslant \Delta > 2$	10	5	3	10	4	5	4	2	3	2	1	5
$2 \geqslant \Delta > 1$	7	5	2	6	1	4	0	2	2	0	1	10
$1 \geqslant \Delta > 0.5$	7	3	2	3	0	1	0	1	0	1	0	2
$\Delta \leqslant 0.5$	2	2	2	3	0	1	1	0	1	0	0	17

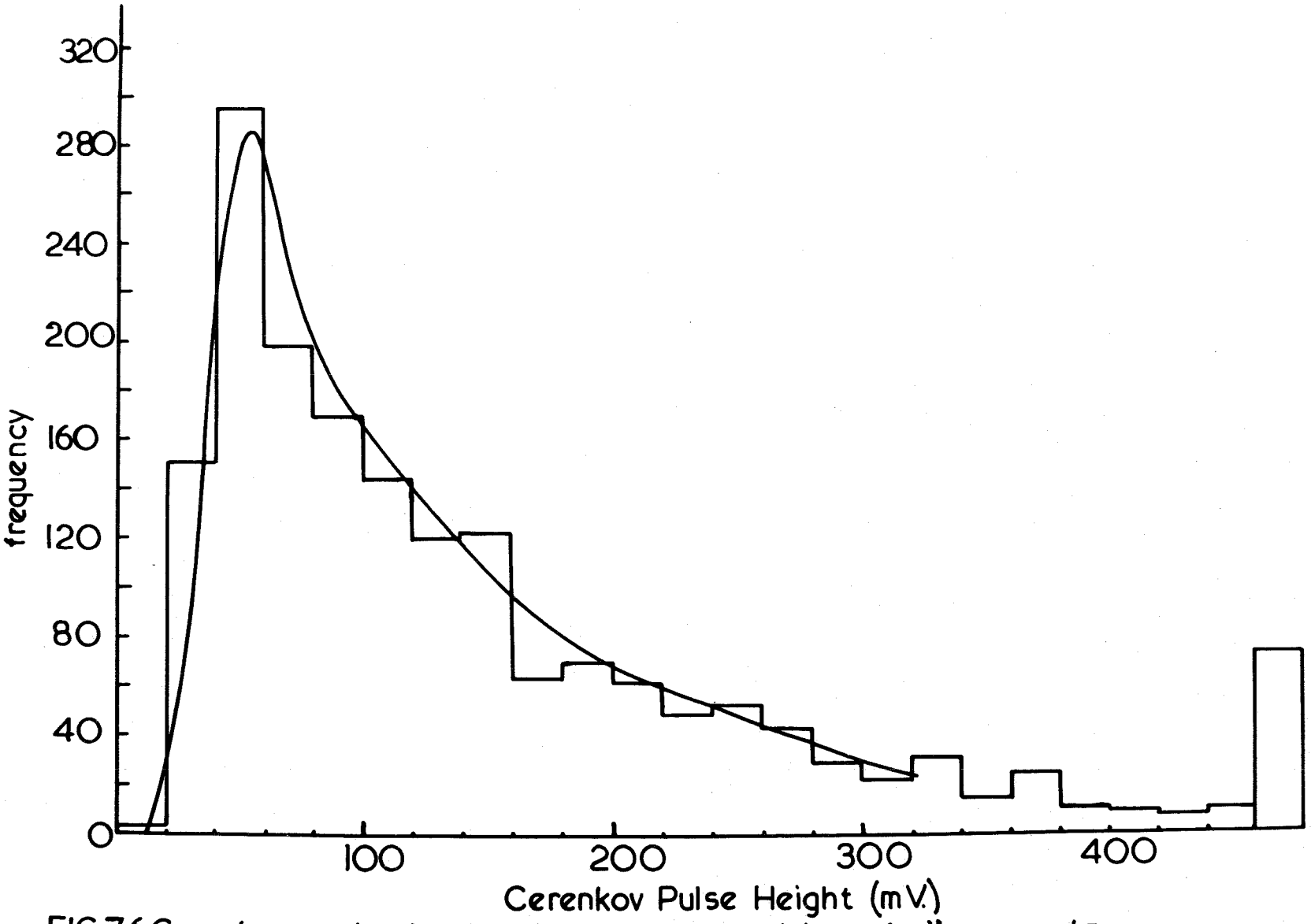

FIG. 7·6 Cerenkov pulse ht. distribution for particles of all momenta

Of these, the photomultiplier effect gives the single largest contributor. This may be estimated as follows. Assuming the pulse heights to follow a Gaussian distribution, the pulse height resolution (Garlick and Wright, 1952; Mullard Manual on Photomultiplier Tubes) in a photomultiplier tube is given by

$$R = \frac{2\sqrt{2 \ln 2}}{\sqrt{f N}} \cdot \sqrt{\frac{\delta}{\delta - 1}} \quad 100\%$$

where N = number of electrons from the photocathode

f = collection efficiency of the cathode/first dynode $\simeq 1$

δ = Average electron multiplication per dynode stage $\simeq 4.3$

therefore,

$$R = \frac{236}{\sqrt{N}} \quad 1.3\%$$

For 18 photoelectrons, $R \simeq 72.3\%$.

The variation in response over the whole counter contributes about 5% to the resolution. Thus for a mono-energetic muon, the total resolution is $\simeq 72.5\%$. This may be compared with the observed resolution $\simeq 84.1\% \pm 4\%$.

The pulse height distribution, as can be seen from fig. 7.6, is a skew distribution with a long tail. When the number of photo-electrons involved is small, as in the present case, the theoretical noise curve obeys a distribution intermediate between a Gaussian and a Poisson distribution.

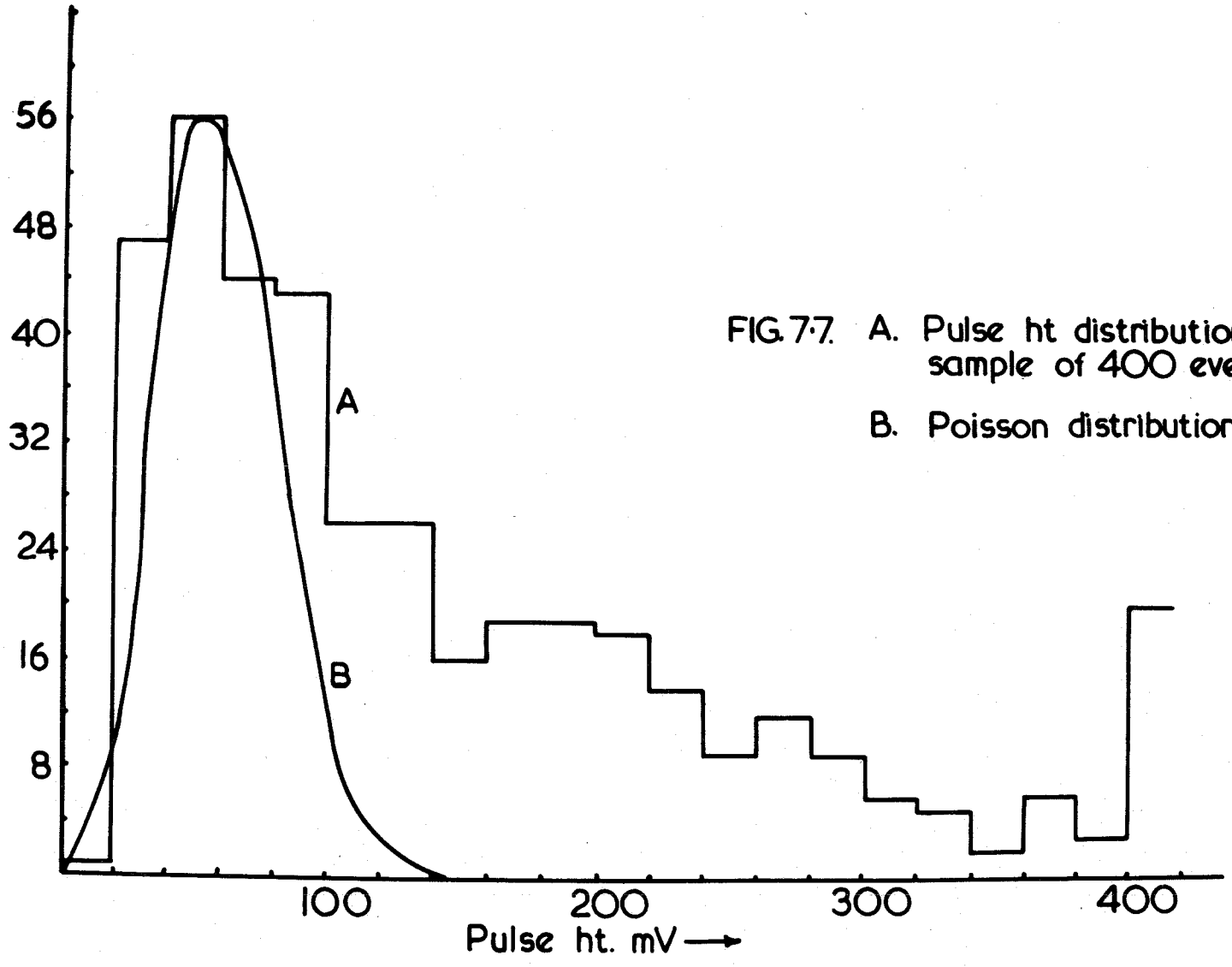

FIG. 7·7. A. Pulse ht distribution for a sample of 400 events.

B. Poisson distribution for 18 p.e.

(Breitenberger, 1956). In fig. 7.7, a Poisson distribution for 18 photoelectrons normalised to the peak position of the pulse height distribution for a sample of 400 events is shown. The observed long tail of the distribution is clearly of a different origin and is considered to be due to the effect of knock-on electrons as indicated in chapter 3, section 5.

7B (d) The Pulse Height Distribution for Positive and Negative Muons:

The pulse height distributions for positive and negative muons are shown in fig. 7.8. The most probable pulse heights of the two distributions are (43.88 ± 0.51) mV, and (43.37 ± 0.87) mV respectively, and their ratio is equal to 1.012 ± 0.036.

7B (e) Grouping of the Data:

As in the ionization loss experiment, the Cerenkov pulses were also grouped into momentum cells, and the results are shown in table 7.6.

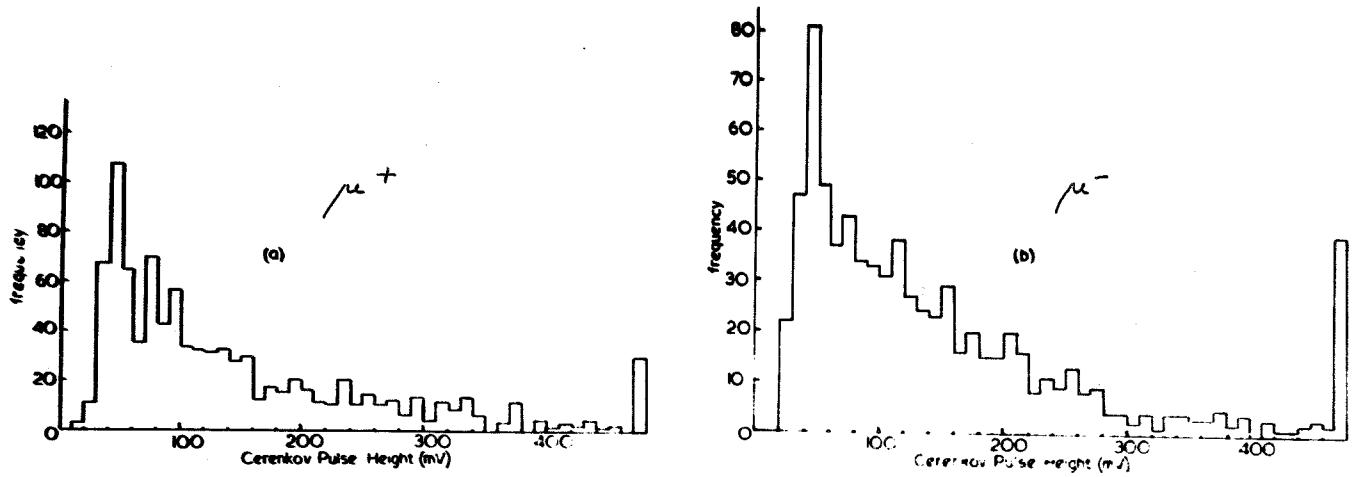

Fig 7·8 Cerenkov pulse ht. distributions for (a) μ^+, (b) μ^-.

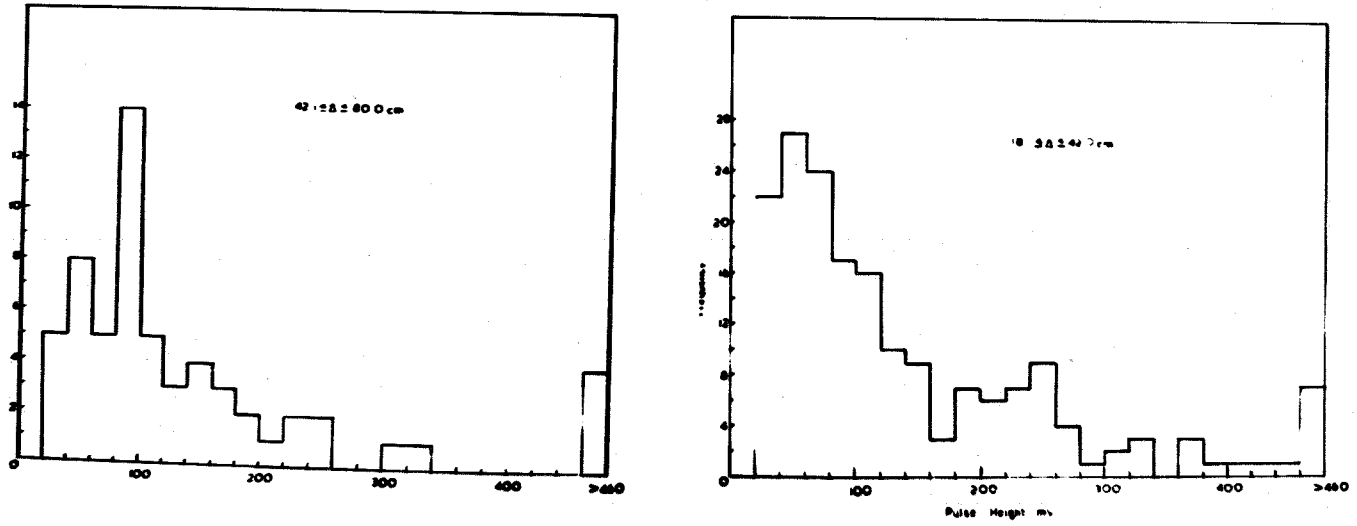

Fig 7·9 Cerenkov pulse height distributions for different momentum cells

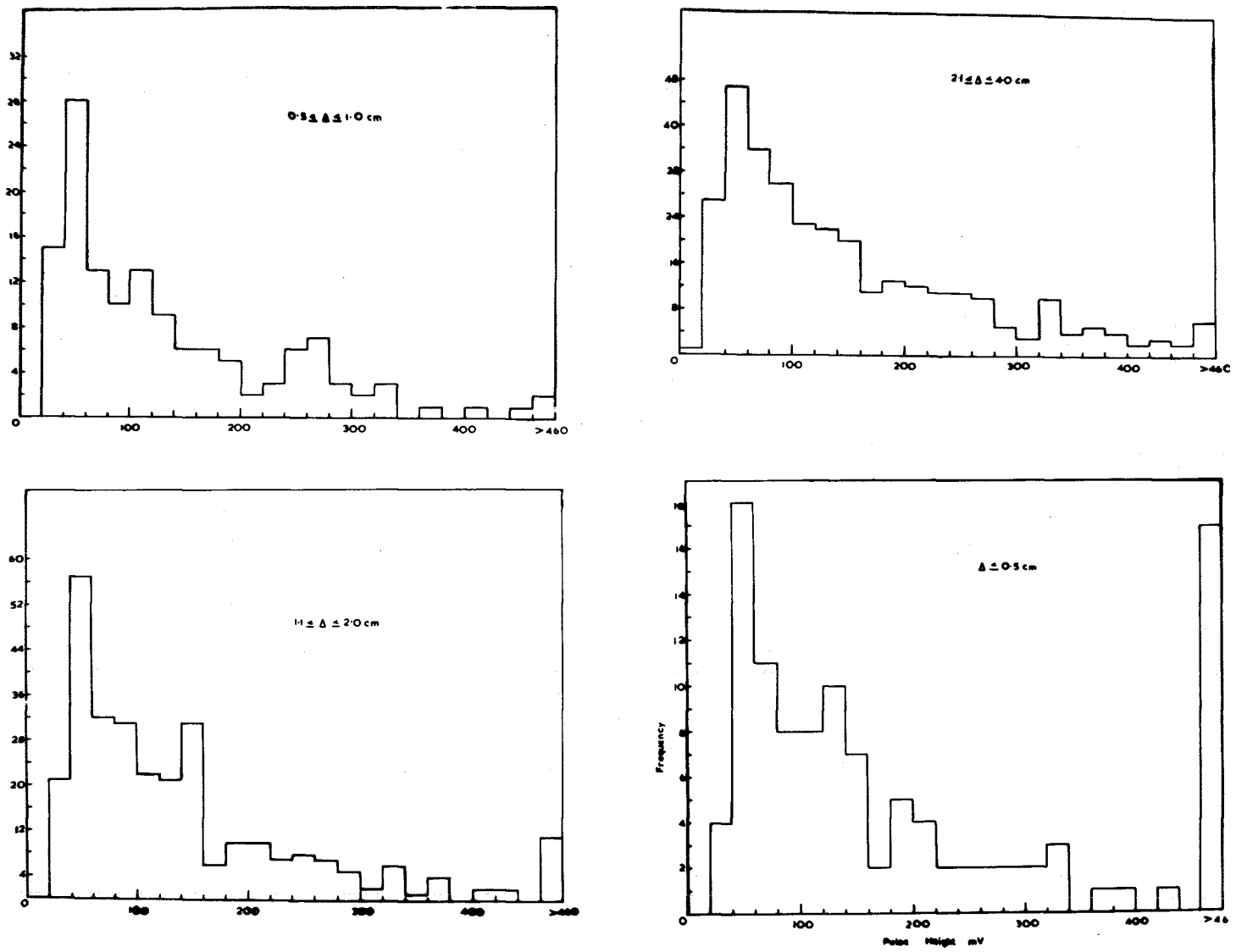

Fig. 7.9 Cerenkov pulse height distributions for different momentum cells.

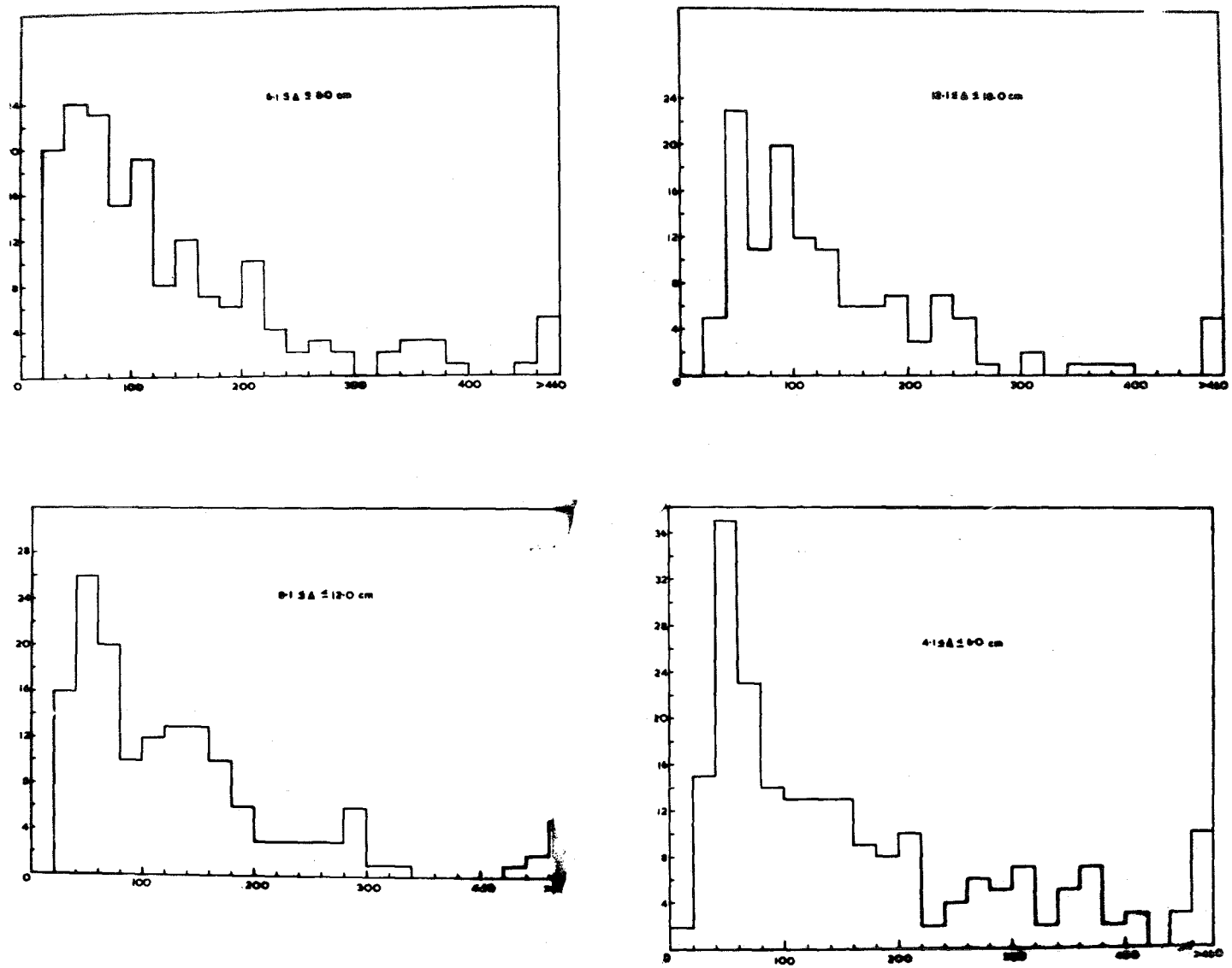

Fig. 7·9 Cerenkov pulse height distributions for different momentum cells.

Table 7.6.

Momentum Cells for Grouping of the Cerenkov Pulses.

Cell Width (cm)	Mean Momentum in the Cell (GeV/c)	No. of Particles (up to 400 mV)
$42 < \Delta \leq 80$	0.355	56
$18 < \Delta \leq 42$	0.723	171
$12 < \Delta \leq 18$	1.50	122
$8 < \Delta \leq 12$	2.32	146
$6 < \Delta \leq 8$	3.18	164
$4 < \Delta \leq 6$	4.56	197
$2 < \Delta \leq 4$	8.04	305
$1 < \Delta \leq 2$	15.2	281
$0.5 < \Delta \leq 1$	30.5	132
$\Delta \leq 0.5$	98.6	92

The histograms for the pulse height distribution for different momentum cells are given in fig. 7.9.

7B (f.) Analysis of the Data:

All three methods used in analysing the data on ionization loss were also tried in the present case. However, only the subjective method was found to be satisfactory in analysing a skew distribution of the present kind.

The reciprocal method was also tried, with different cut off positions, but a good straight line could not be fitted through the points. This is presumably due to the peculiar shape of the distribution, the latter being more Poissonian than Gaussian. The presence of the long tail gave very inconsistent results with the area method. So only the subjective method was used for final analysis. As before, a mean master curve using all the distributions plotted separately in log-linear graph papers was drawn, and the data i.e. all the separate log-normal distributions, were submitted to ten independent observers. The mean of the ten peak values for each group was evaluated. The error on the most probable value was taken as that for a normal distribution of the same width.

The arithmetic mean and the median of each group were also calculated with the tail of the distribution artificially cut off at 400 mV. The accepted values of the mean, median and mode are given in table 7.7.

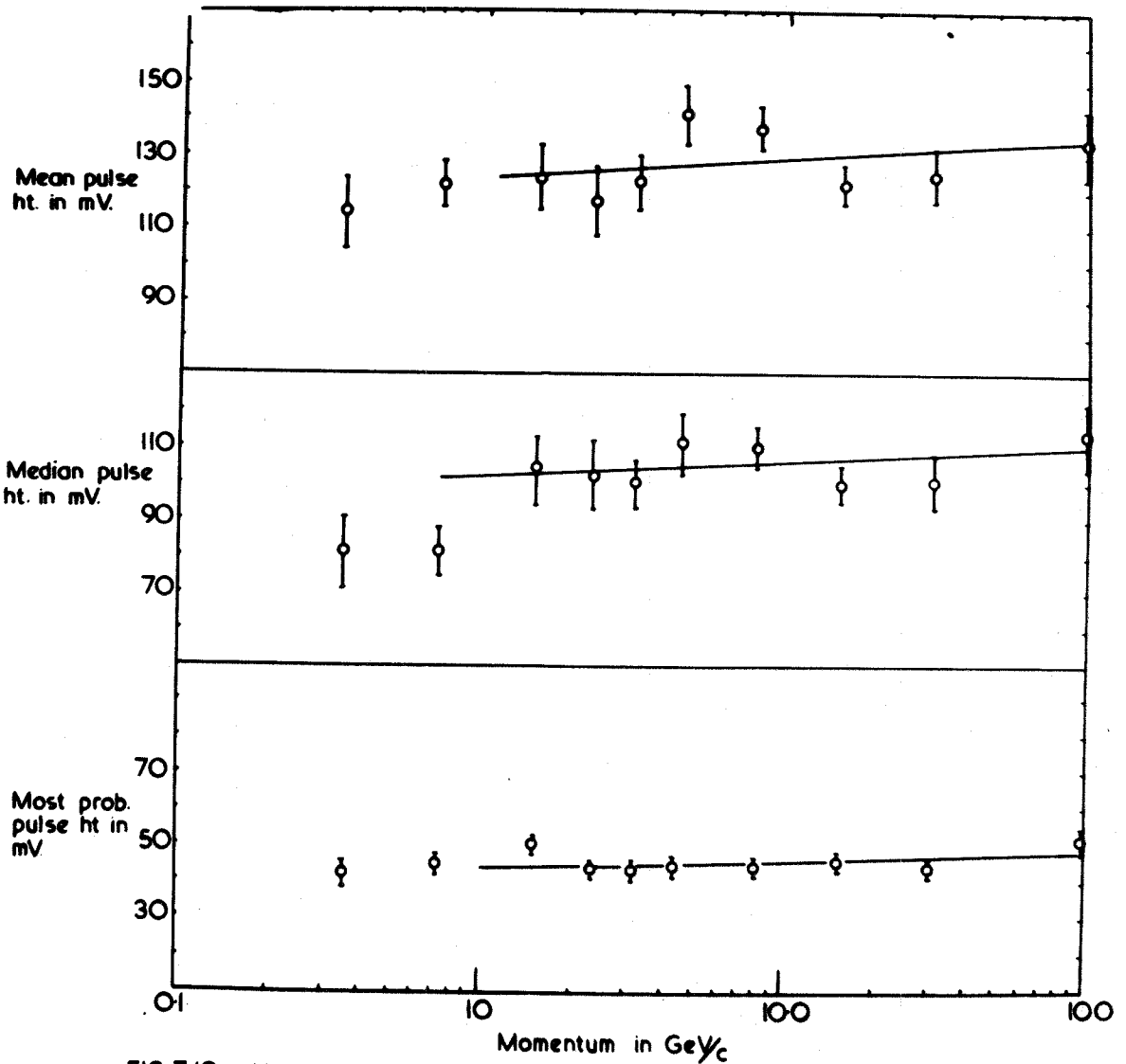

FIG. 7·10. Variation of mean, median & mode of the Cerenkov pulse heights as a function of muon momentum.

Table 7.7

Values of Mean, Median and Mode of the Cerenkov Pulse Height Distributions

Mean Momentum GeV/c	Mean in mV	Median in mV	Mode in mV
0.355	114.3 ± 9.3	81.4 ± 9.3	42.3 ± 3.5
0.723	122.0 ± 6.6	81.5 ± 6.6	45.0 ± 1.7
1.50	123.7 ± 8.9	104.2 ± 8.9	50.5 ± 2.1
2.32	117.4 ± 9.0	102.5 ± 9.0	43.3 ± 2.1
3.18	122.8 ± 7.5	100.5 ± 7.5	43.6 ± 2.0
4.56	141.6 ± 8.6	111.5 ± 8.6	44.3 ± 1.9
8.04	138.1 ± 5.5	110.0 ± 5.5	44.2 ± 1.6
15.2	122.0 ± 4.9	100.0 ± 4.9	46.1 ± 1.4
30.5	124.8 ± 7.7	100.8 ± 7.7	43.9 ± 2.3
98.6	133.9 ± 9.1	113.7 ± 9.1	51.2 ± 2.8

7B (g) The Results.

The mean, the median and the mode values of the Cerenkov pulse height distributions are plotted against the muon momentum in fig. 7.10.

The slope m for each of the three curves for points above 1 GeV/c i.e. in the region corresponding to the plateau value of the classical theory has been calculated

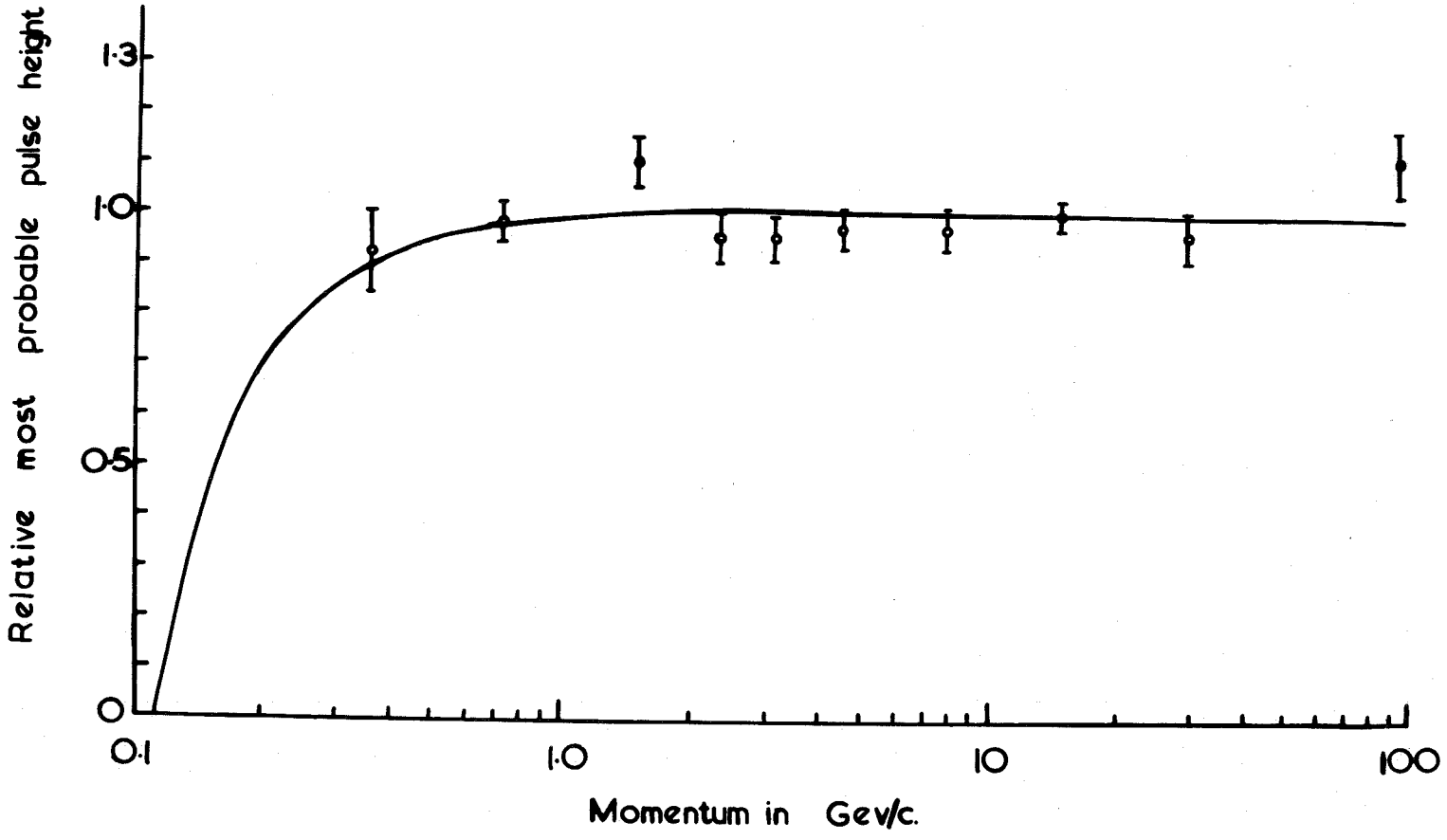

Fig 7·11 Most probable Cerenkov loss as a function of muon momentum.

and found to be equal to

$$m_{mean} = (0.480 \pm 0.862) \text{ per decade of momentum}$$

$$m_{median} = (0.356 \pm 0.253) \text{ per decade of momentum}$$

$$m_{mode} = (0.183 \pm 0.181) \text{ per decade of momentum}$$

The slopes for all the three curves are not significantly different from zero. The percentage rise of the mode values in the classical plateau region above 1 GeV/c is found to be (4.3 ± 4.3) % per decade of momentum. This means that within experimental error, the Cerenkov radiation loss maintains its plateau value from 1 GeV/c onward up to the highest momentum ($\simeq$ 100 GeV/c) measured.

In fig. 7.11, the theoretical curve due to Frank and Tamm, and the observed most probable values normalised to the theory at momentum corresponding to mean of all points above 1 GeV/c are shown.

7B (h) Discussion

As mentioned in chapter 4, section B, there are only a few experiments performed so far to investigate the variation of Cerenkov radiation loss with energy. In the high energy region (GeV range) only two experiments (Bassi et al.(1952), and Millar and Hincks (1957)) have

been reported so far. These workers used cosmic ray muons to cover the energy range up to about 4.2 GeV. The results of Bassi et al. indicated a relativistic rise above that predicted by the classical theory of Frank and Tamm. However, their results were not inconsistent with the theoretical prediction of Budini (1953). But the authors gave only three observed points. As such, the actual magnitude of the observed rise is difficult to estimate. Their last observed point corresponding to energy about 4.2 GeV seems to be about 30% higher than the theoretical plateau value given by Frank and Tamm.

Millar and Hincks (1957), also working in the energy region of a few GeV did not observe any relativistic rise. As such, their results were inconsistent with that of Bassi et al. in the high (GeV) energy range. They concluded that the theoretical Cerenkov intensity as given by the classical theory of Frank and Tamm was valid to within few per cent from the threshold up to the plateau region.

The present work extends to momenta much higher than hitherto. The results indicate that the Cerenkov radiation loss after attaining its plateau value at about 1 GeV/c remains comparatively steady up to the highest momentum measured. Thus, the data are quite inconsistent with the results of Bassi et al., and are in agreement with the results of Millar and Hincks and with the classical theory

of Frank and Tamm. There is no sign of a decrease of Cerenkov intensity above 10 GeV/c ($\gamma > 100$) as predicted by Tsytovich instead, the last point at momentum $\simeq 100$ GeV/c shows, if anything, a small rise above the plateau value.

CHAPTER 8

CONCLUSIONS

8 A Conclusion on the Ionization Loss

From the study on the ionization loss of cosmic ray muons in plastic scintillator, the following conclusions are drawn.

(a) The study on the ionization loss of positive and negative muons indicates that there is no significant dependence of the ionization loss on particle sign, the ratio for positive to negative muons being 1.011 ± 0.035.

(b) Experimental results on the ionization loss above 1 GeV/c show a slight reduction with increasing momentum, a best straight line giving a decrease of $3.6 \pm 1.8\%$ per decade of momentum. The slope above 10 GeV/c is $(2.7 \pm 1.7)\%$ per decade and is considerably smaller than predicted by Tsytovich (1962) for this region.

It is contended that the results are not inconsistent with the 'conservative' predictions of Sternheimer (1952, 1953) who expects a constant value of ionization loss above 10 GeV/c, and this contention is strengthened when a mean is taken of the present data with that of Crispin and Hayman (1964) who used an identical scintillator plastic and who found a small increase in ionization loss with increasing momentum.

8 B Conclusion on the Cerenkov Radiation Loss

The conclusions on the study of Cerenkov radiation are as follows:

(a) The results on the Cerenkov radiation loss on positive and negative muons indicate that there is no significant difference in Cerenkov intensity for the two types of particles, the actual ratio measured for positive to negative muons being 1.012 ± 0.036.

(b) The present results do not show any decrease of Cerenkov intensity at momentum $\geq$ 10 GeV/c ($\gamma \geq 100$) as suggested by Tsytovich from his theory on radiative corrections.

(c) Turning to lower momenta, the results agree with those of Millar and Hincks (1957) and are in disagreement with the only other experiment at a momentum above 1 GeV/c, that of Bassi et al. (1952) which showed a marked increase in Cerenkov loss at $\simeq$ 4 GeV/c.

(d) The present results are in good agreement with the classical theory of Frank and Tamm up to the highest ($\simeq$ 100 GeV/c) momentum measured.

ACKNOWLEDGMENTS

The author wishes to thank Professor G. D. Rochester, F.R.S., for the provision of the facilities for this work and also for his continuous support and interest.

The author is grateful to his supervisor, Professor A. W. Wolfendale for his guidance and encouragement at all stages of the work. It is with gratitude that the author acknowledges the help and also guidance of Dr. M. G. Thompson in completing the work.

Drs. G. Brooke and I. W. Rogers, and Messrs B. Holyoak and M. J. Turner are thanked for help given in repairing the magnet. The author would also like to thank Dr. A. O. Sanni for his help in constructing some of the electrical circuits.

The author wishes to offer special thanks to one of his colleagues, Mr. D. Alexander, for his untiring help in the construction of the spectrograph, without which the work would have been further delayed. He is also grateful to two of his other colleagues, Mr. I. S. Jones and Mr. C. A. Ayre, for their help at various stages of the work.

The technical staff of the Physics Department, in particular Messrs W. Threadgill, E. Lincoln, D. Jobling, K. Tindale, P. Armstrong, M. Lee, and B. Halton and Miss P. Wallace are thanked for their willing help.

He wishes to thank Mrs. J. Lincoln for typing the thesis.

The Education Department, Govt. of Assam, India, are thanked for providing study leave for the period and the committee administering the Fawcus Trust Fund are thanked for helping with financial grants.

Last but not the least the author wishes to express his sincere thanks to his wife, Mrs. A. Pathak, for her continuous encouragement during the whole period of the work.

REFERENCES

Akimov, Yu., K., 1965, Scintillation Counters in High Energy Physics, (Academic Press: London)

Alekseeva, K.I., Zhdanov, G.B., Tret'yakova, M.I., and Scherbakova M.N., 1963, Soviet Phys, JETP, 17, 1254.

Alexander, G., and Johnston, R.R.W., 1957, Nuo. Cim., 5, 363

Allen J.E., and Apostolakis, A.J., 1961, Proc. Roy.Soc. A.265, 117.

Ashton, F. and Simpson, D.A. 1963, Proc. Int. Conf. on Cosmic Rays, Jaipur (India).

Ashton, F., and Simpson, D.A. 1965, Phys. Lett., 16, 78.

Aurela, A.M., 1965, Ph.D. Thesis, University of Durham.

Bakker, C.J., and Segre, E., 1951, Phys. Rev., 81, 489.

Barnaby, C.F. 1960, Ph.D. Thesis, University of London.

Barnaby C.F., 1961, Proc. Phys. Soc., 77, 1149

Barton, J.C., Barnaby C.F., Jasani, B.M., and Thompson, C.W., 1962, J. Sci. Inst., 39, 360.

Bassi, P., Bianchi A.M., and Manduchi, C., 1952, Nuo. Cim., 9, 861.

Beck, G., 1948, Phys. Rev., 74, 795.

Belcher, E.H., 1953, Proc. Roy. Soc. A.216, 90.

Bergeson, H.E., Hilton, L.K., Keuffel, J.W., Morris, M., Parker, J.L., Stenerson, R.O., Wolfson, C.J., 1965, Proc. Int. Conf. on Cosmic Rays (London) P1048.

Bethe, H.A., 1930, Ann. Phys., LPZ., 5, 325.

1932, Z. Phys., 76, 293.

Bethe, H.A., and Ashkin, J., 1952, Exptal. Nucl. Phys., 1, Chap.2. (Wiley: New York).

Bhabha, H.J., 1937, Proc. Roy. Soc. A 164, 257.

Birks, J.B., 1964, The Theory and Practice of Scintillation Counting. (Pergamon Press: London).

Bloch, F., 1933, Ann. Phys., LPZ, 16, 285.

Bohr, N., 1915, Phil. Mag, 30, 581.

Bowen, T., 1954, Phys. Rev., 96, 754.

Bowen, T., and Roser, F.X., 1951a, Phys. Rev., 82, 284.

1951b, Phys. Rev., 83, 689.

1952, Phys. Rev., 85, 992.

Breitenberger, E., 1956, Prog. Nucl. Phys., 4, 56.

Brooke, G., 1964, Ph.D. Thesis, University of Durham.

Brooke, G., Gardener, M., Lloyd, J.L., Kisdanasamy S., and Wolfendale, A.W., 1962, Proc. Phys. Soc., 80, 674.

Budini, P., 1953, Nuo. Cim., 10, 236.

Budini, P., Taffara, L., and Violia, C., 1961, Nuo, Cim., 20, 265.

Bushkirk, F.R., Dyer J.N., Hanson, H.D., Seng, R., and Weidman, R.H., 1964, Proc. 5th Int. Conf. on Nucl. photography, 2,1X -9.

Caglioti, G., Cervellati, R., and Mezzetti, L., 1959, Nuo. Cim., 11, 850.

Cerenkov, P.A., 1934., Dokl. Akad. Nauk., SSSR, 2, 451.

Cerenkov, P.A., 1960, Sci., 131, 136.

Collins, G.B., and Reiling, V.G., 1938, Phys. Rev., 54, 499.

Conversi, M., and Gozzini, A., 1955, Nuo. Cim., 2, 189.

Corsen D.R., and Keck, M.R., 1950, Phys. Rev., 79, 209.

Cousins, J.E., and Nash, W.F., 1962, Adv. in Phys., 11, 349.

Coxell, H., 1961, Ph.D. Thesis, University of Durham.

Coxell, H., and Wolfendale, A.W., 1960, Proc. Phys. Soc, 75, 378.

Crispin, A., 1965, Ph.D. Thesis, University of London.

Crispin, A., and Hayman, P.J., 1964, Proc. Phys. Soc., 83,1051.

Daniel, R.R., Davies, J.H., Mulvey, J.R., and Perkin, D.H., 1952, Phil. Mag., 43, 753.

Eyeions, D.A., Owens, B.G., Price, B.T. and Wilson, J.G., 1955, Proc. Phys. Soc, A., 68,793.

Fano, U., 1963, Ann. Rev. Nucl. Sci., 13, 1.

Fermi, E., 1939, Phys. Rev., 56, 1242.

1940, Phys. Rev., 57, 485.

Fleming, J.R, and Lord, J.J., 1953, Phys. Rev., 92, 511.

Fowler, G.N., and Jones, G.M.D.B., 1953, Proc. Phys. Soc. A, 66,597.

Fowler, G.N., and Hall, A.G., 1965, Proc. 9th Int. Conf. on Cosmic Rays, London, P.976.

Garlick, G.F.J., and Wright, G.T. 1952, Proc. Phys. Soc. B, 65 415.

Frank, I., and Tamm, I., 1937, Dokl. Akad. Nauk, SSSR, 14, 109.

Gardener, M., Kisdnasamy, S., Rossle, E., and Wolfendale A.W., 1957, Proc. Phys. Soc., B70, 687.

Ghosh, S.K., Jones, G.M.D.B., and Wilson, J.G., 1952, Proc. Phys. Soc. A 65, 68

1954, Proc. Phys. Soc. A 67, 331

Ginsburg, V.L., 1940, J.E.T.P., 10, 589.

1940a, J. Phys., (USSR), 2, 441

1942, J E T P., 12, 425.

1943, J. Phys. (USSR), 7, 115.

Halpern, O., and Hall, H., 1948, Phys. Rev., 73, 477.

Hayward, E., 1947, Phys. Rev., 72, 937.

Hayman, P.J., 1962, Ph.D. Thesis, Durham University.

Hayman, P.J. and Wolfendale, A.W., 1962, Proc. Phys. Soc., 80, 710.

Hazen, W.E., 1944, Phys. Rev., 65, 259,

1945, Phys. Rev., 67, 289.

Herz and Stiller, B., 1964, Proc. 5th Int. Conf. on Nucl. Photography, 2, IX-23.

Huybrechts, M., and Schonberg, M., 1952, Nuo. Cim., 9, 764.

Jauneau, L., and Trembley, J., 1955, Nuo, Cim., Suppl.1, 230.

Jelley, J.V., 1953, Prog. Nucl. Phys, 3, 84.

1958, Cerenkov Radiation and its application. (Pergamon Press: London).

1961, Contem. Phys., 3(1), 45.

Jones, D.G., 1961, Ph.D. Thesis, University of Durham.

Jones, D.G., West R.H., and Wolfendale, A.W., 1963, Proc. Phys. Soc., 81, 1137.

Jongejans, B., 1960, Nuo. Cim, 16, 625.

Kepler, R.G., D'andlau, C.A., Fretter, W.B., and Hansen, L.F., 1958, Nuo. Cim., 7, 71.

Keuffel, J.W., 1966, (Private Communications).

Landau, L., 1944, J. Phys, USSR, 8, 201.

Lanou, R.E., and Kraybill, H.L., 1959, Phys. Rev, 113, 657.

Linsley, J., and Horwitz, N., 1955, Rev. Sci. Inst., 26, 557.

MacKeown, P.K., 1965, Ph.D. Thesis, University of Durham.

Mallet, L., 1926, C.R. Acad. Sci., 183, 274.

1928, C.R. Acad. Sci., 187, 222.

1929, C.R. Acad. Sci., 188, 445.

Massey, H.J., and Corben, H.C., 1939, Proc. Camb. Phil.Soc., 35, 463.

Mather, R.L. and Segre,E., 1951, Phys. Rev., 84, 191.

Messel, H., and Ritson, D.M., 1950, Phil. Mag., 41, 1129.

Michaelis, R.P. and Violet, C.E., 1953, Phys. Rev., 90, 723.

Miller, C.H., and Hinks, E.P., 1957, Canad. J. Phys., 35,363.

Nuclear Enterprises Catalogue, 1965, September, P5.

Occhialini, G.P.S., 1949, Nuo. Cim. Suppl., 6, 377.

Parry, J.K., Rathgeber, H.D., and Rouse, J.L., 1953, Proc. Phys. Soc. A 66, 541.

Pickup, E., and Voyvodic, L., 1950, Phys. Rev., 80, 89.

Price, B.T., 1955, Rep. Prog. Phys., 18, 52.

Price, B.T., West, D., Becker, J., Chanson, P., Nageotti, E., and Treille, P., 1953, Proc. Phys. Soc. A., 66, 167.

Rossi, B., 1952, High Energy Particles. (Prentice Hall: New York).

Schiff, L.I., 1955, Quantum Mechanics, P267, (McGraw Gukk Book Co: New York).

Schoenberg, M., 1951, Nuo. Cim., 8, 159.

1952, Nuo. Cim., 9, 372.

SenGupta, R.L., 1940, Nature, London, 146, 65.

Simpson, D.A., 1965, M.Sc. Thesis, University of Durham.

Sommerfield, A., 1954, Optics, P328, (Academic Press: New York).

Sternheimer, R.M., 1952, Phys. Rev., 88,851.

1953, Phys. Rev., 89, 1148.

1953, Phys. Rev., 91, 256.

1956, Phys. Rev., 103, 511.

1959, Phys. Rev., 115, 137.

Stiller, B and Shapiro, M.M., 1953, Phys. Rev., 92, 735.

Swann, W.F.G., 1938, J. Franklin Inst., 226, 598.

Symon, K.R., 1948, Ph.D. Thesis, (Harvard University) (See Rossi, B., 1952, H.E. Particles).

Tamm, I., 1939, J. Phys. (USSR), 1, 439.

Tidman, D.A., 1956a, Nuo. Cim., 3, 503.

1956b, Nucl. Phys. 2, 289.

Tsytovich, V.N., 1962, Soviet Phys. DOKlady, 7, 411.

1962, Soviet Phys. JETP, 15, 320

1963, Soviet Phys. JETP, 16,1260.

Uehling, E.A., 1954, Ann. Rev. Nucl. Sci., 4, 315.

Voyvodic, L., 1952, Phys. Rev., 86, 1046.

Whitemore, W.L., and Street, J.C., 1949, Phys. Rev., 76, 1786.

Williams, E.J., 1929, Proc. Roy. Soc. A, 125, 420.

Wilkinson, D.H., 1950, Ionization Chambers and Counters; Cambridge Univ.Press.

Winckler, J.R. and Anderson, K.A., 1954, Phys. Rev., 93, 596.

Winckler, J.R., Mitchell, E.N., Andersen, K.A., and Peterson, L., 1955, Phys. Rev., 98, 1411.

Wolfendale, A.W., 1963, Cosmic Rays, (Newnes: London).

Zhdanov, G.B., Tret'yakova, M.I., Tsytovich, V.N., and Shcherbakova, M.N., 1963, JETP, 16, 245.

Zhdanov, G.B., Tret'yakova, M.I., Shcherbakova, M.N., 1964, Proc. 5th Int. Conf. on Nucl. Photography, CERN, 2 1X - 4.

Appendix 1

Technical Data for the Plastic Phosphor NE 102A

The phosphor used in all the scintillators was of type NE 102A manufactured by the Nuclear Enterprises Ltd. The following are the technical data for the phosphor as given by the manufactures (Catalogue - September 1965).

General description	Scintillation chemicals in polyvinyl - toluene.
Light output	65% that of an anthracene crystal of the same geometry.
Decay constant	2.2×10^{-9} seconds
Maximum emission	4250 AU
Specific gravity	1.032
Softening temperature	75° C
Refractive index	1.581
Effects of liquids	Soluble in aromatic solvents, acetone etc. Unaffected by water, dilute acids, dilute alkalis or lower alcohols.

No. of atoms per cm barn :

H	: 0.0525
C	: 0.0475
N	: 1.8×10^{-6}
O	: 1.8×10^{-6}

No. of electrons per cc 3.4×10^{23}

Appendix 2

Electronics Circuits

This appendix contains the circuit diagrams of some of the circuits not given in the text but used in the apparatus.

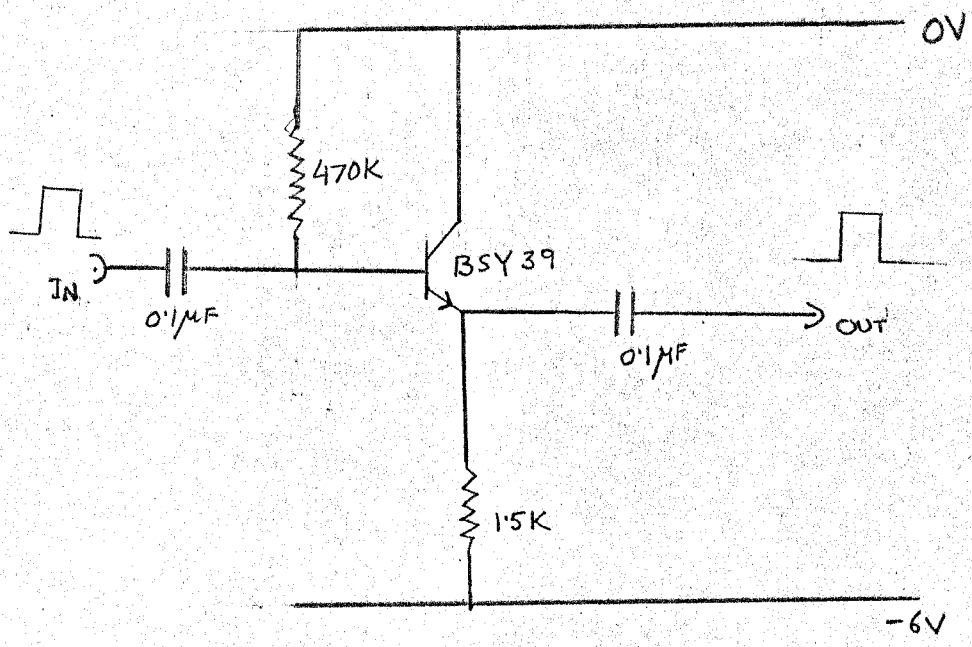

(a)

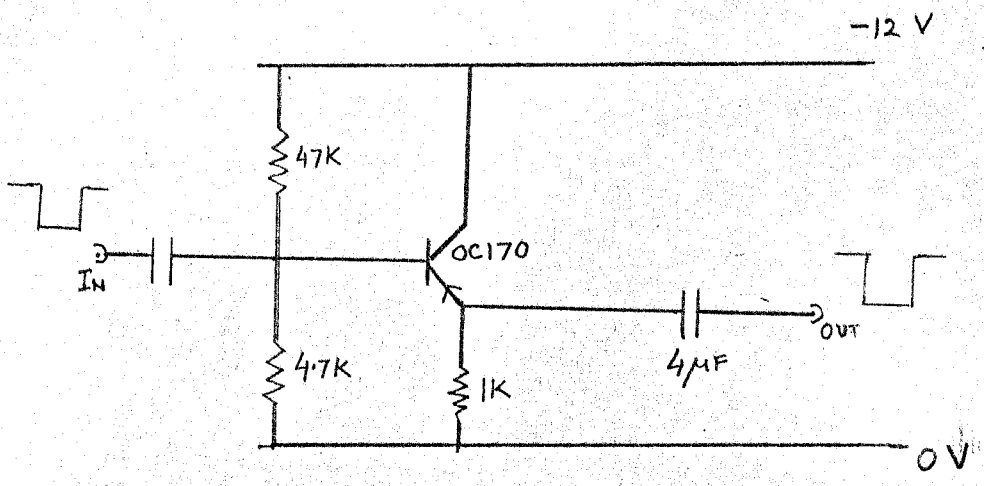

(b)

Fig A2·1. Emitter Followers : (a) Positive input
(b) Negative input

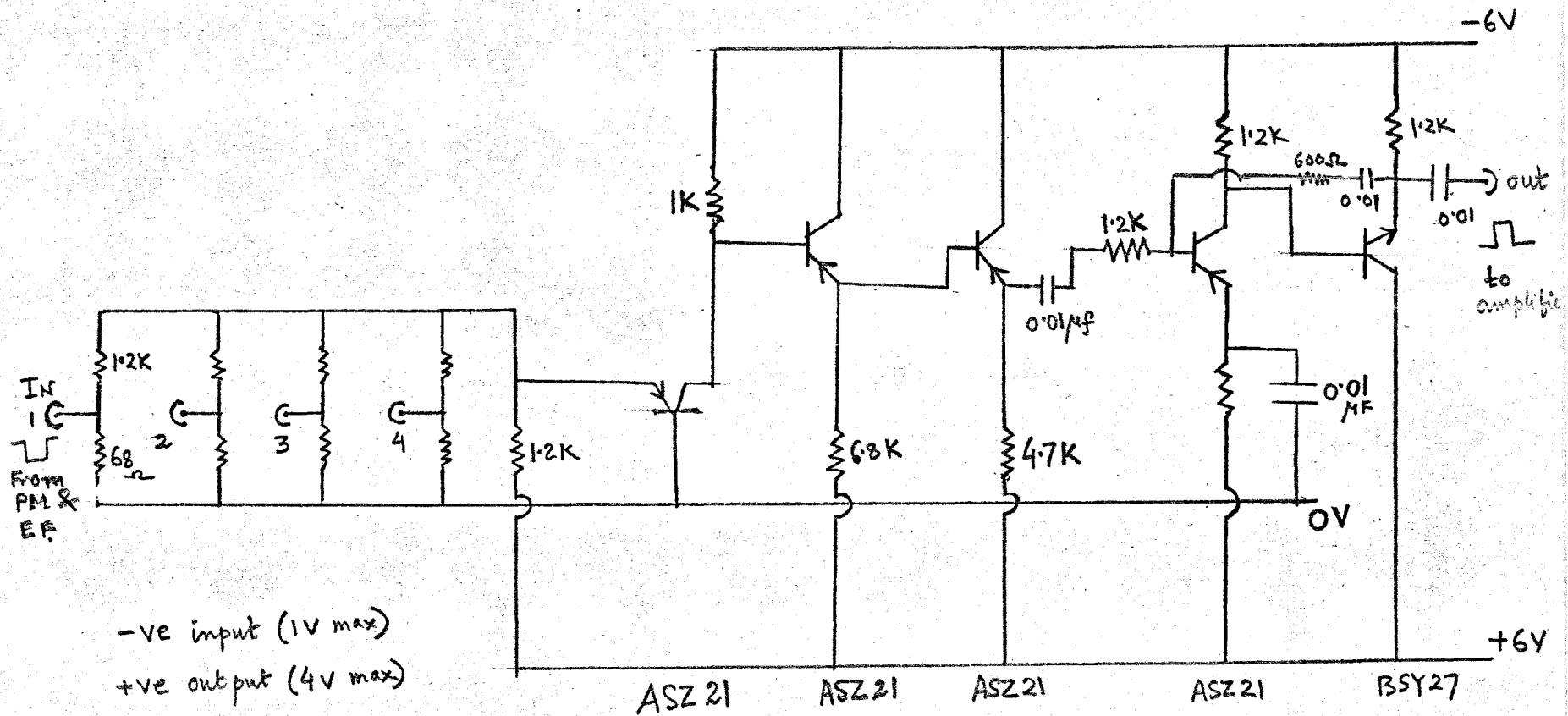

Fig A2.2 Cerenkov Counter Pulse adder & inverter.

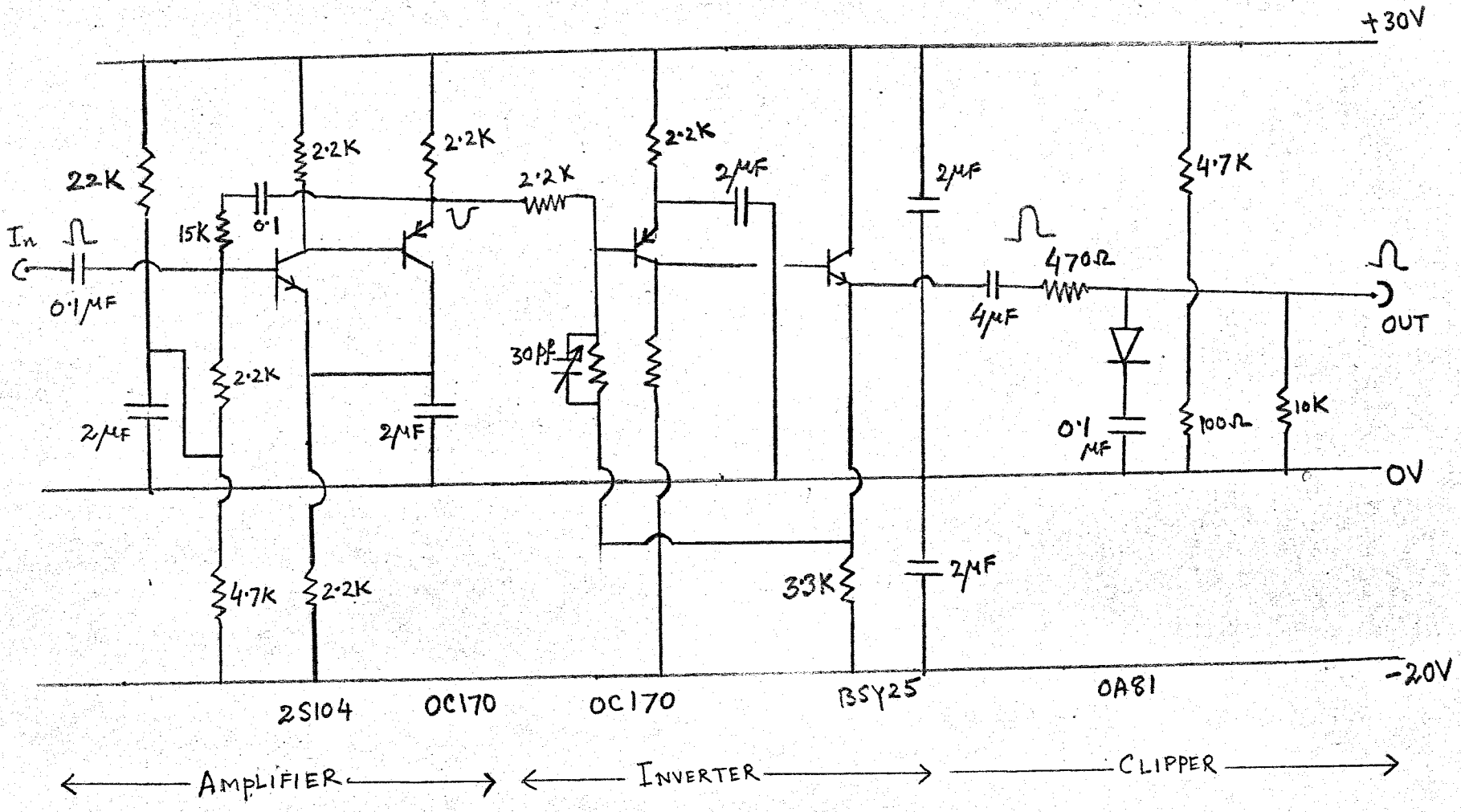

Fig A2.3 AMPLIFIERS IN CERENKOV COUNTER.

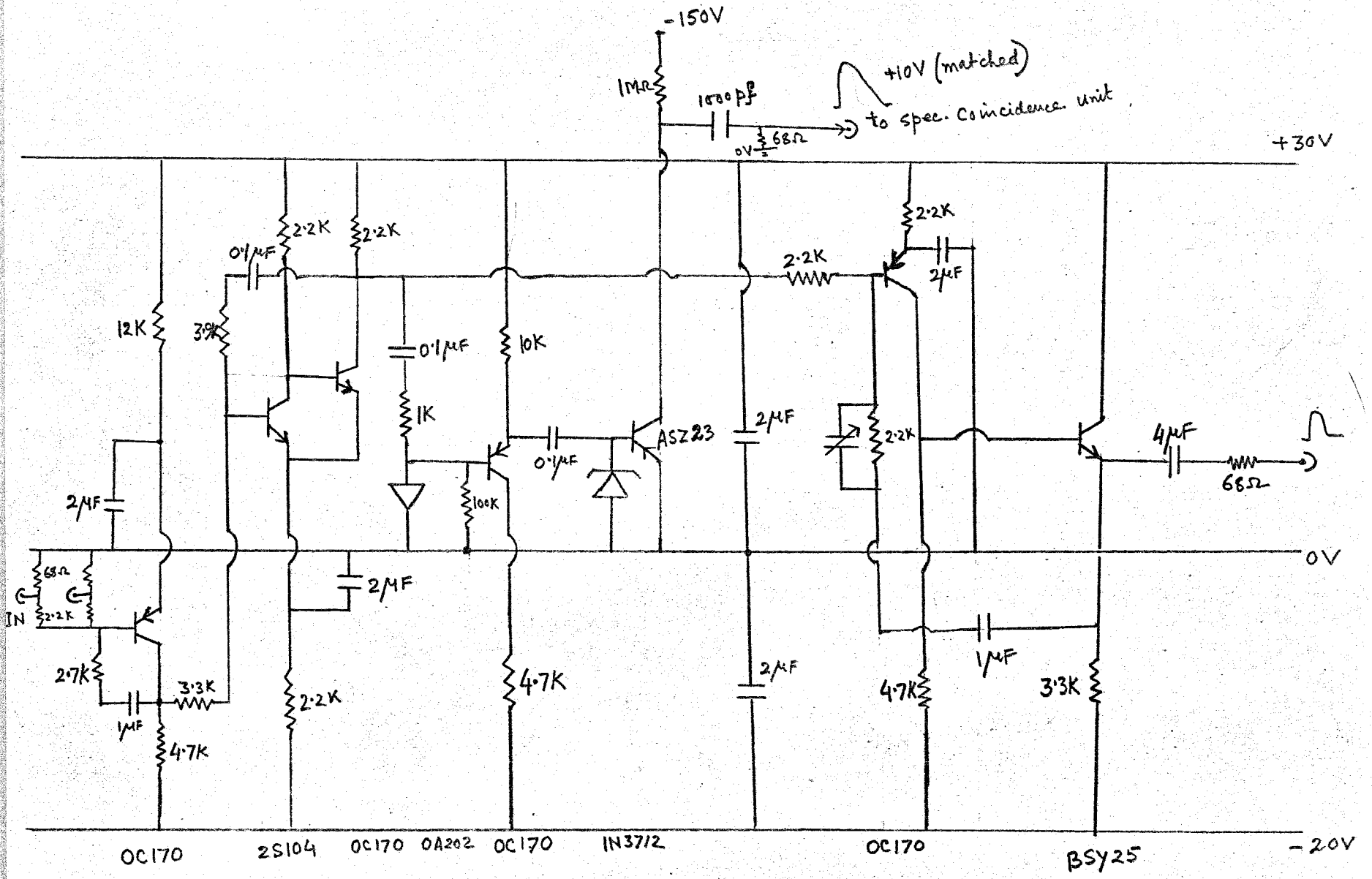

Fig A2.4 Channel Adding Unit with a Discriminator at Fixed Bias Level And Output Drive Circuit. (Scintillation Counter).

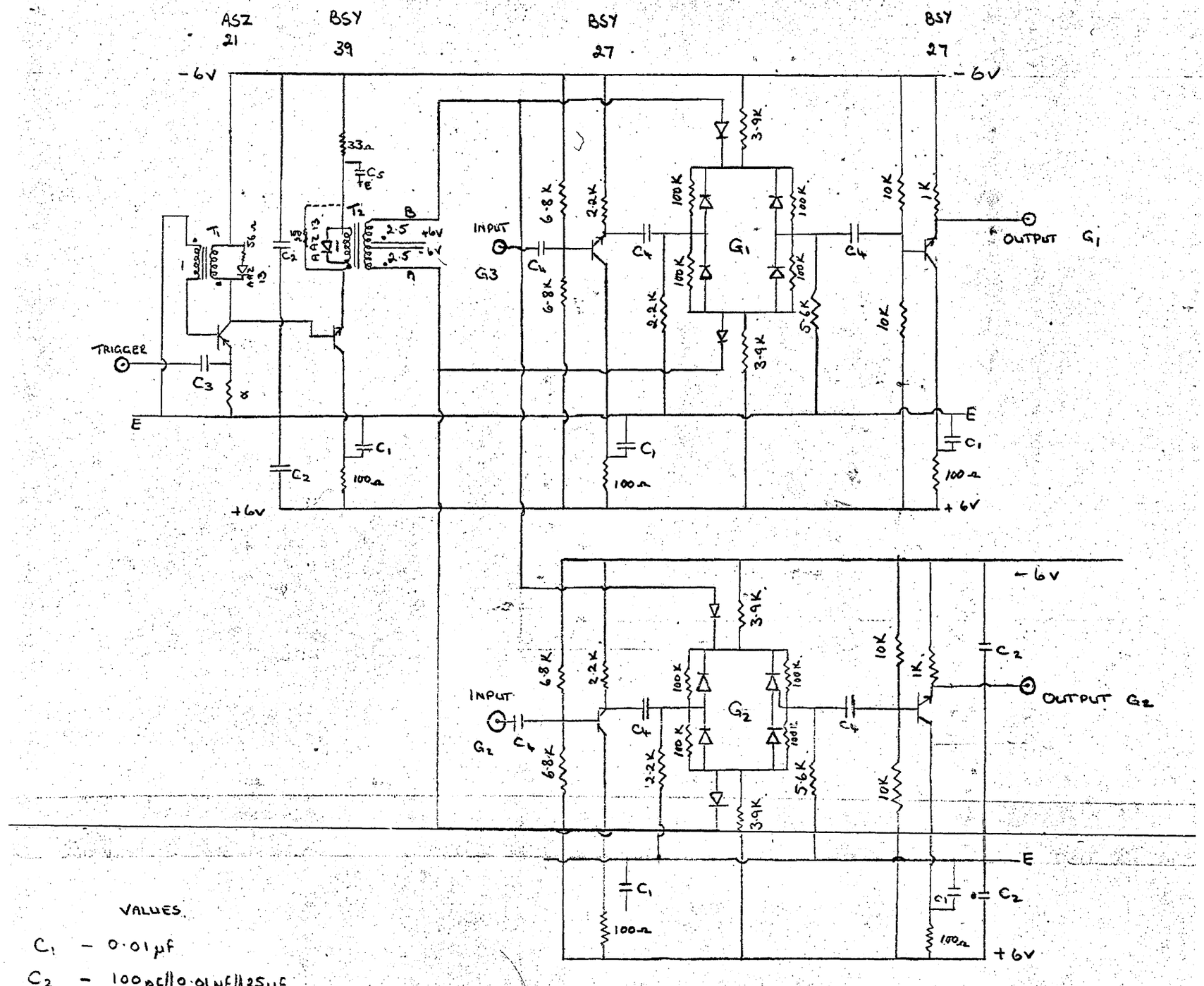

VALUES.

C_1 – 0·01 μf

C_2 – 100 pf ‖ 0·01 μf ‖ 25 μf.

C_3 – 300 pf

C_4 – 0·01 μf ‖ 1 μf

C_5 – 0·01 μ ‖ 50 μf.

OTHER DIODES OA90.

TRANSFORMERS T_1 F x 2236 10:1

T_2 F x 2238 6:12:12

δ – 100Ω

Fig A2.5 GATE CIRCUIT FOR CERENKOV AND SCINTILLATOR PULSES.

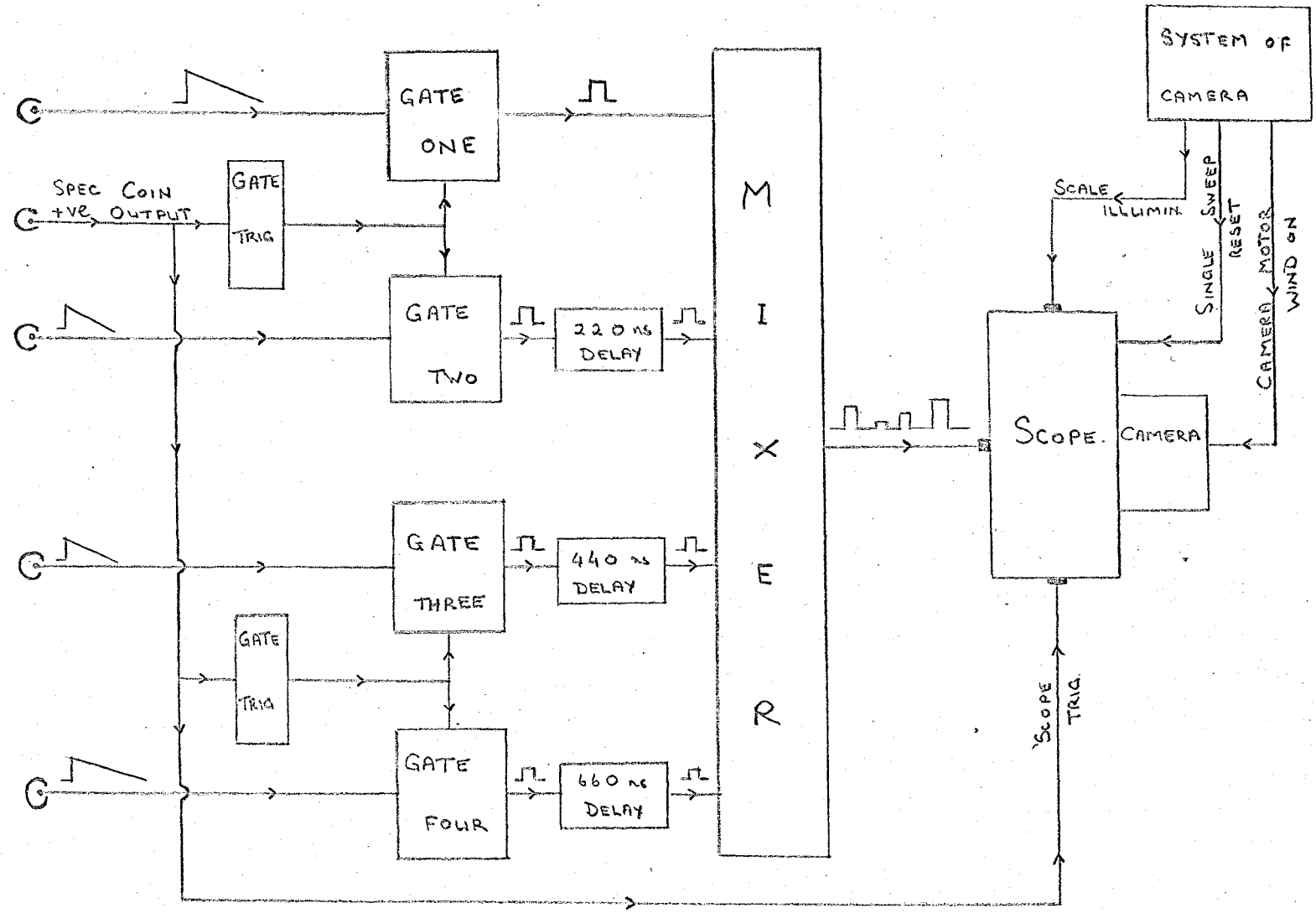

Fig A2·6 OSCILLOSCOPE RECORDING SYSTEM.

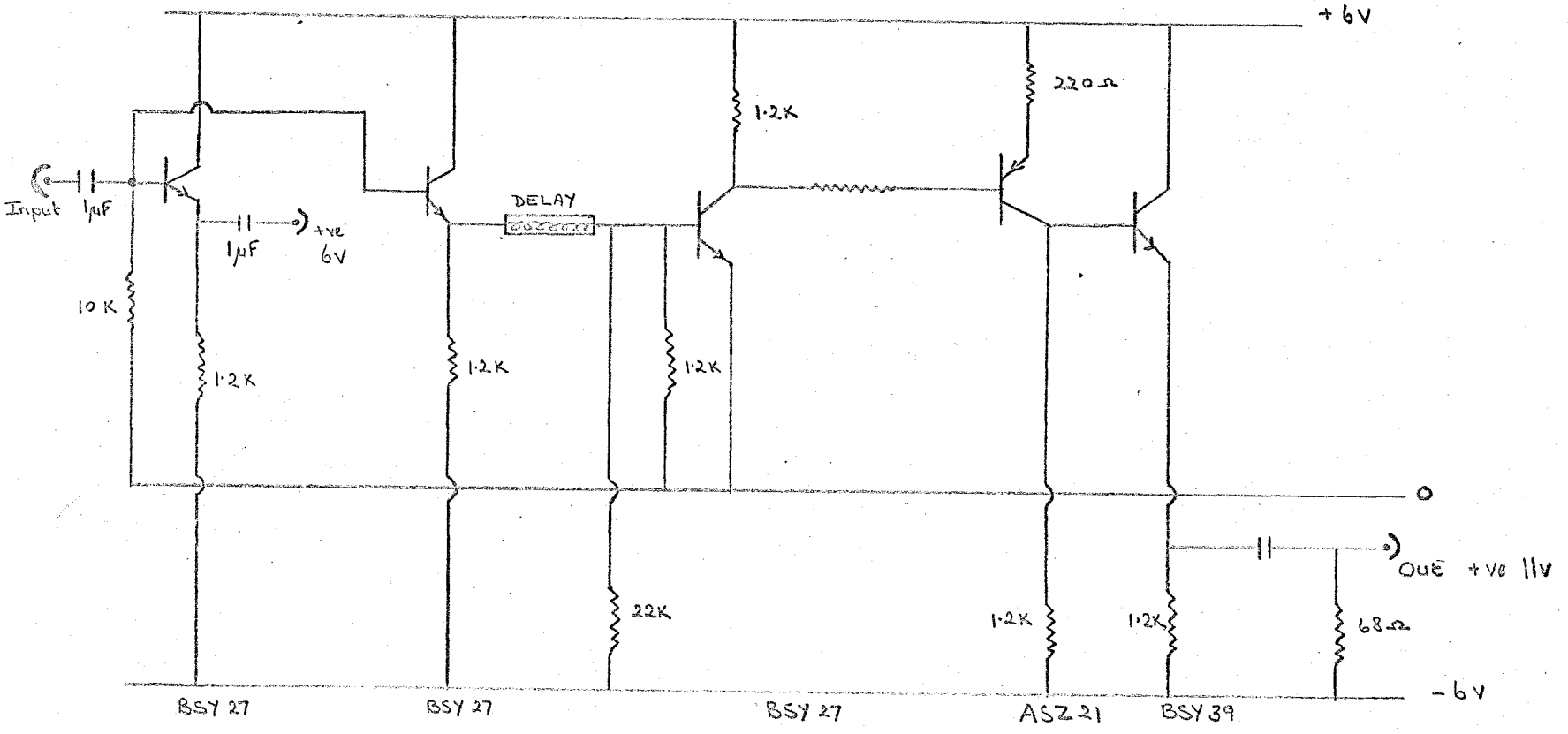

Fig A2·7 SCOPE AND FLASH TUBE TRIGGER UNIT

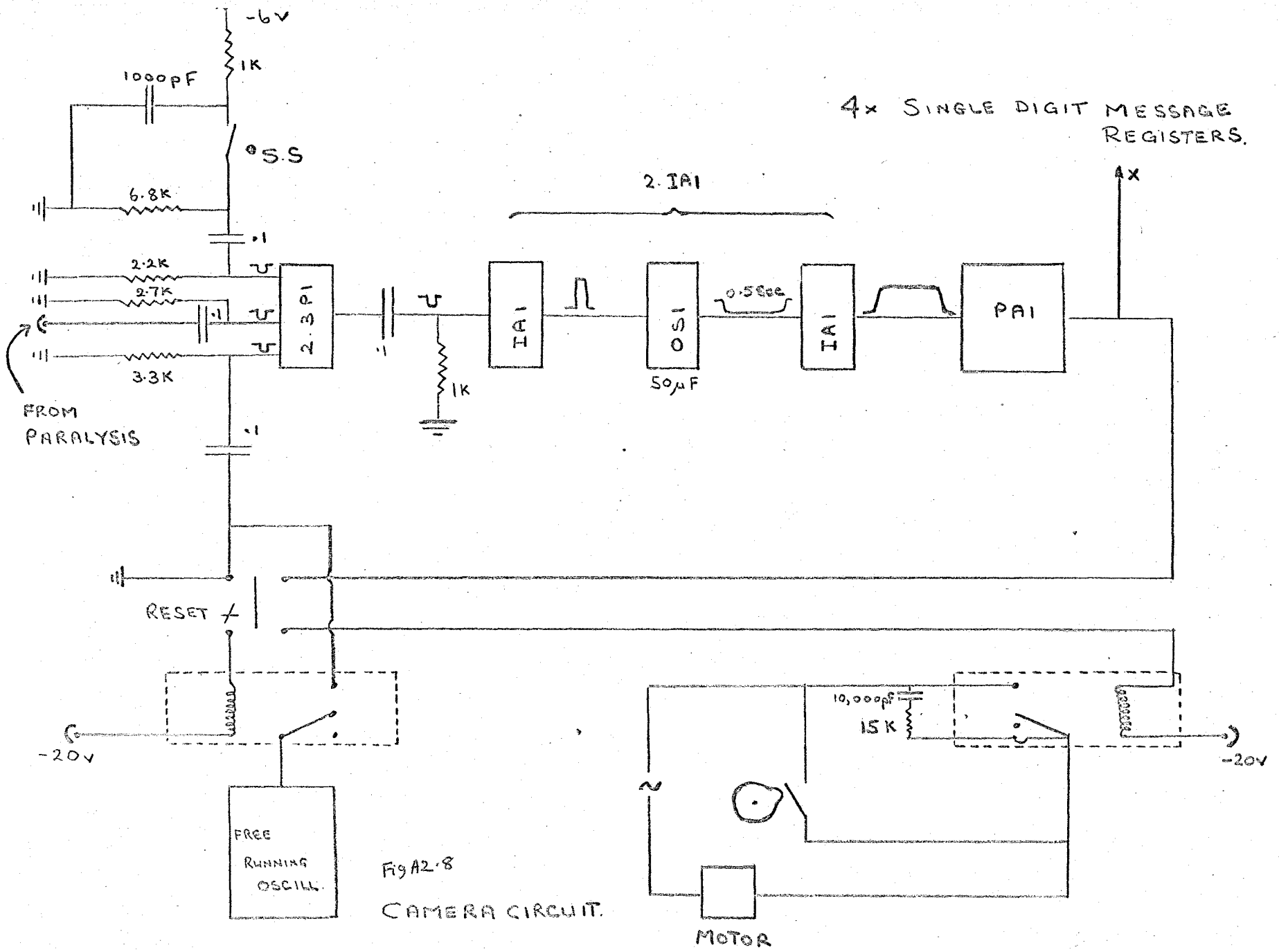

Fig A2·8

CAMERA CIRCUIT.

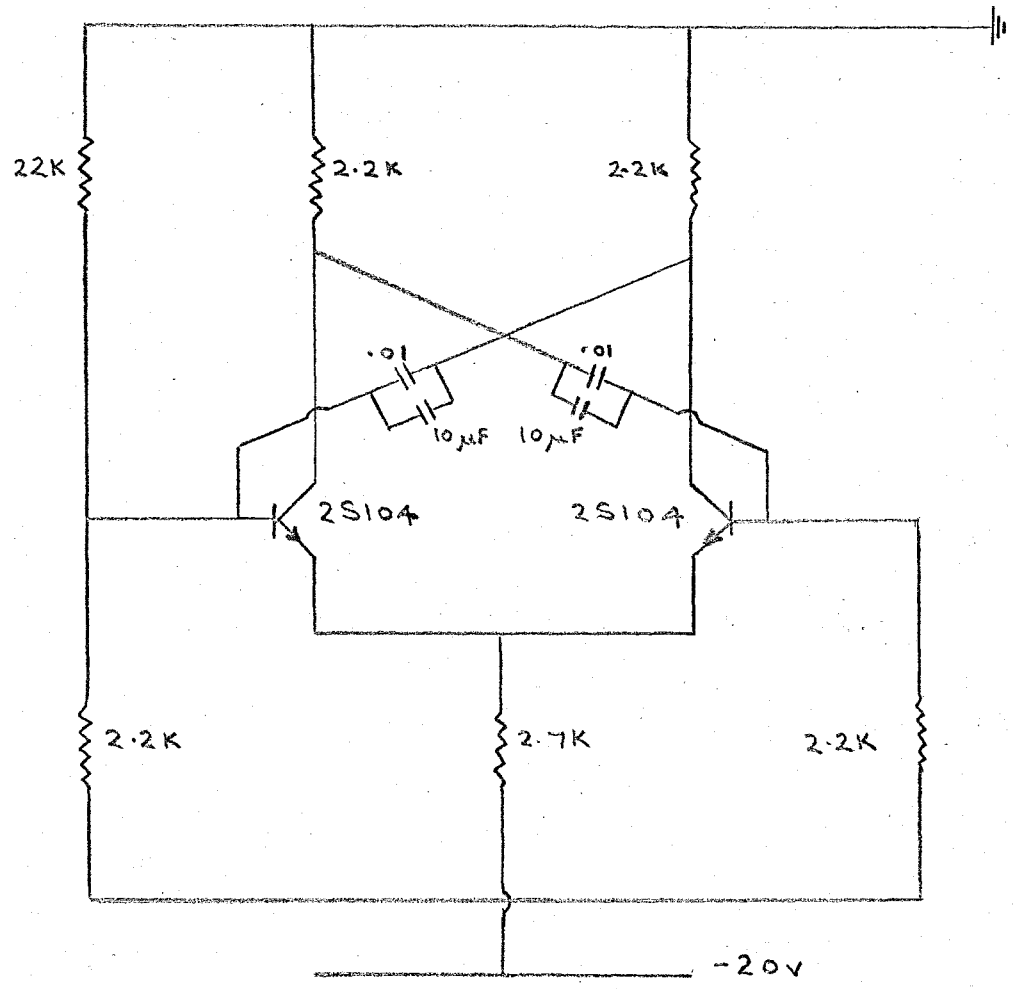

Fig A2.9 FREE RUNNING OSCILLATOR FOR CAMERA CIRCUIT

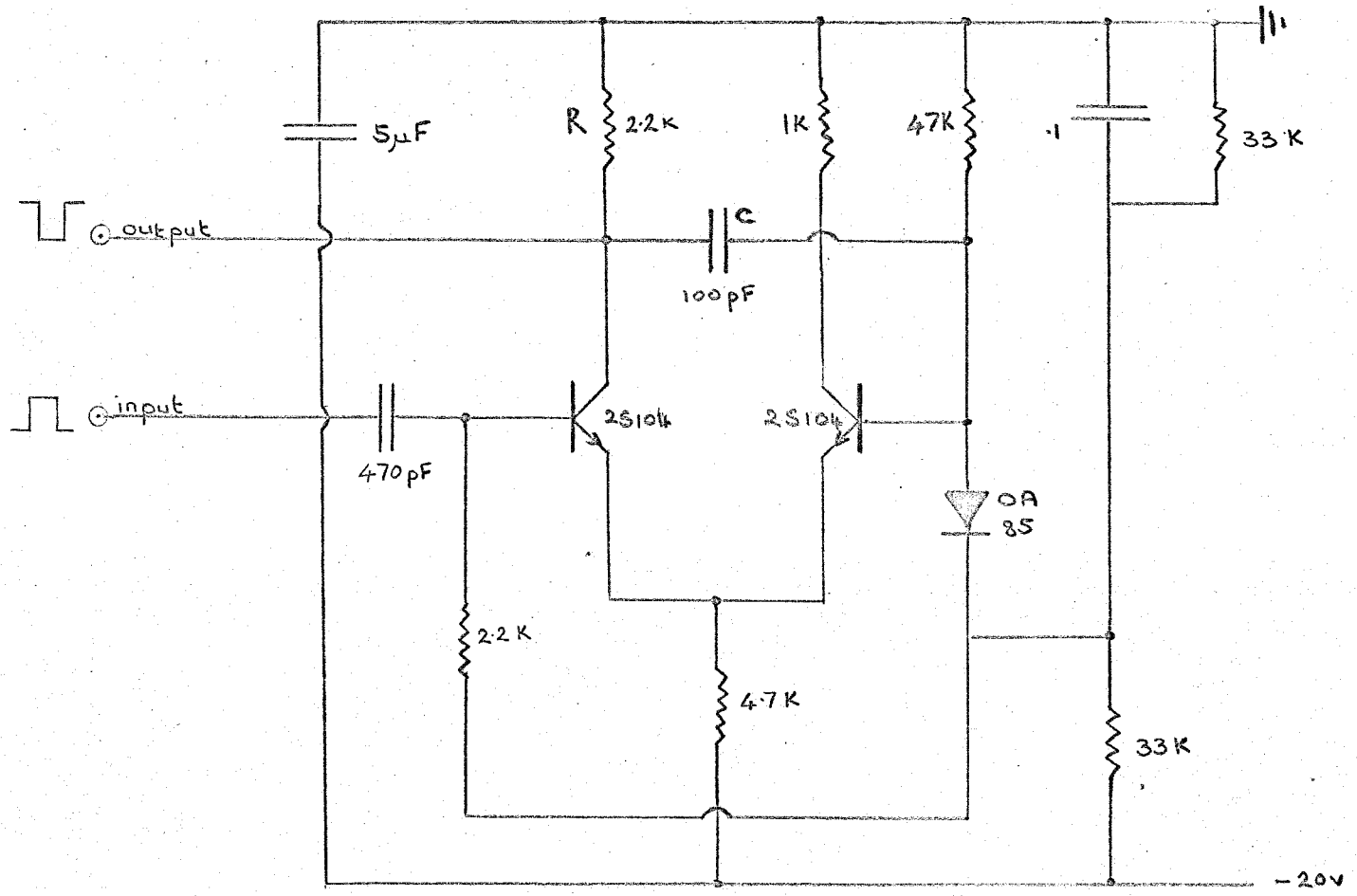

Fig A2·10

PULSE SHAPER FOR ANTI-PULSE, ANTI-COINCIDENCE AND PARALYSIS UNITS.